UNIVERSITÀ DEGLI STUDI DI MESSINA

TESI DI DOTTORATO DI RICERCA IN BIOLOGIA APPLICATA

E MEDICINA SPERIMENTALE

XXXII CICLO

SSD BIO/19

Phage Display as Tool for Marker Discovery, Diagnosis and Targeted Therapy

Candidato:

Dr. LAURA MARIA DE PLANO

Relatore:

Ch.mo Prof.

SALVATORE PIETRO PAOLO GUGLIELMINO

Coordinatore:

Ch.mo Prof.

MARIA ASSUNTA LO GULLO

ANNO ACCADEMICO 2016-2019

INDEX

ABSTRACT

World Health Organization estimates that bloodstream infections affect more than 30 million people worldwide every year causing mortality often due to resistant pathogens. Moreover, heterogeneity of cancer diseases, linked at the crescent cases of manifested neurodegenerative disease, such as Alzheimer disease (AD), are the major expenditure for the public health. Therefore, the costs are predicted to continuously increase over the time due to the necessity of diagnosis and, intensive and prolonged therapies. To reduce health costs, biotechnologies may play a pivotal role by introducing innovative systems cheap and efficient for diagnosis and targeted therapies.

In the present work new biosensors and diagnostic/therapeutic systems based on phage display technology are designed and tuned. New specific, selective and robust phage clones are use as probes for both diagnosis and targeted therapies of pathogen bacteria, cancer cells and misfolded Aβ-amyloid structure associated to AD.

At this purpose, polymeric platform as well as silica, gold, magnetic and latex nanoparticles are functionalized with specific phage clones and associated at conventional (fluorescence microscopy, E.L.I.S.A., Scannig Electron Microscope SEM) and/or innovative (Raman spectrometry and SERS-Raman) detection systems. In addition, bioactivity of phage clones against pathogen agents, such as *P. aeruginosa*, as well as inhibition and disaggregation of amyloid β42-induced cytotoxicity are tested *in vitro*. A new algorithm for the discovery of "self-navigating phage particles" for "smart drug delivery vehicles" is introduced. Finally, *in vivo* biodistribution in nude mice of phage display f8/9 library are performed to identify peptide home-tissue and home-tumor by qPCR and Next generation sequencing.

The results highlight the polyvalent use of phage clones in cheap, innovative and fast detection devices, applicable in several fields (clinical, food and environmental monitoring), as well as in targeted therapy systems for personalized medicine.

LIST OF PUBLICATIONS

Open Researcher and Contributor ID (ORCID): **0000-0003-1152-948X**

Papers:

- **Combinatorial Avidity Selection of Mosaic Landscape Phages Targeted at Breast Cancer Cells-An Alternative Mechanism of Directed Molecular Evolution**
  Petrenko VA, Gillespie JW, Xu H, O'Dell T, De Plano LM.
  Viruses, (2019) 11, 785- | journal-article
  DOI:10.3390/v11090785

- **Bio-hybrid gold nanoparticles as SERS probe for rapid bacteria cell identification**
  Franco D, De Plano LM, Rizzo MG, Scibilia S, Lentini G, Fazio E, Neri F, Guglielmino SPP, Mezzasalma AM.
  Spectrochimica Acta - Part A: Molecular and Biomolecular Spectroscopy 2020 | journal-article
  DOI: 10.1016/j.saa.2019.117394

- **FITC-labelled clone from phage display for direct detection of leukemia cells in blood**
  Franco D, De Plano LM, Rizzo MG, Crea S, Fazio E, Bonsignore M, Neri F, Allegra A, Musolino C, Ferlazzo G, Trusso S, Guglielmino SPP.
  Lecture Notes in Electrical Engineering 2019 | book
  DOI: 10.1007/978-3-030-04324-7_22

- **M13 bacteriophages as bioreceptors in biosensor device**
  De Plano LM, Franco D, Rizzo MG, Crea S, Messina GML, Marletta G, Guglielmino SPP.
  Lecture Notes in Electrical Engineering 2019 | book
  DOI: 10.1007/978-3-030-04324-7_20

- **One-step functionalization of silicon nanoparticles with phage probes to identify pathogenic bacteria**
  Rizzo MG, De Plano LM, Crea S, Franco D, Scibilia S, Mezzasalma AM, Guglielmino SPP.
  Lecture Notes in Electrical Engineering 2019 | book
  DOI: 10.1007/978-3-030-04324-7_21

- **Phage-based assay for rapid detection of bacterial pathogens in blood by Raman spectroscopy**
  De Plano LM, Fazio E, Rizzo MG, Franco D, Carnazza S, Trusso S, Neri F, Guglielmino SPP.
  Journal of Immunological Methods 2019 | journal-article
  DOI: 10.1016/j.jim.2018.12.004

- **Antiadhesive and antibacterial properties of pillar[5]arene-based multilayers**
  Barbera L, De Plano LM, Franco D, Gattuso G, Guglielmino SPP, Lando G, Notti A, Parisi MF, Pisagatti I.
  Chemical Communications 2018 | journal-article
  DOI: 10.1039/c8cc05659e

- **Direct conjugation of silicon nanoparticles with M13pVIII-engineered proteins to bacteria identification**
  De Plano LM, Scibilia S, Rizzo MG, Franco D, Mezzasalma AM, Guglielmino SPP.
  Applied Physics A: Materials Science and Processing 2018 | journal-article
  DOI: 10.1007/s00339-018-2169-1
- **One-step production of phage–silicon nanoparticles by PLAL as fluorescent nanoprobes for cell identification**
  De Plano LM, Scibilia S, Rizzo M.G, Crea S, Franco D, Mezzasalma AM, Guglielmino SPP.
  Applied Physics A: Materials Science and Processing 2018 | journal-article
  DOI: 10.1007/s00339-018-1637-y

- **A water-soluble pillar[5]arene as a new carrier for an old drug**
  Barbera L, Franco D, De Plano LM, Gattuso G, Guglielmino SP, Lentini G, Manganaro N, Marino N, Pappalardo S, Parisi MF, Puntoriero F, Pisagatti I, Notti A.
  Organic and Biomolecular Chemistry 2017 | journal-article
  DOI: 10.1039/c7ob00530j

- **Specific and selective probes for Staphylococcus aureus from phage-displayed random peptide libraries**
  De Plano LM, Carnazza S, Messina GML, Rizzo MG, Marletta G, Guglielmino SPP.
  Colloids and Surfaces B: Biointerfaces 2017 | journal-article
  DOI: 10.1016/j.colsurfb.2017.05.081

- **Rapid detection of Pseudomonas aeruginosa by phage-capture system coupled with micro-Raman spectroscopy**
- Lentini G, Franco D, Fazio E, De Plano LM, Trusso S, Carnazza S, Neri F, Guglielmino SPP.
  Vibrational Spectroscopy 2016 | journal-article
  DOI: 10.1016/j.vibspec.2016.05.003

- **Phage-AgNPs complex as SERS probe for U937 cell identification**
  Lentini G, Fazio E, Calabrese F, De Plano LM, Puliafico M, Franco D, Nicolò MS, Carnazza S, Trusso S, Allegra A, Neri F, Musolino C, Guglielmino SPP.
  Biosensors and Bioelectronics 2015 | journal-article
  DOI: 10.1016/j.bios.2015.05.073

- **Phage-coated paramagnetic beads as selective and specific capture system for biosensor applications**
  Calabrese F, Carnazza S, De Plano LM, Lentina G, Franco D, Guglielmino SPP.
  Proceedings of the 2015 18th AISEM Annual Conference, AISEM 2015 2015 | conference-paper
  DOI: 10.1109/AISEM.2015.7066851

- **Progress toward the development of a lytic bacteriophages-based impedance microbiology for agro-food application**
  Mortari A, Lorenzelli L, Nicolò M, Guglielmino SPP, De Plano L.
  Lecture Notes in Electrical Engineering 2015 | book
  DOI: 10.1007/978-3-319-09617-9_15

Patents:

- Distretto Tecnologico Sicilia Micro e Nano Sistemi S.C.A.R.L. **"Conformational mimotopes for detecting specific antibodies"** (IT/28.11.16/ITA102016000120204). International patent application has been advanced No. PCT/IB2017/057422 Nov 27, 2017.
  Paper about the patent has been submitted at ACS Central science (under review):
  Innovative IgG Biomarkers based on Phage Display Microbial Amyloid Mimotope for State/Stage Diagnosis in Alzheimer's Disease
  De Plano LM, Carnazza S, Franco D, Rizzo MG, Conoci S, Petralia S, Nicoletti A, Zappia M, Campolo M, Esposito E, Cuzzocrea S. and Guglielmino SPP

Awards

- **First poster award CNS 2018 (National Sensors Conference)**
  M13 bacteriophages as bioreceptors in biosensor device
  De Plano LM, Franco D, Rizzo MG, Crea S, Messina GML, Marletta G, Guglielmino SPP
  21-23 February 2018
  University of Catania, Italy

GENERAL INTRODUCTION

Background

The public health costs and the proper allocation of resources are among the most important World's problems. World Health Organization estimates, those bloodstream infections affect more than 30 million people worldwide every year, potentially leading to 6 million deaths, and three out of every ten deaths, due to sepsis, are thought to be caused by resistant pathogens. This linked to the heterogeneity of cancer diseases, both *inter* and *intra* patient, are the major expenditure for the public health. However, the population ageing implies the increase of the neurodegenerative diseases, such as Alzheimer disease, consequently to the need of long-term cares. Therefore, the costs are predicted to increase continuously over the time due to for the necessity of targeted diagnosis and therapies. To reduce health costs, biotechnologies may play a pivotal role by introducing innovative systems cheap and efficient for diagnosis and therapies.

In this context, the phage display technology satisfies the possibility to study the vast diversity of protein–ligand interactions taking place in the nature. For such innovative systems, phage display technology can be exploited as a powerful tool for the research of new peptides, able to selectively bind to targets. As confirmation of the importance of this technology "to take control of molecular evolution and use it for purposes that bring the greatest benefit to humankind", Smith and Winter obtained a Nobel Prize for Chemistry in 2018. Principle of the technique relies on the ability to insert exogenous DNA fragments "in-frame" within one of the genes encoding for the capsid proteins of bacteriophage (also called phage). The expression of exogenous (poly)peptides on the surface of phage provided a physical link between phenotype (the displayed peptide) and genotype (the encoding DNA), and the formation of billion different phage clones, which formed the phage libraries. These large molecular landscapes represent very

powerful tool for "marker discovery" of target-binding proteins performed by screening cycle. In the past 30 years, phage display has undergone multiple advances showing enormous development both in the selection protocols (*in vitro* and more recently *in vivo*), and in the enlargement of target types (including, small molecules, inorganic materials, natural and biological polymers, nanostructures). The screened phages can be used as probes or bioactive molecules to receptor disease-specific, cell-specific or organ-specific peptides, cell epitopes, proteins agonist/antagonist.

The versatility of phages is determined from their shape, charge, robustness, resistance at acid and alkali as well as easy production. These characteristics make them applicable as “probes” in the development of biosensor, cellular imaging and label-free biosensor devises by self-assembling or chemical conjugation with nanomaterial, reducing cost of production and construction time at the same specificity compared to traditionally devises. Moreover, the third generation of drug delivery system has highlighted the possibility to use phage clones or only phage peptides in the drug-targeted delivery systems. Therapeutic ‘magic bullet’ ushers the era of modern ‘precision medicine’ research where targeted drug is delivered into specific target. The mainly use of these constructed in cancer therapy such as in chronic pathology has permitted to optimize the pharmaco-kinetic and pharmaco-dynamic and the dose dependence of the drugs of disease. Moreover, recent advances describe the use of phage display as novel bioactive molecules. This allow to produce new proteins and peptides able to minimize the use of antibodies, antibiotic and cancer drug and overcome the pharmaco-resistance, bringing at new drugs generation in different medical technological areas, including gene therapy, vaccine development and nanotechnology.

Aim of the Thesis

In the present work new biosensors and diagnostic/therapeutic systems based on phage display technology are designed and tuned. Furthermore, a new algorithm for the analysis of phage population peptides is introduced to identify of "self-navigating phage particles". New specific, selective and robust phage clones are use as probes for both diagnosis and targeted therapies of pathogen bacteria, such as *S. aureus, P. aeruginosa* and *E. coli*, cancer cells, associated to blood disorder (chronic lymphocytic leukemia and multiple myeloma), and misfolded Aβ-amyloid structure associated to AD. Finally, in vivo biodistribution in nude mice of phage display f8/9 library are performed to identify peptide home-tissue and home-tumor.

Outline of Thesis

- Chapter 1. Phage display technology and its applications are introduced;
- Chapter 2. "Whole-cells" of Staphylococcus aureus is used in four rounds of biopanning cycle to isolate target-specific peptides able to selectively bind bacteria surface. Selected phage clones, together to other phage clones previously selected against other pathogen agents, are used as probes in sensor-surfaces. Among the developed detection systems, magnetic beads functionalized with phages and coupled with Raman Spectroscopy have permitted to isolate/concentrate/identify bacteria in artificial infected blood, with an efficiency of 10 CFU/7mL.
- Chapter 3. An innovative "double binding" selection method is used to identify amyloid-like structures by interaction with IgGs. The discovered conformational peptides are able to discriminate sera of AD and healthy patients by E.L.I.S.A. Moreover, levels of identified IgG in AD patient show good correlation with the

progression of the pathology, making the phages biomarkers of state/stage in Alzheimer's disease (AD). Moreover, the phages permit inhibition and disaggregation *in vitro* of amyloid β42-induced cytotoxicity in SH-SY5Y cells.

- Chapter 4. "Promiscuous selection" against PBMCs and leukemia/myeloma cell lines is carried out to identify promiscuous peptides able to detect common marker of inter-specific leukemia/myeloma diseases. Therefore, the selected phages are used in one-step production fluorescent phage–probes with silicon nanoparticles or chemical fluorescents and applied in clinical test for diagnosis of chronic lymphocytic leukemia/multiple myeloma.
- Chapter 5. New concept of "self-navigating phage particles programmed" is introduced. Phage population deriving from selection *in vitro* against breast cancer cells is analyzed to highlight mosaic peptides based of CorMs and SLIMs. Moreover, bio-distributed landscape phage library f8/9 in nude mice harboring human breast cancer cell has allowed to study the pharmacokinetic of phage particles in the tissues and in tumor microenvironment.

CHAPTER 1
Phage display: Description and Applications

Phage display technology is a powerful research tool for high-throughput screening of protein interactions with the advantages of simplicity, high efficiency and low cost. This was in the first described by George P. Smith in 1985, which has demonstrated the display of foreign peptides on filamentous phages by the fusion of peptide of interest to N-terminal of gene III [Smith, 1985]. The expression of exogenous (poly) peptides on the surface of bacteriophage (also called phage) provided a physical link between phenotype (the displayed peptide) and genotype (the encoding DNA) [Smith, 1985]. Following Gregory P. Winter and Clackson, in 1991, exploited the phage display methodology to build large libraries of fully human antibody sequences for the treatment of diseases such as multiple sclerosis and cancer [Clackson et al., 1991]. Since then, a large number of phage displayed libraries have been constructed [Bass et al., 1990; McCafferty et al., 1990; Barbas et al. 1991; Smith, 1991; Smith and Scott, 1993; Petrenko et al., 1996; Hoogenboom 2002; Szardenings, 2003], leading to many peptides discoveries in the fields of cell biology, pharmacology, immunology, and drug discovery. The power of the *in vivo* phage display technique was in the first proposed by Pasqualini and Ruoslahti, which proposed the Ehrlich's 'magic bullet' concept for organ- and tumor-targeted drug delivery [Pasqualini and Ruoslahti, 1996; Ruoslahti, 2002; Teesalu et al., 2012]. However, most of the anticancer peptides were designed for exclusively target of one mono-cell type in the cancer complex or for cell of tumor vasculature [Shi et al., 2017]. Recently, Petrenko introduces the concept of 'migration selection' exploring intrinsic capacity of landscape phage display libraries to extravasare from the blood stream to the tumor tissue, migrate through the tumor microenvironment, invade into the tumor and penetrate into the target tumor cells

[Petrenko, 2017]. The collected phages find themselves a way to the tumor and their specific proteins resulted a mosaic of small binding units with expected tissue migrating propensity [Petrenko, 2017]. During 30 years long history the phage display has reaffirmed the power of the method resulting in the development of multiple display techniques need to satisfy the study the vast diversity of protein–ligand interactions taking place in the nature. Confirming the importance of this technology Smith and Winter obtained a Nobel Prize for Chemistry in 2018 for their pioneering works.

1.1 Filamentous Phages as Protein Display Vehicles

For definition, Phage display is a technique that uses bacteriophage, or so-called phage, to display a random molecular landscape. The most commonly phages used for the construction of phage display libraries are Ff filamentous phages (M13, f1 and fd) able to infect a Gram-negative bacteria. They show a high degree of homology [Lowman, 1997; Kehoe and Kay, 2005; Smith, 2011]:

I. Share 98.5% of DNA sequence and can tolerate insertions of foreign DNA up to 12,000 bp in the non essential regions without disrupting phage packaging;
II. Their genome can be isolated as single stranded and double stranded DNA for cloning and library construction;
III. The phage coat proteins can be modified to display foreign proteins without loss phage infectivity;
IV. Can to accumulate in high concentration in the infected bacterial cells due to non-lytic propagation.

These phages are F+ *Escherichia coli* strains. In fact, the coat protein pIII interacts with the receptor on the outer surface of bacteria F pili. The following contraction of the pili, due to do not understood sequences of events yet, lead to the bound of phage-pIII coat protein with secondary receptor, TolQRA, located in the inner membrane of Gram-

negative host. The phage transfers its viral genome inside the host cell involving in a chronic infection which is not kill host cells but slow the cell growth, due to stress in the production of phage particles. The single-stranded DNA helped from cytoplasmic enzymes of bacterium converts itself to double-stranded DNA known as replicative form (RF). The phage replicates as an episome producing more replicative forms and synthesizing more phage proteins, which are localized on integral inner membrane thanks leader sequences. When a critical pV concentration is reached, itself bind to the genome packing sequence and initiate virion assembly [Paschke, 2006; Sidhu, 2000; Newton and Deutscher, 2008]. The other viral coat proteins encapsulate the single stranded DNA during its secretion from the host cell. The lack of replication regulation and the ability of the episome to be transferred to daughter cells during cellular division allow the production of the first generation, about 1000 phage particles. This number decreases to 100 to 200 particles in the next generation [Hill and Stockley, 1996; Webster, 1996]. Together, high titer viral stocks ($\sim 10^{13}$) and the effortlessly purification are major factors for the success of the phage display platform. All three Ff phages are used for phage display technology; however, the M13 bacteriophage is the most chosen. Therefore, for simplicity, the successive sections will be limited to M13 phage.

1.2 Phage Capsid Structure and Chemical-Physic Properties

M13 phage consists in a rod of (6–7) nm in diameter and 900 nm long with cover a circular ssDNA [Stopar et al., 2003]. The 6407 nucleotides, which composed the ssDNA, encode 2700 copies of the major coat protein PVIII, distributed in the entire length, and five copies each of four different minor coat proteins (PIX, PVII, PVI, PIII) located at the ends (**Figure 1**).

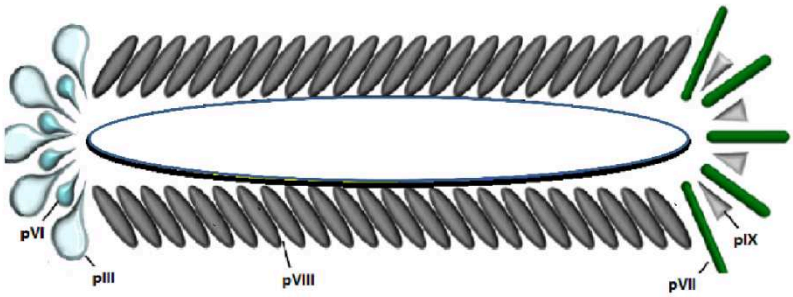

Figure 1. Structure of the phage M13. Phage M13 is a ssDNA virus infecting *E. coli* F+ strains.
The wild-type particle is approximately 900 nm long built from 2700 molecules of the major capsid protein, PVIII. The ends of the capsid rod are composed with minor capsid proteins, PIII, PVI, PVII, and PIX.

The major coat protein pVIII constitutes ~85% of the total virion mass; the ssDNA ~12%, and five copies for each of the minor coat proteins (pIII- pVI at one and pVII - pIX at the other end) restante 3% of the total virion mass [Hemminga et al., 2010; Morag et al., 2015]. The surface area of filamentous phages are about is 18700 nm^2 with number of charged residues at the surface of 8800 at pH 7.4 and charge density of 0.48 eq/nm [Zimmermann et al., 1986]. The capsid characteristic and conformation are mostly due to the major coat protein such as the chemical-physic properties. pVIII consists of primary sequence of 50 amino acids with molecular weight of about 5240 Da organized at α-helix. It can be divided into three distinct regions [Stopar et al., 2002]:

I. N-terminal composed by first 20 amino acids, is rich in acidic residues which give a low isoelectric point of the phage particle;
II. Central region composed by a 19 hydrophobic amino acidics which have structural support;
III. C-terminal composed by 11 amino acids rich in positive charges due to the lysines residues, neutralize the negatively charged viral ssDNA making.

The organization is sandwiched with a hydrophobic face inside and a hydrophilic face exposed outside of the phage particle, mostly stabilized of hydrophobic forces that can be solubilized by amphiphilic molecules. The hydrophobic parts of the pVIII protein

neighboring protein in the phage particles protect the inner part of the coat proteins and the DNA against the approach of hydrophilic solutes and macromolecules. Consequently, only the outer region of the phage is accessible to the external environment and gives the physicochemical properties at the entire phage structure. Zimmermann et al. showed that only the amino acids below residue in position 21° of the pVIII sequence are exposed to the aqueous solution and accessible to polyelectrolyte [Zimmermann et al., 1986]. Consequently, the four negative charges, in the N-terminal of the pVIII, located in 2°, 4°, 5° and 6° position, influenced the isoelectric point (pI) at acid value, theoretically calculated and experimentally confirmed as pH 4.2 [Zimmermann et al., 1986]. During the capsid formation, the pVIIIs interact to form pentamers, where the following pentamer is shifted 16.0/16.15 Å and twist between 33° and 36° compared to the next pentamer [Marvin et al., 1994; Papavoine et al., 1998]. Each subunit consists of a single curved, right-handed at an angle of ∼20° respect to the viral axis, with a C-terminal based on α-helix (residues 6–48), positively charged and directed on the interior to interact with the DNA (negatively charged), and a N-terminal based on type II β-turn (residues 1-5) which is instead exposed on the exterior of the phage particle. Each protein in the pentamer has axial and tangential interactions with 10 neighboring along the helical array defined (**Figure 2**).

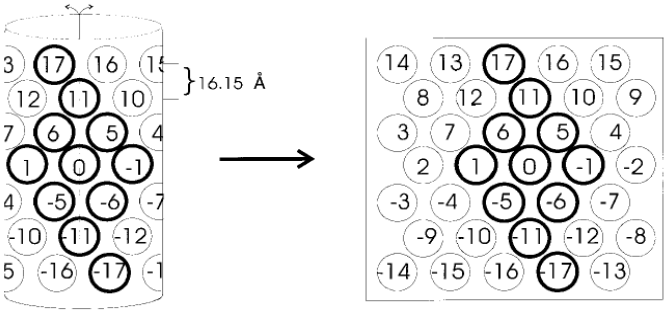

Figure 2. **Representation of the arrangement of the M13 coat proteins**. Starting from the protein "0" there are tangential interactions with 29 amino acids residues of the protein in position 11 and 5 with located proteins in position 17. The mentioned residues are directed in the interior of the phage and between them the phenylalanine amino residues in position 11 of the protein 17 with Phe42 and Phe45 residues on protein 0 giving integrity at the phage particle. All other residues, 41, 10 and 1 amino acid residues from proteins in position 6, 5 and 1 respectively, are directed outside of the phage. In particular, the Trp26 of protein 0 is in contact with Gly34, Ala35, Gly38, Ile39 and Phe42 of the protein 6. [picture comes from Stopar D et al., 2002].

Successively, Morag et al performed atomic-resolution structure of non-crystalline assembled of the M13 capsid model by magic angle spinning solid-state NMR, and made one 3D model deposited in the Protein Data Bank (PDB ID code 2MJZ) [Morag et al., 2015]. The model confirm that the first exposed five residues of each pVIII N-terminal are structurally unconstrained, making an optimal target for genetic engineering. In fact, this space can be filled with extra amino acids genetically added (up to 10 amino acids can be added) in the phage peptide display technology without significantly impairing the viability of the phage [Makowski et al., 1994].

However, look at accessibility of other coat proteins in the context of intact phage particle Endemann et al. showed that the most important coat proteins spaces are in middle and N- terminus of pIII (406 residues) and N-terminus of pVIII (50 residues), but pIX, is accessible in intact phage in N-terminus [Endemann and Model, 1995]. Moreover, some parts of pVI and pVII are able to take foreign peptide in C- and T – terminus, respectively [Smith and Petrenko, 1997; Sidhu, 2001] (**Table 1**).

Protein	Number of amino acids	Molecular weight	Copies per phage	Type of Display
P3	406	42500	~5	N or C
P6	112	12300	~5	C
P7	33	3600	~5	N
P8	50	5200	~2700	N or C
P9	32	3600	~5	N

Table 1. M13-based phage display alternatives.
Table shows the amino acid number addable for each coat phage proteins.

1.3 Types of Phage Libraries

The phage display constructs are classified in:

I. ***Monovalent*** when one or even fewer peptides displayed per phage particle advantageous when the goal is a high monovalent affinity of displayed peptides to the target;

II. ***Polyvalent (or multivalent)*** when the foreign peptide is fused to all copies of the protein present on the viral coat.

High and low densities of the exposed peptides are due to size of the peptide need to display. This in turn decides the library engineering in the arrangement of the coat protein genes [**Figure 3**, Smith and Petrenko, 1997]. In particular, in a "type 3" vector, only a single phage chromosome (genome) carrying to engineered gene III with "in-frame" with foreign DNA and the all other normal genes need to lead a progeny phage. It will encode a single type of pIII molecule displaying the peptide theoretically on all five pIII coat protein on virion. Similar is "type 8" for the engineering of the gene pVIII. However, only short hexogen peptides (≈ 8 amino acids) can displayed on all copy of coat proteins. In fact, if the foreign peptide is large, proteolytic enzymes in the host bacterium often remove the foreign peptide from most copies of proteins. Moreover, dramatically alteration of physical and biological properties of the virion's mass can interfere with the coat protein function in viral packaging and bacterial infectivity. In a type "33" or "88" vector, the phage genome carrying two genes of the some protein, one is recombinant (has a foreign DNA insert) and the other wild-type, as well as the other genomic code. The resulting virion comprised of both wild-type and recombinant pVIII molecules consist of a mosaic where the engineered forms usually predominate. This allows hybrid pVIII proteins with quite large foreign peptides to be displayed on the virion surface, overcome the limit of phage assembly cannot. A type "3+3" or "8+8" system differs from a type 33 or 88 systems because the two genes are on separate genomes. The wild-type protein version is on a phage (usually called the "helper" phage) which genome carry to all proteins need to give a virions particles, while the engineered protein version is on a plasmid called a "phagemid." The genome of the phagemid carries a "plasmid replication origin" that allows it to replicate in *E. coli* host, "filamentous phage replication origin", which is activates when the cell is co-infected with the helper phage and an "antibiotic resistance gene" that allows plasmid-bearing host cells to be selected. When a phagemid virion infects a cell, the cell acquires the

antibiotic resistance by the phagemid. However, it need that helper phage virion co-infects cell host, to produce progeny virions in the normal way. This lead at two types of secreted progeny virions: particles with helper phage DNA and particles with phagemid DNA both with a mosaic of recombinant and wild-type pVIII proteins on own coats. In monovalent or polyvalent forms, another difference there is in the use of pVIII or pIII (or other minor engineered protein) libraries, the avidity effect caused by the display valency. Only 3–5 copies of pIII per phage particle are present in the coat surfaces compared to the 2700 copies pVIII. Generally, this leads to significant differences in the affinity of the proteins or peptides that can be selected by pIII or pVIII display libraries to the same target. Relatively high affinity peptides and proteins can be isolated with dissociation constants (Kd) of 1–10 mM from pIII libraries, whereas pVIII-fused peptides tend to have lower affinity (Kd of 10–100 mM) due to higher number of the displayed peptides [Smith, 1991; Noren and Noren, 2001; Kay et al., 2001].

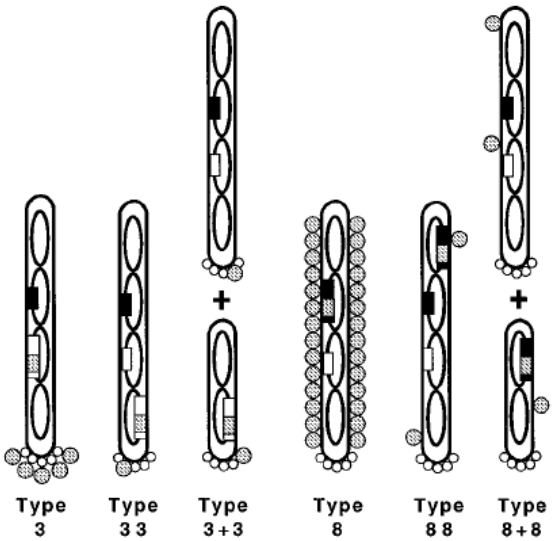

Figure 3. Types of phage display systems. The long vertical ovals represent phage virions, and the shorter vertical ovals represent the phagemid virions. The twisted line inside each virion represents the single-stranded viral DNA, the segments encoding coat proteins pVIII and pIII being designated by black and white boxes, respectively. The hatched segments within these boxes represent foreign coding sequences spliced into a coat-protein gene, and the hatched circles on the surface of the virions represent the foreign peptides specified by these foreign coding sequences. The five white circles at one tip of the virions represent the N-terminal domains of the five pIII molecules; foreign peptides displayed on pIII are either appended to the N-terminal domain (type 3 systems). In type 8 systems, the foreign peptide is displayed on all copies of the major coat protein pVIII (type 8 systems). [Picture comes from George P. Smith and Valery A. Petrenko, 1997].

1.4 Key Steps in Phage Display Technology

The key advantage of phage display is the possibility to identify target-binding proteins from a library of zillions of different random peptides without the need to screen each molecule individually. Phage display cycle can be divided in three steps: library creation, biopanning and selected clone analysis [Hoogenboom, 2005].

1.4.1 Library Creation

The process starts with library design, which could contain zillions of DNA clones harboring sequences of interest. In phage random peptide libraries, the DNA inserts derived from "degenerate" oligonucleotides, since 20 different natural amino acids exist, the number of different peptide sequences that can be obtained by randomizing N residues is 20^N. In the degenerate sequence is synthesized by adding an equal mixture of Adenine (A), Guanine (G), Cytosine (C) and Tyrosine (T) to a growing nucleotide chain assisted by incorporating only a mixture of guanine and thymine or guanine and cytosine in position three of the codons to enhance the formation homogenously distributing sequences. This strategy leads to the elimination of two of three stop-codons, while the remaining stop codon, TAG, can be suppressed by a supE *E. coli* strain used for phage propagation that contains genes for the corresponding tRNA, which eventually results in the incorporation of a glutamine residue at the position of the stop codon during translation, albeit with varying efficiency. The entire base sequence is an equimolar mixture of over a million different molecular species collectively encoding all possible residue peptides. A typical random peptide library has about a $10^{14} – 10^{19}$ different phage clones.

1.4.2 Biopanning

The selection of phage clones from randomized peptide libraries is a fundamental strategy for the development and identification of target specific ligands [Pande et al., 2010; Bakhshinejad et al.; 2016]. The screening cycle of phage display peptide libraries represent the platform need to reach specific binders to the target. This process consists of two steps, namely biopanning and amplification.

Biopanning involves following steps (**Figure 4**):

I. **Target choice**: it could be an organic or inorganic molecule; moreover, it is even possible to use tumor bearing animals for in vivo selection. Follow the targets immobilization that it can be by passive adsorption to a modified 96-well polystyrene microtiter plates or active functionalization on magnetic beads, or leaving the target free in buffer solution;

II. **Phage binding**: The naïve phage display random peptide library is incubated with the target and left to interact. It is important to start the first round with a large and highly diverse library for a better chance of isolating peptides of interest.

III. **Removing unbound phage**: the washes, need to delay the unbound-phage, are less stringent in the first round. However, the stringency of selection can be increased by more extensive washes in subsequent rounds to isolate phage with higher affinity. In fact, due to stability of the filamentous phage, at pH, ionic strength, denaturants, limited proteolysis or sonication can be used for non-specific elution of the target bound phage.

IV. **Phage elution**: the target bound phage can be obtained by acid solution, which carried out mix of free target and competing ligand.

After biopanning, the phage eluate is amplified in infecting bacterial cells to increase the number of only the phage that have bonded to target of interest clones at each round [Matochko et al., 2014]. This “secondary library” is used as input population for the

next round of biopanning. In order to restrict the selection to phage clones with greater avidity towards the target of interest, biopanning is repeated from three to six times. Finally, a step of extraction and subsequent analysis, by Sanger sequencing, of DNA is carried to identify the amino acid sequences of the foreign peptides displayed by the selected phage clones.

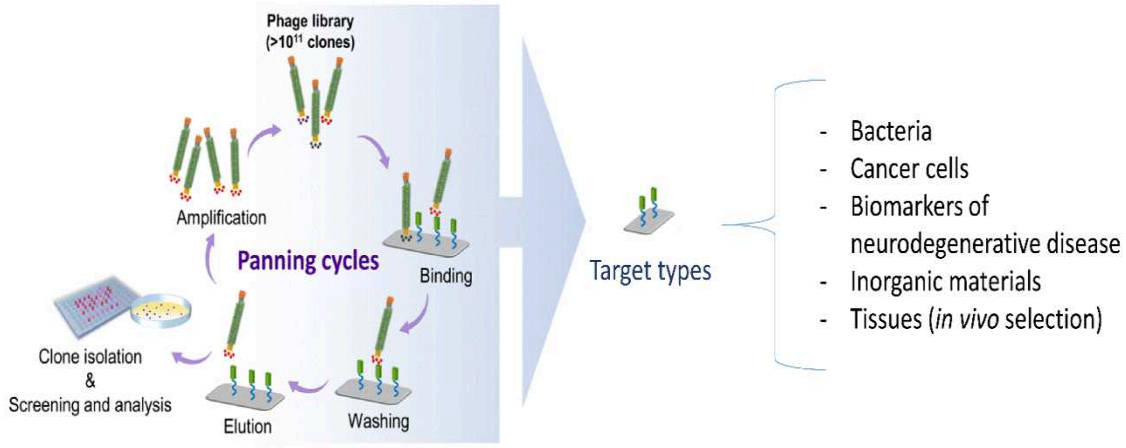

Figure 4. Schematic representation of biopanning cycle. Phage library is incubated with the target, then the phage unbound where washed and the phage bound the target where eluted. This cycle is replied for three, four time.

From the initial round of the selection can be expected less than 1 percent of the initially used library that bind to the target prior to extraction and amplification in E. coli. Considering an amplification factor of three for a selectively binding clone, the library would consist of 81% binding individuals after four cycles as illustrated in **Figure 5.**

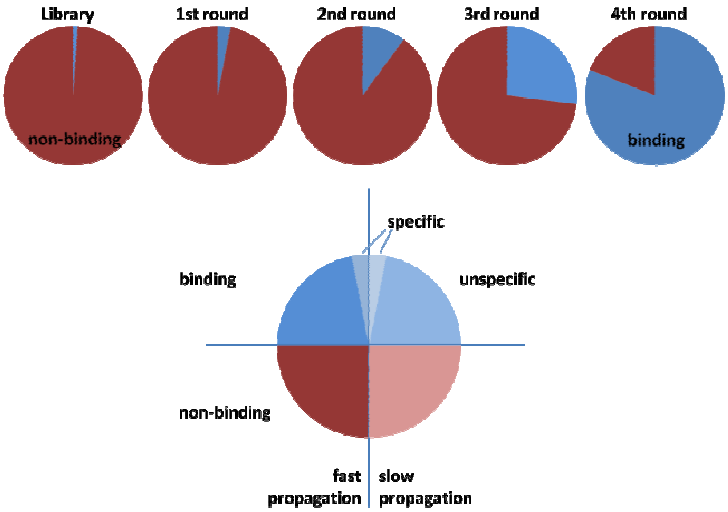

Figure 5. Enrichment phages by affinity selection up line. Schematic representation of the different type of phage respect to their target binding and evolutionary fitness.

The clones present in a library bind the target to three categories: non-binding, unspecific binding and specific binding all with high or less fitness. To decrease the unspecific binding phages, it is good to depress the phage display with a negative panning round against naïve molecules. The subsequent positive panning is then performed with a population that is depleted from unselective clones. However, the phages subpopulation amplification needs to expand the number of binding-target phage clones for each round, could be risk to compromise the diversity due to non linear propagation of the individual clones for the different fitness. Recently the advanced technologies have permitted to accelerate and improve the selection process. The next generation sequencing (NGS), which can to sequence millions of inserts in parallel [Bentley, 2006], was proposed as innovative molecular technology to deeply peptide phage display library after the first rounds of biopanning. In this way only one round could better to identify all the specific binding phage clones.

1.4.3 Selected phage clone analysis

A few hundred individual clones, from an eluate round of the selection, can be separated on “plaque lifts” and tested for ability to bind the receptor. Typically, standard selective tests are the so-called phage enzyme-linked immunosorbent assay (phage-E.L.I.S.A.), immune-screening and/or western blot, these can evaluate the affinity and specificity of individual clones or entire eluate populations after biopanning. Those save the cost of synthesis of peptides which may have been enriched due to artifacts in the screening process described above. Successively, to assure a reasonable significance, 50–100 phage clones should be sequenced and frequency of each amino acid and the distribution in the peptide fragments evaluated. All the data lead to identify the peptides ability and the contribution in the bound with targets of their amino acids. The find peptides can be “epitope”, that is the part of a ligand with which the receptor makes

specific contact, when show ability against the target. These epitopes will be "continuous," if the sequence motif in the selected peptides matches with the primary amino acid sequence of the natural ligand, or "discontinuous" when carry of critical binding residues that are distant in the primary sequence but close in the folded native conformation. Geysen and colleagues introduced for the first time the term "mimotope" to refer at small peptides that specifically bind a receptor's binding site without matching the natural epitope in the amino acid sequence, considering just cases of these "conformation-dependent" epitopes or where the natural ligand is non proteinaceous [Geysen et al.,1986]. Recently, start on the concept that 'elementary binding units' is usually formed of two /three amino, which are important to give function, it is possible to discern different motif inside of the short peptide sequences up 9-20 amino acids [Meszaros et al., 2009; Petrenko, 2017]. The phenomenon of "promiscuous peptides" is of two types: peptides recognizing distinct receptors in the same cells target, and peptides recognizing the same receptor overexpressed in different cells target. The first is based on the concept that multiple functions are associated with a single peptide structure. The peptides are like mosaic structure where are identified more 'elementary binding units' or motifs, which are assembled in the phage-displayed peptides during consecutive circles of affinity selection [Gross et al., 2016; Gillespie et al., 2016; Ruoslahti, 2017]. In the second cases the motif is common at more than target against it was performed the selection. Sometime it talk about receptor overexpress in tumor cells or ubiquitous in all the cells (Ruoslahti, 1996; Zou et al., 2012; Cardó-Vila et al., 2008].

1.5 Phage Applications

The phage display technology born for identification novel interacting protein-proteins. In this prospective, phage libraries is used to predicted the potential binding residues that involved in different conditions such as between: bacterial membrane transport

proteins; intracellular interactions of distinct protein domains (molecular mapping) [Fack et al., 1997; Caberoy et al., 2010]; to map epitope involved in specific interaction receptor/antibody or receptor/intrabody [Bratkovic, 2010]. In enzymology, phage display is used to develop modulators positive or negative of both the active and allosteric sites of the enzyme or for structure and function of receptors. Moreover, due to that filamentous phage is resistant to broad range of proteases; it is used in identification of substrates of various proteases [Lehmann, 2008; Hiraga et al., 2009]. Recently, phage display is applied in the identification of protein and/or amino acid involved in the interaction with inorganic materials [Chen and Rosi, 2016]. The versatility of phages is determined by their shape, charge, robustness, selective modification [Chung et al., 2014], resistance to heat and to many organic solvent [Royston et al., 2006; Bruckman et al., 2008; Brigati et al., 2004] acid and alkali as well as a low-cost production [Petrenko and Smith, 2000; Petrenko and Vodyanoy, 2003]. Specific phages could be used in different forms. Therefore, phage has been applied in a several fields such as biosensing [Lee at al., 2013], cellular imaging [Cochran and Cochran, 2010], vaccine development [Aghebati-Maleki et al., 2016] and drug and gene delivery [Sioud, 2019]. Moreover, recent advances describe the use of phage display in the discovery of novel bioactive molecules to produce proteins and peptides able to minimize the use of antibodies, antibiotic and cancer drug.

1.5.1 Phage in Biosensor

1.5.1.1 Biosensor composition

Nowadays biosensors have a several range of applications that aim to improve the quality of life. Biosensors are ubiquitous in applications such as monitoring of treatment and disease progression, detection of pollutants, food and environmental control, disease-causing microorganisms and markers that are indicators of a disease in bodily

fluids (blood, urine, saliva, sweat) and many more. A biosensor is a smart device that measures biological or chemical reactions by generating signals proportional to the concentration of an analyte in the reaction.

Traditional biosensor consists in the following components (**Figure 6)**:

I. **Analyte**: Substance of interest that needs detection;

II. **Bioprobe**: Molecule able to recognize the analyte. The most molecules used, as bioreceptor or bio-probe, are enzymes, cells, aptamers, deoxyribonucleic acid (DNA) and antibodies. The interaction between analyte and bioreceptor generates a signal in the form of light, heat, pH, charge or mass change, etc. defined as bio-recognition;

III. **Transducer**: The transducer is an element that converts one form of energy into another. The role of the transducer is "energy converter", i.e. converts the bio-recognition event into a measurable signal in a process known as signalization. The produced signals are usually proportional to the amount of analyte–bioreceptor interactions**;**

IV. **Electronics:** It consists of complex electronic circuitry that converts the signals from analogue into the digital form. Then the processed signal is quantified by the display unit of the biosensor that generates the output such as numeric, graphic, tabular or an image, depending on the requirements of the end user.

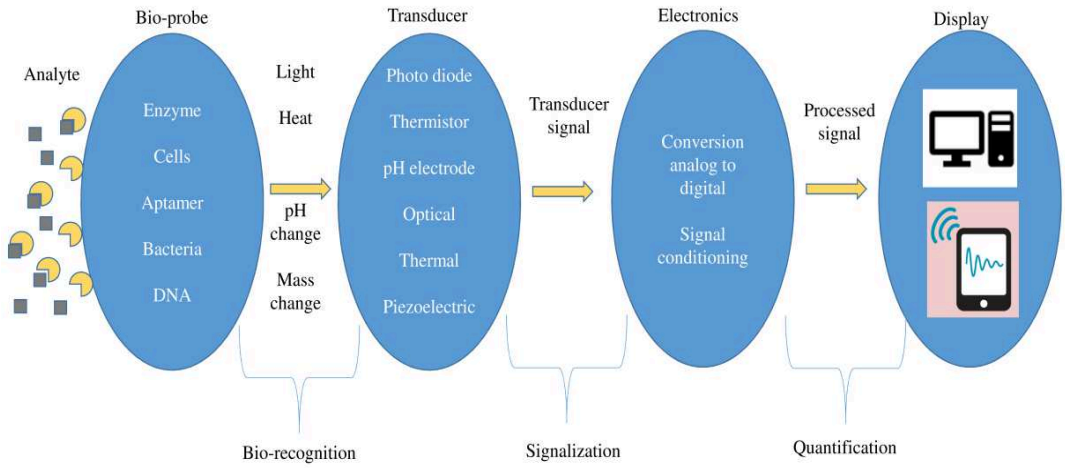

Figure 6: Schematic representation of the biosensor composition.

1.5.1.2 Bioprobes

Selectivity is perhaps the most important feature of a biosensor. This is due to the ability of a bioprobe to specifically detect an analyte in a sample containing other contaminants. Antibody-based systems represent the gold standard in biosensors. However, in the last decade, novel affinity reagents are showed to substitute antibodies in biosensors, in particular, synthetic aptamers or peptide, oligonucleotide, microRNA, polysaccharide. The necessity to find a substituted biomolecules is essential for the development of commercially viable biosensors cheaper and more stable then antibodies based assay. In this context, several studies employed phage clones like a better alternative of classic and modern bio-probes like traditional and/or new bio-probe for several advantages such as:

I. Multiple target-binding sites in one bioactive molecule, which increases avidity in specific target bond;
II. Massive generation of progeny phages, due to their short replication time;
III. Ability at tolerance critical conditions like organic solvents and large range of pH and temperature;

IV. The ductility of the phage making its suitable to a wide range of transduction systems, including electrochemical, optical and acoustic-sensitive sensors, lateral flow systems or integrate micro-fabrications.

1.5.1.3 Transducer

Guided micro-Raman Spectroscopy. Noninvasive and label-free vibrational spectroscopy and microscopy methods have shown great potential for clinical diagnosis applications. Spectroscopy is an analytical technique for the study of the interaction between an electromagnetic radiation and atoms or molecules. When a photon collides with a molecule, its energy can be unaltered and keep same frequency (elastic or Rayleigh scattering) or, otherwise, be transferred to or from the same molecule, causing a variation in the frequency of the incident photon (inelastic or Raman scattering). On the latter phenomenon is based Raman scattering, for which the difference in energy between the incident and scattered photons corresponds to the energy of the molecular vibration [Wachsmann-Hogiu et al., 2009] and can be associated with the vibration of a particular chemical bond (or a single functional group) in the molecule [Choo-Smith et al., 2002]. Due to its immediacy, convenience and easy-to-use, Raman spectrometry is increasingly considered in the development of diagnostic applications, label-free and alternatives to imaging fluorescence. However, practical uses of Raman spectroscopy is strongly limited by scattering signal [Qian and Nie, 2008] and the richness of information, often representing a noise for the correct analysis of the sample, especially in complex and highly variable systems, such as cellular ones. Surface-enhanced Raman scattering (SERS) allows to exceed these limits by exploiting the giant electromagnetic field enhancement from noble metal nanostructures to localize surface plasmon resonances and to obtain an enhancement of Raman signal [Le Ru et al., 2007; 2009]. In this context, an increasingly common approach is the controlled assembly of bio-hybrid

nanostructured materials, consisting in metal nanoparticles (NPs), and a probe, such as antibody, peptide or increasingly common phage, to guide the detection to the target of interest. In this case, an enhancement signal of the target of interest alone can be obtained from a dry sample (for example fixed biological samples) or in a prospective optical SERS sensor for biomolecular detection in liquid (in LIQUId SERS sensOR, or simple LIQUISOR) [Fazio et al., 2016].

Guided Fluorescence imaging. Another application based on biohybrid structures is fluorescence. In fact, fluorescence remains one of most diffused diagnostic tools, because extremely versatile and continuously improved by new emerging techniques. For this reason in recent years, the increasing availability of fluorescent dyes has directed researchers to development of non-invasive methodologies in diagnostic imaging field. Among them, various nanotechnology platforms have been developed to allow the simultaneous real-time evaluation of a broad range of disease markers by non-invasive techniques [Riehemann et al., 2009]. Semiconductor nanocrystals and nanoparticles with dimensions in the order of nanometers can have peculiar optical and electronic properties, such as tunable emission in visible range, high levels of brightness and photostability [Chan et al., 2002]. These nanostructures, when illuminated by UV light, can undergo to transition of an electron to a state of higher energy, from the valence to the conductance band. The return back of the electron to the valence band involves a releasing of its energy by the emission of light or photoluminescence. Respects to conventional organic fluorophores, inorganic nanoparticles have longer fluorescence lifetime, photostability and high resistance to metabolic degradation [Walling et al., 2002]. However, the potential toxicity of some semiconductor nanocrystals due to their chemical composition (i.e. cadmium, selenium or other heavy metal ions) limited the use in biological applications [Derfus et al., 2004]. In this

contest, biocompatible and fluorescent silica-based nanoparticles (SiNPs) have the potential to permit fluorescence imaging techniques of real-time and non-invasive visualization of biological events in vivo and in vitro test. Despite these advantages, conventional approaches for the preparation of SiNPs functionalized with biological molecules involve appropriate technique for surface modification and consequently onset of impurities in the final preparation and lost of the activities of biological molecules. In opposition, pulsed laser ablation in liquids (PLAL), widely used for the fabrication of metal NPs of different composition, morphology and size without generating external impurities [Rao et al., 2014], has been considered as a successful method for the conjugation of pure NPs with various conjugated biomolecules such as proteins, peptides and oligonucleotides [Bagga et al., 2013].

1.5.2 Phage in Therapeutic Applications

One of the dominant problems in modern pharmacology is to find drugs that act directly on the target disease and have minimal toxicity on healthy tissues, organs and cells. Recently, research groups use phage display technology in medical science, to find innovative drugs. The standard use of the phage display in therapy application is the identification of bioactive molecules. Peptide agonists and antagonists for receptors, characterization of new protein/peptide-DNA interactive [Bratkovic, 2010; Liu et al., 2014], protein functional against epitopes [Marino et al., 2009], [Pande et al., 2010; Soendergaard et al., 2011; Wang et al., 2012] are the standard phage-peptide drug application. Several papers report that the number of patent applications involving peptide-related technology has grown in the last decades, a large part of them initially derived by screening of a peptide-displaying phage library [Nixon et al., 2014]. In particular, the actually approved and commercialized peptides discover by phage display technology are described below. Adalimumab (Humira®; AbbVie Inc., formerly

Abbott Laboratories, North Chicago, IL), the first antibody obtained with this methodology, is a human IgGκ antibody that binds tumor necrosis factor (TNF) and blocks activation of TNF receptors approved for treatment of psoriasis, inflammatory bowel and rheumatoid arthritis diseases in 2002 [Nixon et al., 2014]. Ranibizumab (Lucentis®; Genentech) is an antigen-binding fragment (Fab) and neutralizes the activity of vascular endothelial growth factor A (VEGF-A), approved for the treatment of wet age-related macular edema in 2006 [Demidova-Rice et al., 2012]. The first marketed peptibody has been Romiplostim (Nplate®; Amgen) in 2008, like agonist of the thrombopoietin receptor, for the treatment of immune thrombocytopenic purpura [Bussel et al., 2006]. Ecallantide (Kalbitor ®; Dyax Corp., Burlington, MA) approved in 2009 as potent inhibitors of human plasma kallikrein for the treatment of acute hereditary angioedema (HAE) [Stolz et al., 2010]. Belimumab (Benlysta®; GlaxoSmithKline, London, UK) is a human IgG1λ binds the soluble form of human B-lymphocyte stimulator (BLyS), preventing its interaction with its receptors, approved in 2011 for the treatment of systemic lupus erythematosus (SLE) [Stohl, 2012]. Raxibacumab (GlaxoSmithKline, London, UK) is a human monoclonal IgG1λ antibody approved for the treatment and prevention of inhaled anthrax in 2012 [Huang et al., 2012]. More others are in clinical trial phases but still not on the market.

Moreover, based on the “magic bullet concept” by Paul Ehrlich [Strebhardt and Ullrich, 2008; Bertrand et al., 2014; Vigevani and Valcarcel, 2014], the phage display technology exploits peptides specify for drugs delivery to the desired location ensuring interaction between a drug and the target [Nemudraya et al., 2015]. Several nanocarriers have utilized peptides for targeted drug delivery systems like liposomes, micelles, polymers, nanoparticles and stem cells [Blanco et al.; 2011; Wang et al., 2012; Cao et al., 2014 B]. Moreover, chemical drugs can be conjugated on phage surface by chemical modification or gene drugs can also be inserted into the genome of phage by

recombinant DNA technology [Ju and Sun, 2017]. Today, the fast development of the research led to commercialization or in late-stage clinical trials of phage display-derived antibody and peptides for various diseases such as autoimmune and inflammatory diseases, cancer, metabolic and allergic disorders.

1.5.2.1 Phage library *in vivo* bio distribution

There are many knowledges about the peptides able to recognize a range of different human antigens, including cell surface-expressed tumor antigens thanks to phage libraries *in vitro* selection against purified antigens or whole tumor cells. However, the clinical application of these tumor-specific peptides depends on their ability to target tumor *in vivo*. Numerous studies have failed to demonstrate a correlation between the *in vitro* binding characteristics of antibodies and the *in vivo* tumor targeting properties. Consequently *in vivo* panning represents a significant new application of phage display technology, may allow the identification of peptides that recognize biologically relevant tumor targets. The successful of applications in *in vivo* panning for the isolation of specific-tumor peptides needs mainly understanding of the pharmacokinetics of phage display landscape libraries. This includes phage bio-distribution in the tissues, clearance from the circulation and extravasation capacity for in the interstitial compartments by optimization of incubation times, phage extraction and propagation procedures. Consequently, the peptides that home to a desired antigen/organ can be identify. As described in the previously chapters, the conventional biopanning cycle is based of several rounds, where the amplification of the bound phage is performed. However, the latter step could enriched the phages that do not necessarily explain the most bound-ability but are faster in the amplification. This condition is increased in *in vivo* selection due to the necessity to extract phages maintaining the infectivity. The use of the advance of next generation sequencing (NGS) able to sequence millions of inserts in

parallel [Bentley, 2006; 2008; Margulies et al.., 2005], overcomes the problem permitting both DNA quantification and peptides sequences detection contextually.

1.5.2.2 Next Generation Sequencing (NGS)

Next generation sequencing (NGS) is considered the parallel sequencing of massive DNA sequences. This revolutionary technique has permit to sequence entire human genome in a single day, at the contrast, of the previous Sanger sequencing technology, which has required over a decade foe the same purpose. The conventional use of NGS in clinical application permits to improve patient care of insertions and deletions of DNA, small base changes (substitutions), large genomic deletions of exons or whole genes and rearrangements such as inversions and translocations. Moreover, NGS in microbiology is substituted at conventional method morphology, staining properties and metabolic criteria with a genomic definition of pathogens. The successive bioinformatics analyses are used to elaborate the wide volume of data by mapping the individual reads to the human reference genome. in the phage display context, in tandem qPCR, for DNA detection, and sequencing by NGS, for sequences knowledge, represent a new gold standard for phage display selection thanks to accuracy, running time, diversity coverage, and cost-effectiveness [Dias-Neto et al., 2009]. Is has been demonstrated that NGS can already found after one round of selection the some positive peptides generally selected after several round of selection using traditional method of sequencing, identifying itself as a good alternative fast, accurate and relatively low cost [’t Hoen et al., 2012; Yang et al., 2017].

CHAPTER 2
Biosensor for Rapid Detection of Pathogenic Agents

Infectious diseases, due to their high mortality risk, are the main problematic for community health and subsequent care. In addition, the rapidly increasing of antibiotic resistant strains [Richter et al., 2018], coupled to spread allogeneic strains, favored by the increase in trade and tourist travel, makes very difficult the control and monitoring of the possible contamination.

Blood infection, so-called sepsis, is a systemic inflammatory response, characterized of the presence and persistence of microorganisms in the bloodstream [Polat et al., 2017]. More of 96 microorganisms, including bacteria, viruses, parasites or fungi, can be involved in blood lethal infections. Among them, *Staphylococcus aureus*, *Pseudomonas aeruginosa* and *Escherichia coli strains* the most have been found to be the most frequent.

Regardless of the type of detection tools, one of the most encountered problems is the recognition and isolation of the pathogenic agent, especially when it is present at low concentration. Therefore, rapid, selective and sensitive system tools for the detection and recognition of pathogens are highly demanded in environmental monitoring (infection prevention), clinic diagnosis and disease control to prevent disease progression and to reduce complications that can be serious. The isolation of the few number of the bacteria (1-10 colony forming units, CFU) from a large volume of the water, beverages or blood samples (10-100 mL) represents the arduous problem of the strains identification for which the standard procedures required days of incubation to allow the bacteria growth. Indeed, the gold standard used is culture system, which allows detecting the presence of the bacterium by grown on the agar plates, following by genotypic and phenotypic assays to its specific identify. However, these procedures

are time consuming and led the results after several days or weeks [Braga et al., 2013]. Recently, molecular techniques, such as real-time polymerase chain reaction [Tatavarthy and Cannons, 2010] are entered in diagnostic assay but, though more faster, their use is limited because the often not efficient isolation of microbial DNA from high concentration of blood cells, can left inhibitor that make difficult the DNA polymerase reaction.

Phage display can be used to find probes that selectively bind bacteria targets of infection, more ductile and resistant then antibodies or other standard probes (such as aptamers, olygomers, DNA/RNA molecules) and able to be functionalized on several sensor-surfaces for different detection systems.

As described in the previous chapter, a biosensor consists in three main components: probe, platform (on which the probe is allocated) and detection system (transducing the bound between probes and analyte in signal).

In this prospective, the chapter describes several approaches of bacteria detection using phage as bio-probe coupled on several platforms. In particular:

- Firstly, phage clones were selected using biopanning cycle against "whole-cell" of bacteria target in four rounds, in order to isolate target-specific peptides able to selectively bind cells surface;
- Afterward, selected clones were used in the functionalization of several sensor-surfaces by physisorption of charged materials, which mica, APTES and PEI, and gold nano-particle, and by covalent bound with latex and magnetic beads. Then the phage/target complexes were identified by appropriate detection systems;
- Finally, a proof-of-concept of innovative clinical diagnostic system was proposed coupling phage-magnetic-separation with Raman spectroscopy.

Moreover, a new therapeutic approach is developed by using phage as both detection-probes and anti-bacterial molecule. A short hint was made at phage biological activity found, as antibacterial and anti-biofilm, in *in vitro* tests against *P. aeruginosa*.

2.1 "Whole-cells" biopanning against *Staphylococcus aureus*

M13 pVIII-9aa Phage Display random peptide Library was used to affinity selection of peptides capable of specific binding to "whole-cell" *S. aureus* ATCC 29213 [De Plano et al., 2017]. The selection procedure provided the interaction in suspension of phage clones library with *S. aureus*, in order to do not block the interacting molecules in a forced form. In this way, the natural conformation of the bacteria was maintained. After the fourth rounds, thirty phage clones were individual randomly selected and their DNA sequenced to determine the peptide sequences displayed in their engineered major coat protein (**Table 1**).

Phage clone ID	Motif sequence	Frequency
St.au9IVS1	RVRSSPVVQ	1
St.au9IVS2	RVRSIPHVA	1
St.au9IVS3	RVRSYSPHL	6
St.au9IVS4	RVRSNAASM	3
St.au9IVS5	RVRSAPSSS	17
Consensus by MEME server	RVRS-P-S-	

Table 1. Peptide sequence, displaying on the major coat protein of the engineered phage isolated of the phage display selection against *S. aureus* ATCC 29213.

The motif based on the four amino acids RVRS was present with a high frequency, suggesting that the group was essential for the recognition of bacterium target. The amino acids more represented were the hydrophilic amino acid serine (S) in the 4 and 7 positions, the basic amino acid arginine (R) in 1 and 3 positions, the hydrophobic amino acids valine (V) in the 2 positions, and alanine (A) in the 5 position. Due to the most representative and significant similarity with consensus sequences, the phage clone named St.au9IVS5 was chosen to estimate the specificity and selectivity interaction to bacterium target by E.L.I.S.A. affinity assay. The selected St.au9IVS5 clone was found

to interact more efficiently (roughly a factor 4) with the selection target, *S. aureus*, than to each of the others tested bacteria, both gram positive and gram negative (**Figure 1**).

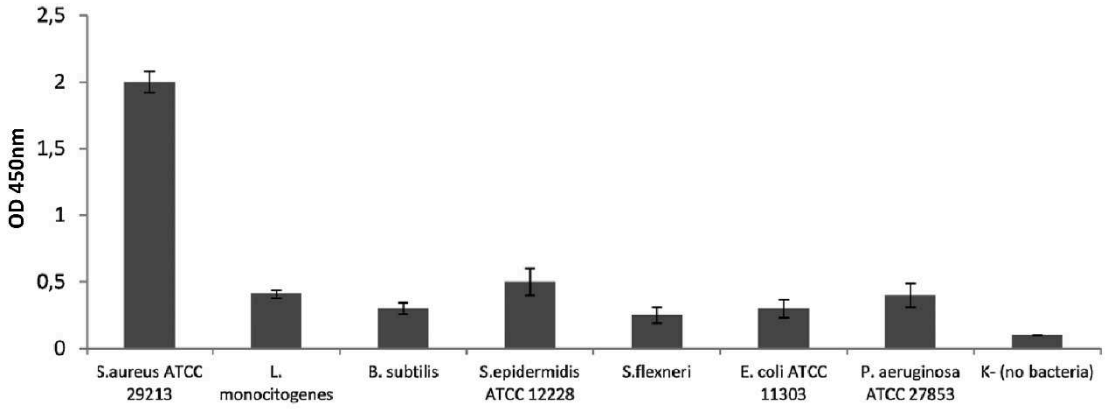

Figure 1. Specificity of St.au9IVS5 phage as determined by E.L.I.S.A. The ability of clone St.au9IVS5 to preferentially interact with the selection target (*S. aureus*) was compared to other potential targets, including Gram-positives bacteria as *S. epidermidis, L. monocytogenes, B. subtilis*, and Gram-negatives bacteria as *Escherichia coli* ATCC 11303, *P. aeruginosa, S. flexneri*. Mean OD_{450} is the average of three separate tests with multiple cultures. Error bars indicate standard deviations. Paired t-test indicates a significant difference ($P < 0.0001$) for St.au9IVS5 binding to *S. aureus* with reference to all the other challenge bacteria.

In addition, St.au9IVS5 binding capacity was evaluated against 9 clinical *S. aureus* isolates strains, including a methicillin-resistant *S. aureus* (MRSA) strain (**Figure 2**). E.L.I.S.A. assay confirmed that the St.au9IVS5 was the most specific and selective phage clone for all tested *S. aureus* strains, including the MRSA strain.

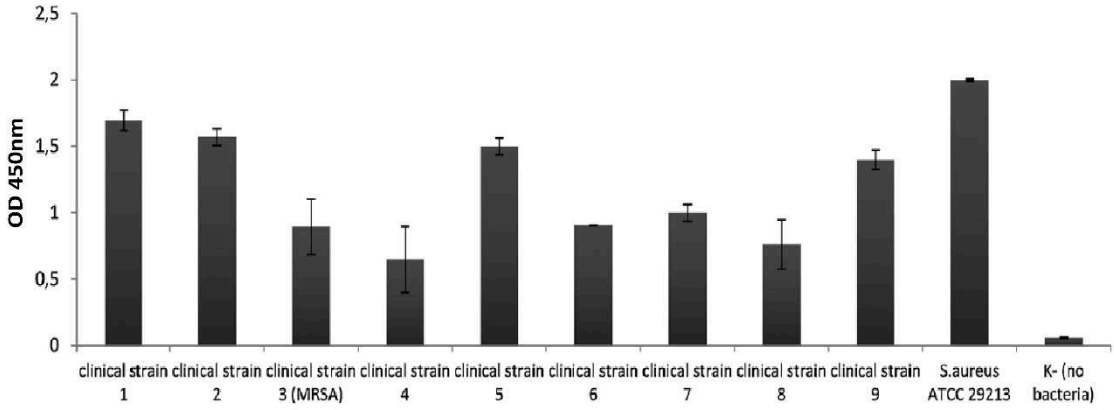

Figure 2. St.au9IVS5 phage capacity to detect clinical *S. aureus* isolates determined by E.L.I.S.A. Mean OD_{450} is the average of three separate experiments with multiple cultures. Error bars indicate standard deviations.

Western blot analysis revealed that St.au9IVS5 bound a protein with a mobility band of about 78 kDa, confirming its selective and specific binding to *S. aureus* cell surface (**Figure 3**).

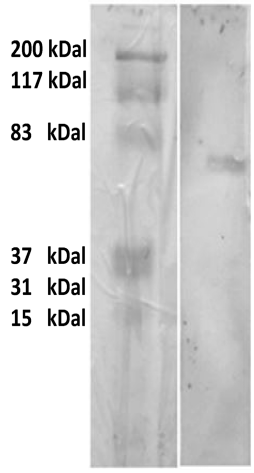

Figure 3. Western blot analysis with the selected phage-displayed clone. Proteins isolated from *S. aureus* ATCC29213 strain were separated by SDS-PAGE and blotted onto nitrocellulose membranes. The membrane was explored with phage clone St.au9IVS5. SDS-PAGE broad-range pre-stained markers were used (Bio Rad, MW indicated in kDa).

Probably, this band was associated at a specific cell-division membrane protein of *S. aureus*, as demonstrated by absence of reactivity against both other gram positive and gram negative bacteria [Nandakumar et al., 2005].

To evaluate the times of interaction between phage clone and its bacterium target, a kinetic phage-E.L.I.S.A assay was performed (**Figure 4**). St.au9IVS5 showed the initial bound at 15' which increased during the incubation time [De Plano et al., 2019].

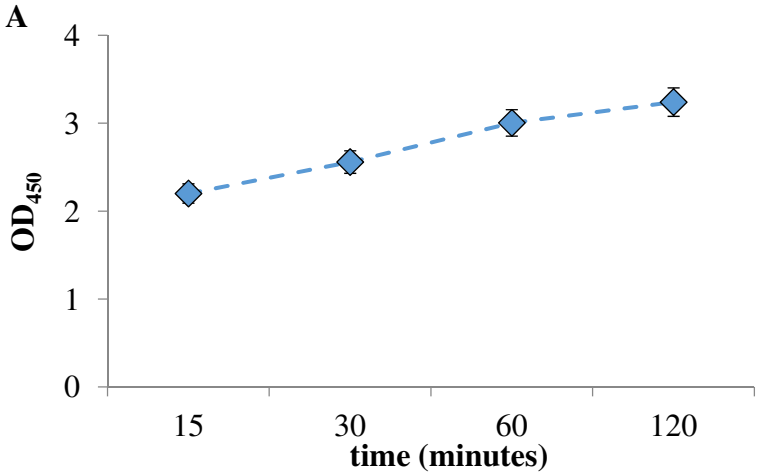

Figure 4. Kinetic phage-capture E.L.I.S.A. between St.au9IVS5 against *S.aureus* ATCC 29213. The test was conducted at four different times15', 30', 60' and 120' at 37 °C with shaking. The Mean OD_{450} is the average of three separate tests with multiple cultures. Error bars indicate standard deviations.

2.2 Phages functionalization of platforms for sensors

The selected phage clone St.9IVS5, specific in the recognition of *S. aureus,* was used in the functionalization of several sensor-surfaces. Approaches were extended to other phage clones, namely P9b and Li5, previously selected [Carnazza et al., 2008 ; De Plano et al., 2019] for their ability to identify *P. aeruginosa* and *E. coli,* respectively. All phage clones were used as "bacteria-binding probe" for detection tools.

2.2.1 Phage-Physisorption on polymeric surfaces

It is known that M13 capsid structure is responsible for the great resistance of phage when exposed to various physical and chemical stresses (i.e. heat, both acidic or alkaline organic solvents, and variations in pH values). Moreover, the major coat protein, pVIII, influences the isoelectric point (pI) of the whole charge expressed on the capsid at pH 3.94/4.2 [Zimmermann et al., 1986]. Therefore, the phage clones, displaying foreign peptide "in frame" to the wild-type amino acids sequences of pVIII, shifted the pI at a different values.

Indeed, theoretical pI values, predicted by protein calculator v3.4, for the peptide sequences exposed on the surfaces of St.au9IVS5 and P9b phage clone were and 4.87, 6.3, respectively (**Table 2**).

	wild-type vector pC89	**St.au9IVS5**	**P9b**
pH7	-3	-1	-0.1
pI	Neutral (pH: 3.92)	Neutral (pH: 4.87)	Neutral (pH:6.3)
pH 9	-4.1	-2.2	-1.7

Table 2. Theoretical pI value and charges exposed at pH 7 and 9 of the exposed N-terminal pVIII of the wild-type phage and the phage clones by ExPASy tool.

To evaluate the effect of different pI on physisorption, wild-type vector pC89 (without foreign peptide), P9b and St.au9IVS5 were used for functionalization in charged, PEI and APTES, and no-charged, mica, surfaces. Due to their pI, at pH 7 charge exposed on surface of wild-type vector pC89, P9b and St.au9IVS5 resulted -3, -0.1 and -1,

respectively. Otherwise, at pH 9 charge exposed on surface of wild-type vector pC89, P9b and St.au9IVS5 resulted -4.1, -2.1 and -1.7, respectively.

The performed test-matrices aimed to verify the different behavior of the phage clones, due to their peptides exposed, during the functionalization according to pH, buffer solution and the characteristics of surface (**Figure 5**).

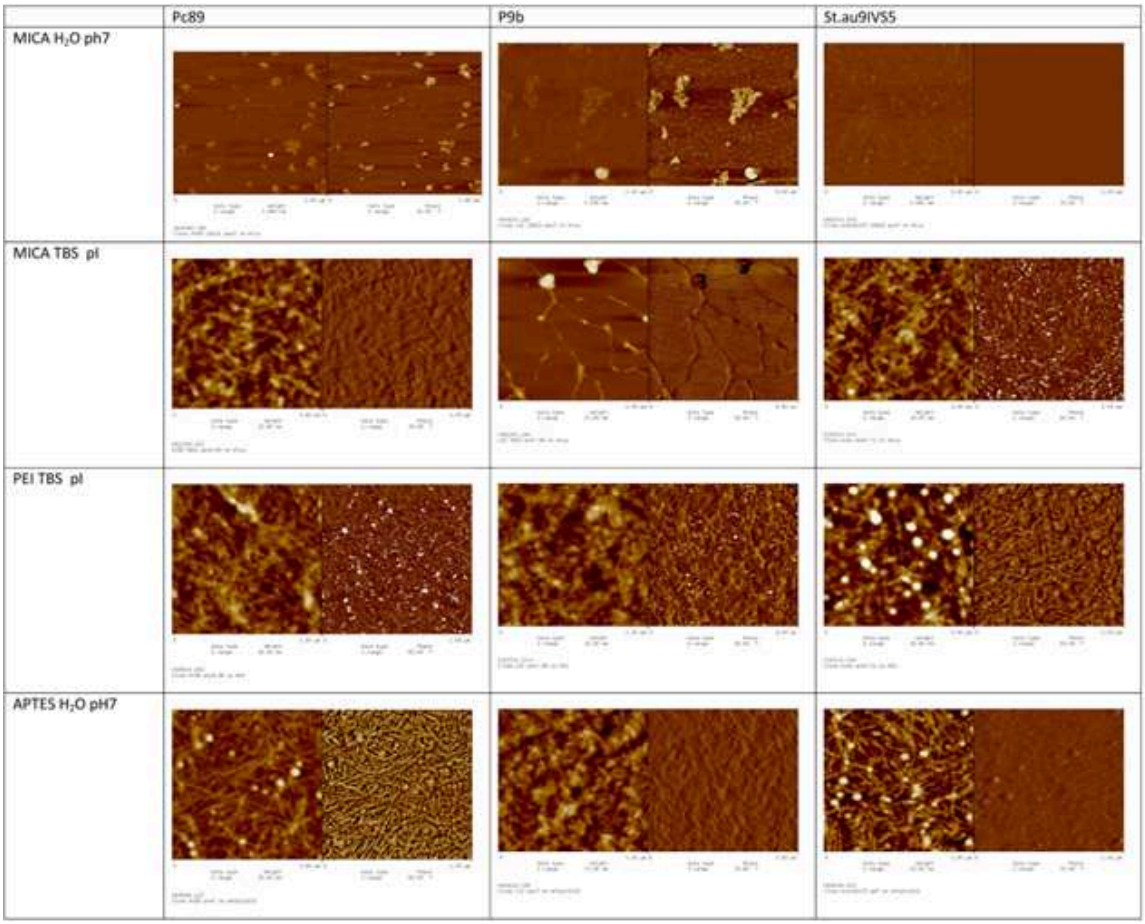

Figure 5. **AFM images of wild-type vector pC89, P9b and St.au9IVS5** on mica in H2O at pH 7 (the first line), mica in Tris-buffered saline (TBS) buffer at pI (the second line), PEI in TBS buffer at pI (the third line), APTES in H2O at pH 7 (the last line).

On mica surface in deionized water pH 7 only few bubbles for wild-type vector pC89 was observed, like St.au9IVS5 which poor sporadic adhesion showed. Instead, P9b phage clone showed an adhesion in insula disposition at pH 7, condition in which its charge was near at neutrality. The repulsion between phage clones and mica surface was attributable to electrostatic effects, mica had a surface with negative potential in turn, the phages at pH 7 exposed negative charges, consequently never electrostatic

interaction flocked. When the phage clones were in TBS pI buffer the ions present influenced the wild-type vector pC89, which covered whole surface; likewise St.au9IVS5 phage clone had a similar behavior; however, a better arrangement was observed along the surface. Differently, P9b phage clone, at pH corresponding to pI, showed sporadic adhesion in thin phage bundles elongated on the mica surface. Probably the peptide played an significant role in the stabilization of salt–bridge, which was highly dependent upon factors such as the cost of desolvating the charged groups and the relative flexibility of the side chains involved in the ion pair. Moreover, the acid pH at pI for wild-type vector pC89 and St.au9IVS5 led to the formation of reactive ions species into the TBS buffer (in particular Na^+ and H^+) which could interact with phage surfaces to stabilize salt–bridge with the surfaces. This condition did not occur in the pI of P9b, which was 6.3 near the neutrality of the buffer. In the same way, the surfaces stratified with positive polymers, namely APTES and PEI, had been exploited. Wild-type vector pC89 in deionized water pH 7 was strongly attracted of the positive surfaces permitting the multi-stratification of the phage on the surfaces. However, in TBS pI, the present Na^+ ions covered phage surface and reduced the interaction with the positive charges exposed on surface leading better stratification. St.au9IVS5 clone had a better distribution in salts presence (TBS pI) compared to deionized water pH7 where the phage clone was conditioned in the self-assembling only for its negative charges exposed. About P9b phage clone, which surface charge was neutral at pI and even closer to the neutrality at pH7, the immobilization on positive surfaces produced the formation of highly reticulated phage-networks roughly covering the whole substrates. TBS at pI permitted an organized stratification of the phage on the surface compared to deionized water pH7. **Table 3** shows the percentage of coverage of the surfaces by integrated density analysis.

		Mica		APTES	PEI
		H2O	TBS	H2O	TBS
wild-type vector pC89	pH7 (-3)	5.9%	no	59% monolayer	no
	pI (pH: 4.2)	no	60% Multilayer	no	60% multilayer
St.au9IVS5	pH7 (-1)	21% Sporadic adhesion	no	68% multilayer	no
	pI (pH: 5.4)	no	65% multilayer	no	58% multilayer
P9b	pH7 (-0,1)	8.6% Sporadic adhesion	no	53% multilayer	no
	pI (pH: 6.3)	no	10%	no	59% multilayer

Table 3. Percentage by integrated density analysis of coverage of the surfaces. no: not tested condition.

In summary, the specific peptide displayed on the coat of the phage clones was the most important element to consider, in order finding the correct condition for an organized phage-probe surface. In deionized water, the stratification was conditioned only of electrostatic interaction between phages and surfaces and permitted the partial coverage only when the charges of the two elements were in opposition. In presence of TBS buffer and electrostatic interaction, the surfaces were covered with thinker bundles helped lateral aggregation between phages induced by divalent metal ions present in the solution [Butler et al., 2002; S. Huang et al., 2008]. However, organized phage-networks was found only when TBS buffer was at pH corresponding to pI. Based on findings that this combination of elements allowed to lower the natural aggregation between phages (thank to neutral condition of the coat charge), then the formation of salt-bridges for the connection of surfaces and phages were facilitated.

The optimal condition of immobilization was observed on PEI in TBS pI for P9b clone and mica in TBS pI for St.au9IVS5. In these surfaces, phage networks showed a two-levels organization:

I. In the first-level, phage self-assembly in short fibers (less than 200 nm wide) and large bundles (5.68±0.68 nm thick and 34.42±3.29 nm wide);
II. In the second-level, organization mode occurs on the phage bundles with circular platelets (3.13±0.24 nm thick and of 40.04±2.56 nm average diameter).

In order to evaluate the maintenance of phage binding activity, detection test of the bacteria targets was performed on functionalized surfaces. *P. aeruginosa* and *S. aureus* bacteria cells were stained with 4',6-diamidino-2-phenylindole dihydrochloride (DAPI) and the bacteria cell captured were visualized by fluorescence microscopy. In particular, *P. aeruginosa* and *S. aureus* displayed the same pattern of the P9b-physorbed and St.au9IVS5-physorbed, confirming that both phage clones maintained their capacity to bind the targets. These data were confirmed by statistical analysis in terms of integrated density (I.D.) which showed mean values at 15' significantly higher ($P < 0.005$) compared to the surfaces physisorbed with wild-type vector pC89; the difference in bound target increased during the time get to $P < 0.0001$ at 1 h (**Figure 6**). The selectivity surfaces functionalized with St.au9IVS5 and P9b phage clone were evaluated by testing with also other potential targets (in particular *Listeria monocitogenes* and *Escherichia coli strains*). Only a sporadic adhesion of tested bacteria was observed and assigned to non-specific bond of the bacteria to the functionalized surface (data not shown).

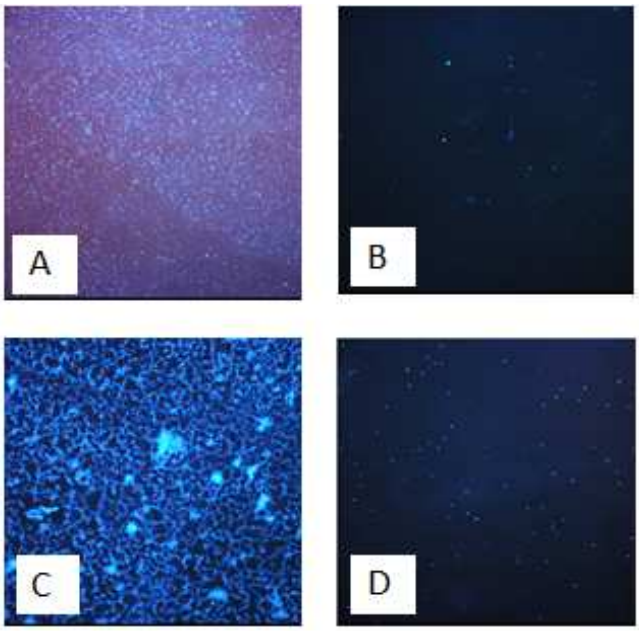

Figure 6. **Fluorescence microscopy images of *S. aureus* and *P. aeruginosa* attached to the surface of funcionalizated surface**. *S. aureus* attached on mica with the affinity-selected St.au9IVS5 (A) and PEI with wild-type vector pC89, as negative control phage (B); *P. aeruginosa* attached on PEI with the affinity-selected P9b (C) and PEI with wild-type vector pC89, as negative control phage (D).
20× magnification after 1h of incubation.

Therefore, the analysis of the isoelectric point of the phage clones, it is important element that needs to be considered in the optimal organized phage-absorption and maintenance of the recognition capability of cells target. The phage-biosensor-platform proposed is a model performed to capture about 50% of *S. aureus* cells and *P. aeruginosa* in a few minutes. Moreover, the proposed approach can be extended to other targets by changing the phage clone. The phage-biosensor-platform could find application as biochip for developing of miniaturized sensor to detect and monitoring of pathogen agents, as well as also cancer cells, virus or toxin to which a corresponding phage was selected for.

2.2.2 Bio-hybrid gold nanoparticles

The small size of the bacteria cells, such as the density and/or the contaminants present in samples make difficult to obtain the Raman signals. For this region, to increase the Raman signals of bacteria cells, noble metals, as gold and silver nano-particles, are used as molecule amplifiers of signal in so-called SERS (previously described in the previous chapter). Also in this case, the functionalization of noble metal nano-particles with probes allows a direct amplification of signal to target of interest, providing important information about the latter. Peptide guided SERS by silver nanoparticles (AgNPs) conjugated with specific phage clone, directed to the membrane of leukemic cells (specifically U937 cell line) has previously been proposed in a previous work [Lentini et al., 2015].

Exploiting the previously data about advantage/disadvantages to maintain correct folding of displayed peptide, due to changes in pH values [Lentini et al., 2015; Scibilia et al., 2016], in section the activity about the self-assembling of phage clones with gold nano-particles (Au-NPs) is described [Franco et al., 2019].

In particular, firstly, 99.9% purity Au target, immersed in distilled water was abled using the beam going from a neodymium-doped yttrium aluminum garnet (Nd:YAG) laser (model New Wave Mod. Tempest 300) focused (532 nm wavelength, 10 Hz repetition rate) to obtain Au nano-colloids. The characteristics in UV–vis optical absorption spectrum and the Au-NPs size were showed in **Figure 7.** The Au nano-colloid had band at about 510 nm typical of AU in UV-vis analysis, and dimension of about 10 nm and 35 nm with a PDI value of 0.5.

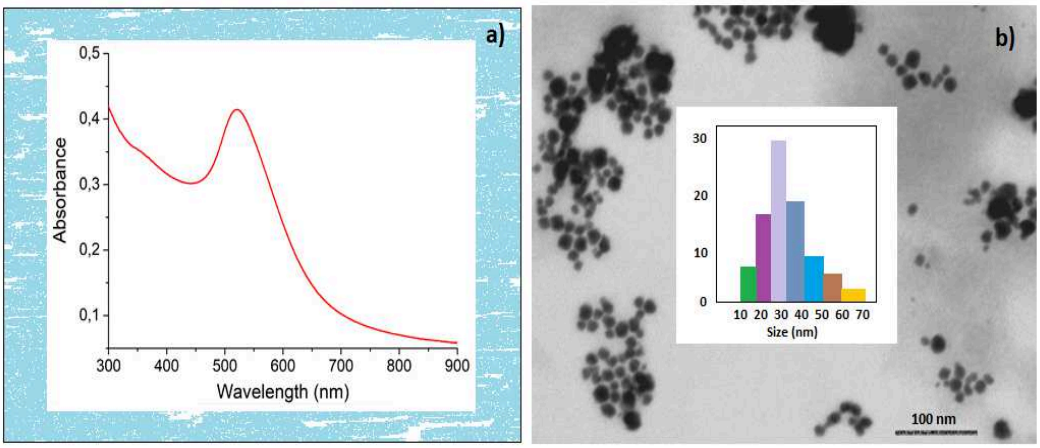

Figure 7. (a) UV–vis optical absorption spectrum of Au nano-colloid with a band at about 510 nm and (b) STEM image of Au-NPs with corresponding size histogram, obtained by DLS in agreement with STEM, of about 10 nm and 35 nm with a PDI value of 0.5.

Moreover, Au-NPs were characterized by Z potential value of -40 mV. Therefore, P9b phage/Au-NPs networks (**Figure 8**) carried out by electrostatic self-assembling, incubating P9b in ionic buffer at pH7, condition in which its positive charges were exposed. The presence on the assembled phage network of both elements was indicated by the EDX, which estimated species: C (25%), O (10%), N (12%) and Au (53%) assignment to phage and Au respectively. The phage clone is able to be efficient probes only when their peptides are in the correct form, then able to bind the bacteria target. Consequently, the efficiency of phage Au-network to detect the *P. aeruginosa* was verified putting the complexes in a solution with a suspension of bacteria target.

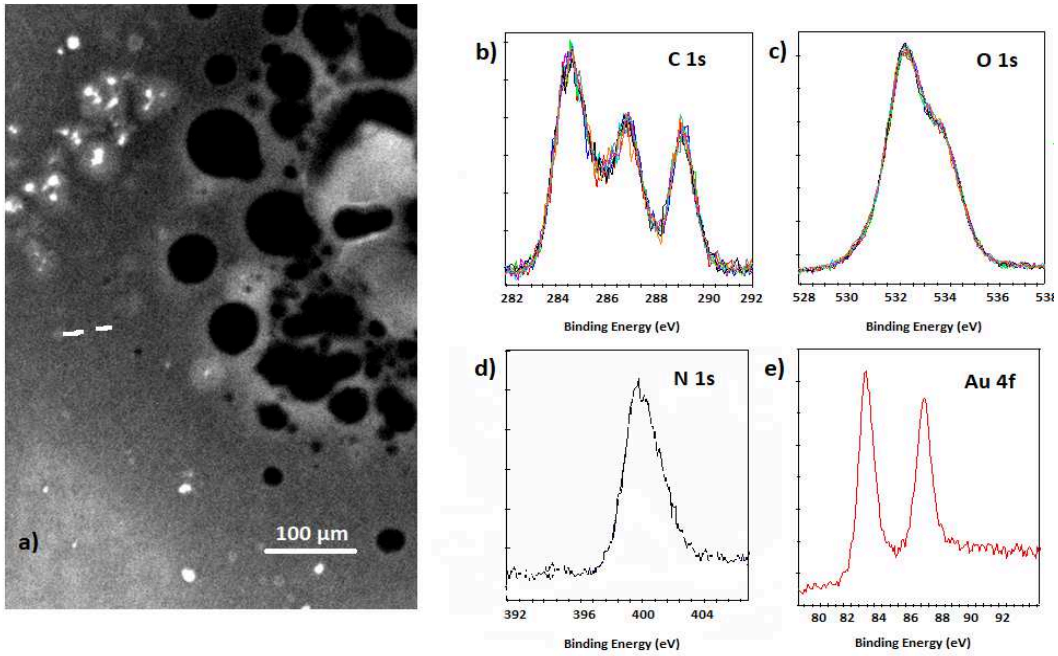

Figure 9. SEM image (a) and XPS spectra (b-e) of the Au NPs- P9b phage complex

The comparison of *P. aeruginosa* Raman spectra alone and after mix with phage-network solution has permit to confirm the complex maintain the ability to recognize the bacteria target. In fact, the Raman signal of the *P. aeruginosa* (PA) mixed Au-NPs@P9b samples was increased about 2 times with respect to *P. aeruginosa* alone (PA) and highlight new Raman features (**Figure 10**). In particular, the bands in the 800–1200 cm^{-1} region remain almost unchanged, while a sharp and intense peak appears at about 750 cm^{-1} due to the ring-stretching mode of DNA/RNA bases thymine. While spectrum of *P. aeruginosa* targeted by Au-NPs@P9b network (**Figure 10-C**) showed the presence of new contributions at about 1580 and 1655 cm^{-1}, ascribed, respectively, to the DNA bases ring breathing and Amide I stretching modes. This observation lead to suppose SERS effect was due to nearness with Au-NPs of the phage network, while the new signals are due to phage interaction on bacteria surfaces.

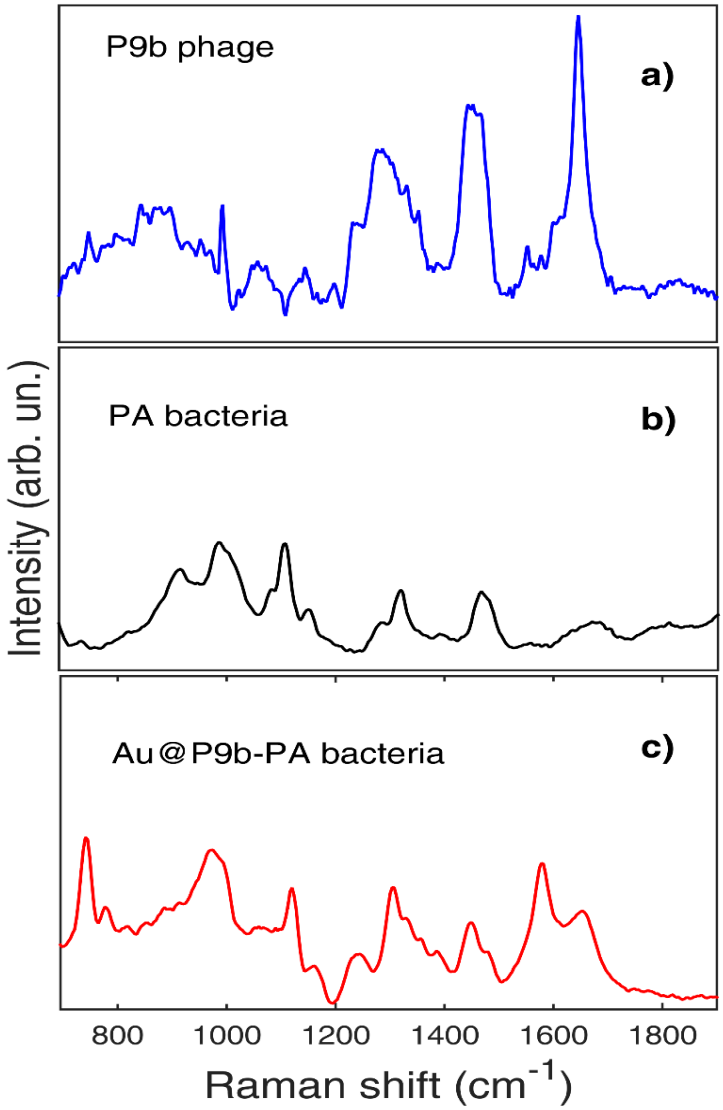

Figure 10. Raman spectra of P9b phage (a), *P. aeruginosa* (PA) (b) and Au-NPs@P9b networks in PBS (pH 7.18) mixed to PA (c).

The "proof of concept" proposed use P9b consequently the detection of *P. aeruginosa* by SERS. However, this phage clone has been used as a model, indeed the concept can be extended to the other bacteria or eukaryotic cells changing the specific-phage clone associated to the Au-network.

2.2.3 Phage-based beads for liquid samples

In this section, the optimization of phage-functionalization on surface of commercial beads (that are latex or magnetic beads) with different characteristics (materials, size, chemical functionalization) by covalent bonds is described. In addition, for each

functionalization procedure, the ability of the phage-coated beads to recognize and bind the bacterial targets (10^3 CFU/mL) has been evaluated and integrated in phage-based capture and concentrating systems for single step detection of pathogens in liquid samples. Covalent bound between phage and beads was obtained by activation of carboxyl groups (present on the phage or bead) that react with the amino groups on the counter part's surface. The chemical process provided the activation of EDC (1-Ethyl-3[3-Dimethylaminopropyl] Carbodiimide) in MES buffer (2-(N-Morpholino) Ethanel Sulfonic acid), which reacting with the carboxyl groups (COO-), formed highly reactive O-acylisourea species that in turn react readily with the amino groups (NH_2). Specifically, to perform phage-coated latex beads, the activated carboxyl-groups, exposed on bead surface, covalently bond specific NH_2 phage-chemical groups. On the contrary to obtain phage-coated magnetic beads the phage clone bond covalently the amino groups exposed on magnetic beads, due to intermedia of reaction formed on the COO- phage-chemical groups.

In both cases the data showed an efficient coupling of phage onto beads compared to the negative control (**Figure 11-A**). The results of capture efficiency were reported as percentage average of captured bacteria (**Figure 11- B and C**).

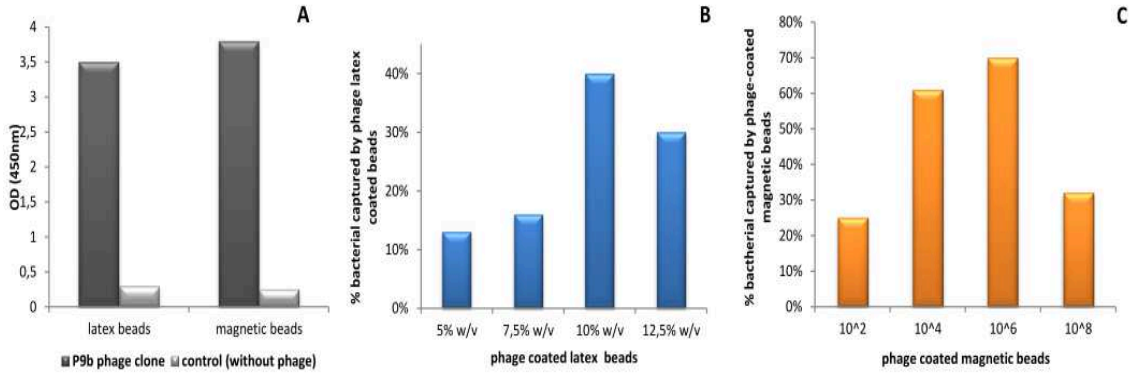

Figure 11: A) E.L.I.S.A: assay on phage-coated beads. Beads functionalized with P9b phage clone and respective negative controls (not coated beads); B) Dependence of capture efficiency on the amount of used phage-coated latex beads; C) Dependence of capture efficiency on the amount of used phage-coated magnetic beads. All tests were performed in triplicate and results were reported as percentage average of capture.

The phages, coated on the beads using both NH_2 or the COOH present on their surface, maintained the recognition capacity on both type of functionalization despite the covalent bind. In particular, % of cells captured by the phage-coated latex beads increased from 13% to 39.63% when phage-coated beads increased from 5% w/v to 10% w/v. On the contrary, the capture efficacy decreases from 39.63% to 30% when phage-coated beads further increase, suggesting that the ratio between phage-coated beads and *P. aeruginosa* cells was a major factor influencing the capture efficiency [De Plano et al., 2019; Lentini et al., 2016].

Similarly, phage-coated magnetic beads, at same bacteria concentration (10^3 CFU/mL), the capture efficiency were clearly increasing until 67% only until at one optimal concentration of 10^6 phage-coated magnetic beads. This is possible because the probability meeting between two elements is low when was presented both small and high quantity of phage-coated beads in the solution with same bacteria concentration. The data showed that 10% w/v of P9b-coated latex beads and 10^6 P9b-coated magnetic beads permitted the better capture efficiency of bacteria target. In summary for facility in the use and for better capture efficiency compared to the latex beads, the magnetic beads represent a good material to use in biosensor prospective. Similar trends were obtained by using of the other phage clones with the same type of beads.

2.2.4 Phage-magnetic-separation in blood

Indeed, beads play an important role in biosensor development since they have a three-dimensional structure with a higher surface area to volume ratio compared to a flat surface, consequently providing more binding sites for target. Moreover, another advantage is their easy manipulation in fluids in addition to a low cost also for the detection of antibodies with a low titer [Hansenová-Maňásková et al., 2016; Sutarlie et al., 2016].

In this prospective, phage-magnetic-separation was exploited in the capture efficiency in the blood. P9b, St.au9IVS5 and Li5 covered on magnetic beads were used to concentrate and rapidly detect *P. aeruginosa*, *S. aureus* and *E. coli* microorganisms responsible for the most frequent bloodstream. The capture-trend of each bacteria individually in 7 mL blood solution showed a coherent progression compared to the scalar concentration of the phage-factionalized magnetic beads present in solution (**Figure 12**).

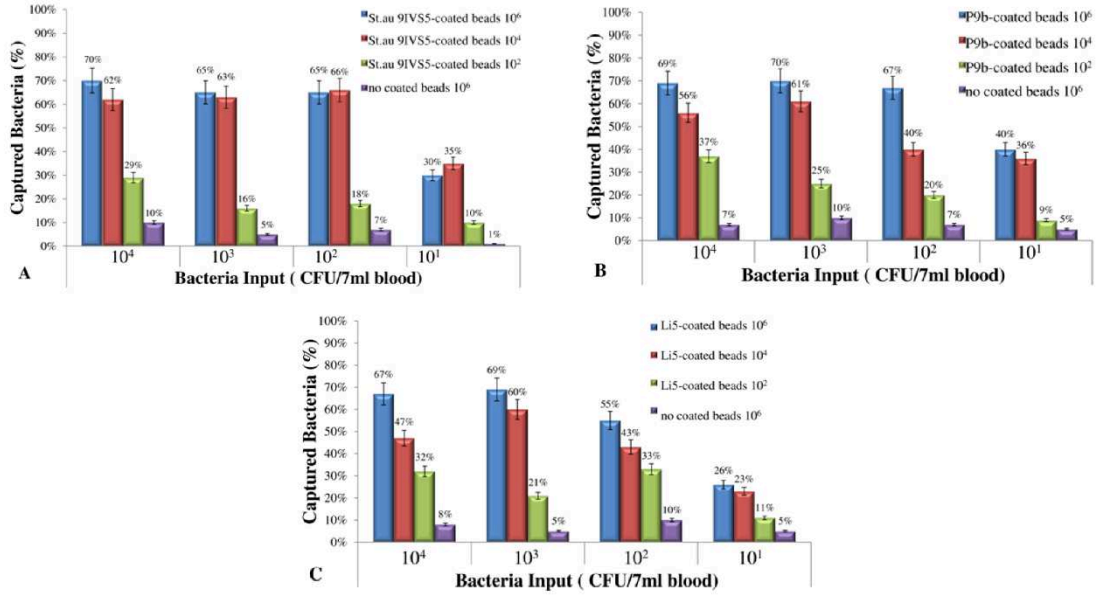

Figure 12. Capture efficiency of phage-coated beads, with the specific phage clone, in capture test against bacterium target. A) St.au9IVS5-coated beads against *S. aureus*; B) P9b-coated beads against *P. aeruginosa* and C) Li5-coated beads against *E. coli*. Mean is the average of three separate experiments with multiple cultures.

In particular, for 10^2 phage-coated beads the capture efficiency resulted lower compared to tests with 10^4 and 10^6 phage-coated beads, for all the phage clones used in the system. Instead, 10^4 phage-coated beads with St.au 9IVS5 captured 60% of bacteria targets. Similar and/or higher percentages were obtained when using 10^6 St.au9IVS5 and Li5 coated beads. Consequently, 10^4 St.au9IVS5-coated beads were considered the optimal concentration to capture S. *aureus* bacteria in the blood solution. The best P9b-coated beads concentration resulted 10^6, with a maximum of 70% of captured *P.*

aeruginosa, likewise, Li5-coated beads which showed the highest efficiency in the capture of *E. coli* with the value of 69% in 15'of reaction. Moreover, the results show that uncoated beads recover a media percentage around 5–10% of bacteria target, and that this interaction is probably due to electrostatic bonds or van der Waals like forces, as reported by other authors [Foddai et al., 2010]. Consequently, the relative amount of bacteria and beads in the solution played an important role in the collision frequency between the two, then, the capture efficiency was influenced of the probability meeting between phage-coated beads and bacteria targets. The capture efficiency, evaluated in comparison with uncoated beads, was 10 CFU/7 mL, when was used the optimal concentration of each phage coated beads. did not observe any negative interaction when all the different phage-coated beads were dispersed in the same solution (data not shown).

2.3 Phage-based assay for rapid detection of bacterial pathogens in blood by Raman spectroscopy

In biosensor prospective, the complexes were analyzed by Raman spectroscopy. The bacteria bound at phage-magnetic particle were incubated in rich-medium for 4 h at 37 °C in agitation. Then, grown bacteria were concentrated in 10 μL PBS and deposited onto a slide for micro-Raman spectroscopy measurements. The specificity of molecule vibrational provided information about bacteria strains permitting the distinction between them. [Chan et al., 2006; Cheng et al., 2005; Shetty et al., 2006; Kast et al., 2008; Stone et al., 2004].

Particularly, the regions considered for the discrimination, in light gray, show vibrational features mostly due to proteins (amide I, II, III), aromatic amino acids (phenylalanine (Phe)) and nucleic acid components (guanine (G), adenine (A)). In the 1500–1550 cm^{-1} spectral region, Raman signal of proteins and relevant bacteria matrix

components could be also influenced by the interaction with the carotenoids [Jehlicka et al., 2013], whose main skeletal features are: C=C stretching centered at around 1520 cm^{-1}, C-C stretching around 1150 cm^{-1} and C=CH bending around 1000 cm^{-1}. (Figure 13 and table 2).

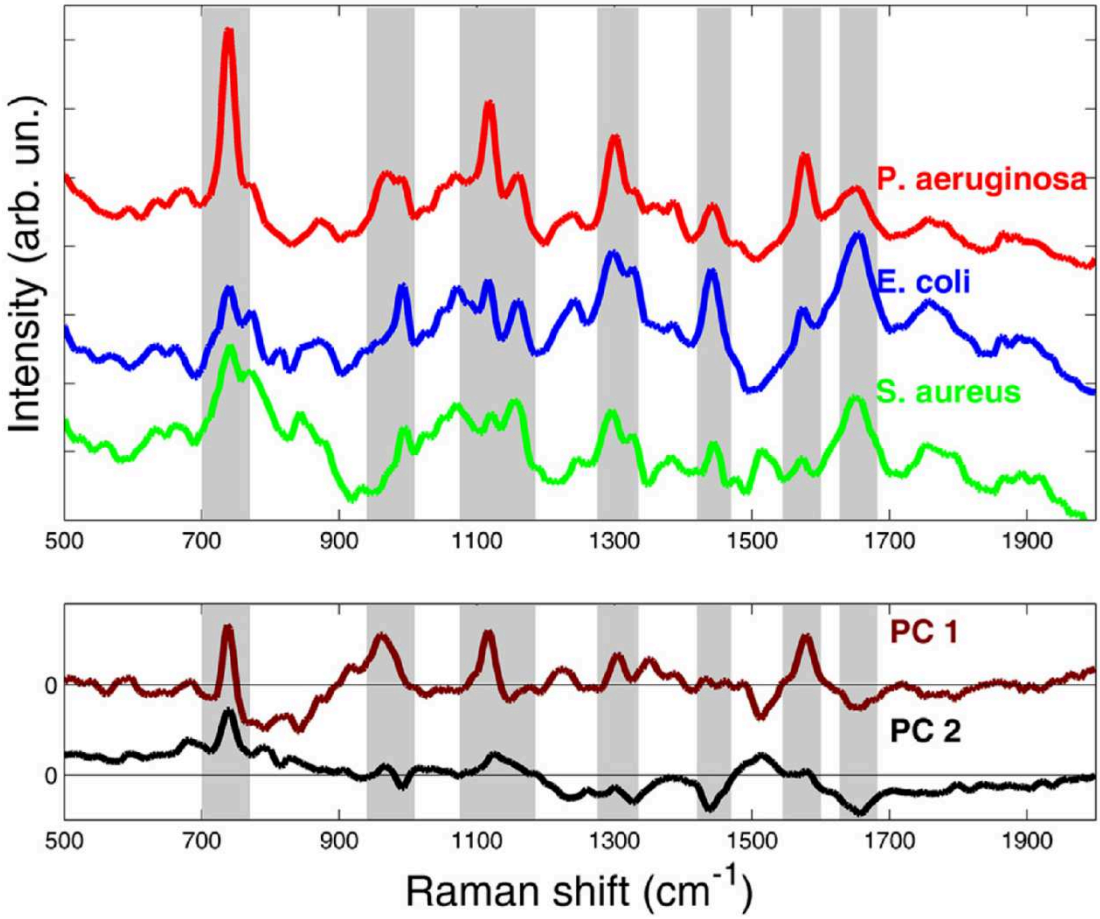

Figure 13. Representative micro-Raman spectra of *P. aeruginosa* (red line), *E. coli* (blue line) and *S. aureus* (green line). The shaded area that encloses each curve represents the standard deviation values limits, while the gray bands highlight the main vibrational contributions due to proteins, lipids and nucleic acids (upper panel); PC1 and PC2 as a function of wavenumber (lower panel).

Specifically, pretreated spectra from considered bacteria were used as an input set for the principal component analysis (PCA) procedure. Then, hierarchical cluster algorithm (HCA) was applied to the PCA results in order to identify statistically similar groups (Figure 14). HCA output show that bacteria were exactly clustered into three different groups, also highlighting some existing intra-species subgroups, probably due to a

different metabolic state within the same cell population (**Figure 14**) [Kloß et al., 2013; Münchberg et al., 2014].

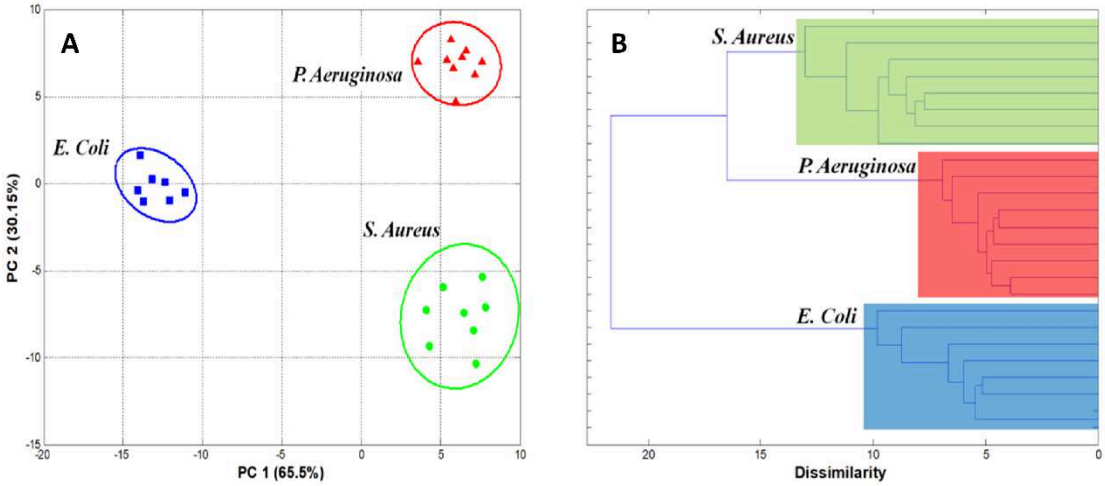

Figure 14. **Output by PCA (A) and HCA (B) analysis of bacterial spectra.** The points enclosed in the ellipses and the different color (blue, red and green) refer to the clusters, as they were identified by the HCA algorithm. Spectra input, from each bacterium strain, are identified by different symbols (square for E. coli, circle for S. aureus and triangle for P. aeruginosa) in the PCA graph. (For interpretation of the references to color in this figure legend, the reader is referred to the web version of this article.)

Raman band (cm^{-1})	**Vibrational modes**	**Assignments**	**References**
710-760	Symmetric ring breathing mode	DNA/RNA bases	Chan et al., 2006
		Protein	Cheng et al., 2005
940-1010	Skeletal modes	Lipid	Shetty et al., 2006
	Symmetric ring breathing mode	Protein	Cheng et al., 2005
1070-1170	ν(C–C) or ν(C–O)	Lipid	Kast et al., 2008
	C–C, C–N stretching	Protein	Chan et al., 2006
1270-1320	Amide III	Protein	Stone et al., 2004
	CH2 deformation	Lipid	
1420-1450	Ring breathing modes	DNA/RNA bases	Chan et al., 2006
	$\delta(CH_2)$, $\delta(CH_3)$	Lipid	Kast et al., 2008
1550-1600	C= C stretching	Protein	Cheng et al., 2005
	Symmetric ring breathing mode	DNA bases	Chan et al., 2006
1630-1670	Amide I	Protein	Cheng et al., 2005
	C= C stretching	Lipid	Stone et al., 2004

Table 2: Raman band used as molecular species-specific fingerprint, corresponding vibrational modes and their assignments. ν stretching mode; δ, bending mode.

Therefore, the systems of combination between phage-magnetic separation and micro-Raman spectroscopy, schematized in **Figure 15**, was validated using 27, 34 and 23 blood samples artificially infected from *S. aureus*, *P. aeruginosa* and *E. coli* respectively.

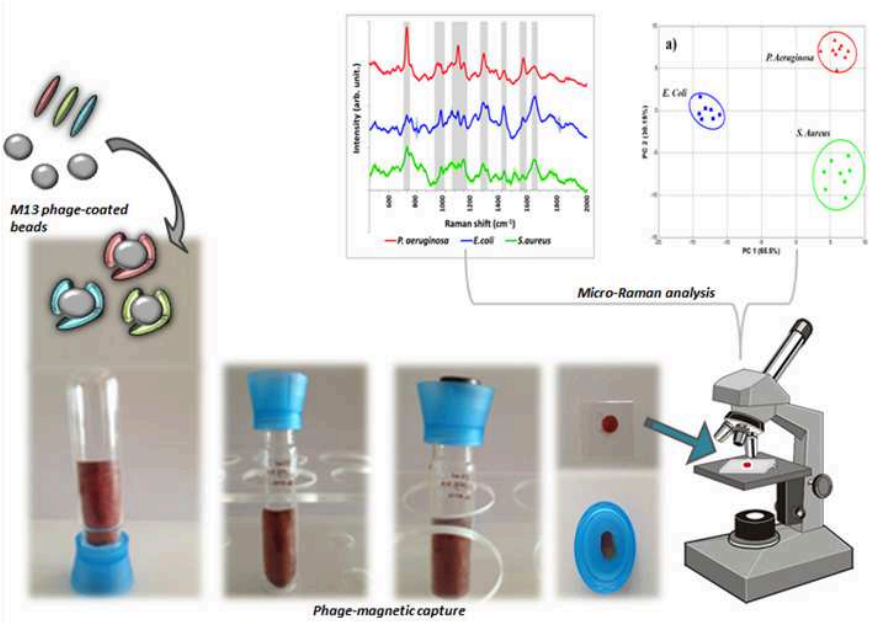

Figure 15. **Schematic representation of the proposed proof-of concept.** In the first, phage clones were functionalized on the magnetic beads. Then the phage-magnetic separation of the bacteria carried out in 7 mL of blood samples in 15'. Therefore, the complex amplified in broth bacteria culture and analyzed in micro-Raman spectroscopy in about 5h. All the process carried out in less 6h**.**

The biosensor had detection limit of 10 CFU in 7mL blood volume, which are amplified and concentrate in small volume (10µL) and rapidly detect by Raman-spectra in less 6h with sensibility of 100% for *P. aeruginosa* and *S. aureus* and 96% for *E. coli* (**Figure 16).**

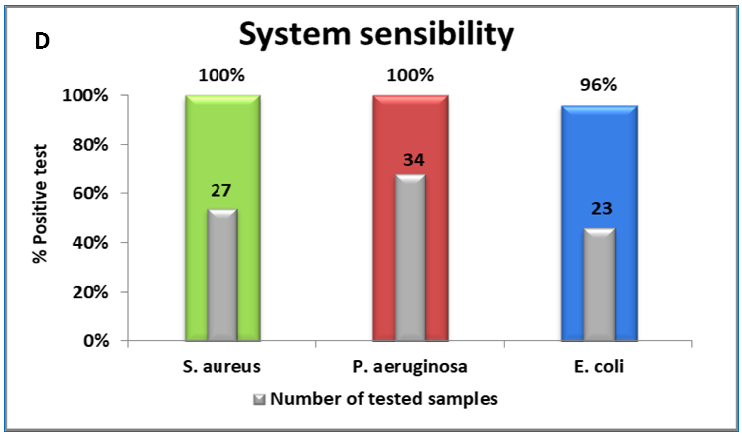

Figure 16. Sensibility of the system. The detection accuracy of: 100% for *S. aureus* (27 samples /27 samples), 100% for *P. aeruginosa* (34 samples/34 samples) and 96% for *E. coli* (22 samples/23 samples).

2.4 Phages like antibacterial and antibiofilm molecules

Recent advances describe the use of phage display in the discovery of novel bioactive molecules. This technology leads to produce proteins and peptides able to minimize the use of antibodies, recently become major causes of human mortality and disability worldwide due to drug-resistant bacteria strains. Many research groups have used the phage display in the discovery of new drugs. Consequently, banks online about phages, or more generally, peptides with antibacterial activity are in continue growth. Starting from the knowledge present in the literature and in the online tools, clones selected against S. *aureus* and P. *aeruginosa* have been sorted with existent naturally or synthetic antimicrobial peptides (AMP) by AP-prediction (http: //aps.unmc.edu/AP/prediction/prediction_main.php) AMP bank server **Table 5.** Moreover, the probable toxicity and the penetrant activity were investigated by TOXIN-PRED (http://crdd.osdd.net/raghava/toxinpred/) and CELL-PPD (https://webs.iiitd.edu.in/raghava/cellppd/submission.php) , respectively (**Table 5**).

Bacteria target	Peptide sequences	Ap-prediction	Toxin-pred	Cell-PPD
	RVRSSPVVQ	no	no	no
	RVRSIPHVA	no	no	no
S. aureus	RVRSYSPHL	no	no	no
	RVRSNAASM	yes	no	No
	RVRSAPSSS	no	no	no
P. aeruginosa	QRKLAAKLT	yes	no	no

Table 5. shows the bioinformatics analysis of the probable ability of the peptides exposed on the phage clones selected against *P. aeruginosa* and *S. aureus*.

Among all, the peptide, QRKLAAKLT, displayed on the pVIIIs of the P9b and specific to recognize the P. *aeruginosa,* result to have α-helix structure and antimicrobial peptide probable activity. In particular, the most relevant homology, about 42.85 %, is with the $(KLAKLAK)_2$ peptide which is part of ligand targeted agents against cancer and obesity [Javadpour et al., 1996]. This peptide has been proposed like synthetic drug candidates in its D-enantiomer version, commercialized of "AnaSpec" company (https://www.anaspec.com/), for its pro-apoptotic induction. The amino acids _KLA—

KL-_ in P9b were involved in the homologies with $(KLAKLAK)_2$ showing some motifs "KLA" (lysine–leucine -alanine) and "KL" (lysine–leucine). Moreover, the non-toxic and the penetrating probable ability have made this a peptide able to be use in *in vitro* analysis. Therefore, several phage concentrations of P9b were test in broth culture with several *P. aeruginosa* cell input to evaluate the minimal inhibition concentration (MIC) (**graphic 1**). The P9b showed anti-bacterial grown ability at all the condition with p-value (p) <0,01, however never condition showed the total inhibition of the cell grown, suggesting that the phage had a bacteriostatic action. According to the phage-doses used, decreasing concentrations of the phage clones added at the broth culture increase the vitality of the cells after 24h. In particular, the high phage concentration, 10^{11}/mL, led to decrease of 62% and 49% of the bacteria growth when the input of the bacteria cells was 10^2 and 10^5 PFU/mL respectively. Consequently, the MIC was evaluated at 10^{11}phages/mL. Probable the high phage concentration of P9b phage clones in the solution covered all the specific receptor on the bacteria membrane inhibits the interchange between inter- and extra- cell environment, preventing the vitality and leading at bacteriostatic induction of *P. aeruginosa* cells.

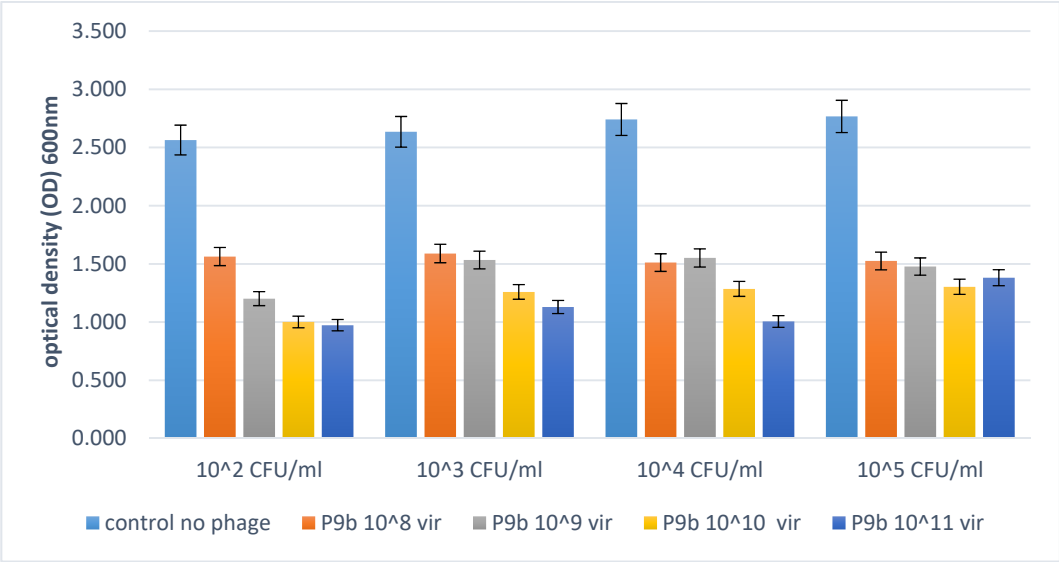

Figure 17. Inhibition of grown of *P. aeruginosa* in broth culture. Several phage concentrations of P9b were incubated with several P. aeruginosa cell input in broth culture and evaluated after 24h.

The ability to cause infection of *P. aeruginosa* has also been correlated with its tendency to form bacteria complex [Lee and Yoon, 2017; Trøstrup et al., 2017]. The formation of bacteria complex starts with bacterial adhesion on solid surfaces, which represents a rational step of action to eliminate biofilms or to prevent biofilm formation [Harmsen et al., 2010]. For this, several times of incubation were used to verify the inhibition and destabilization of the *P. aeruginosa* adhesion on the substrate when incubates with P9b clones at 10^{11} PFU/mL (**Figure 18**). The results confirm that the P9b alters the adhesion ability of the phage when inoculate in the first 4h. The interaction of the phage was present only in the early steps of the bacteria adhesion, probable after this the bacteria cells change any cells surfaces receptors preventing the phage clones bound.

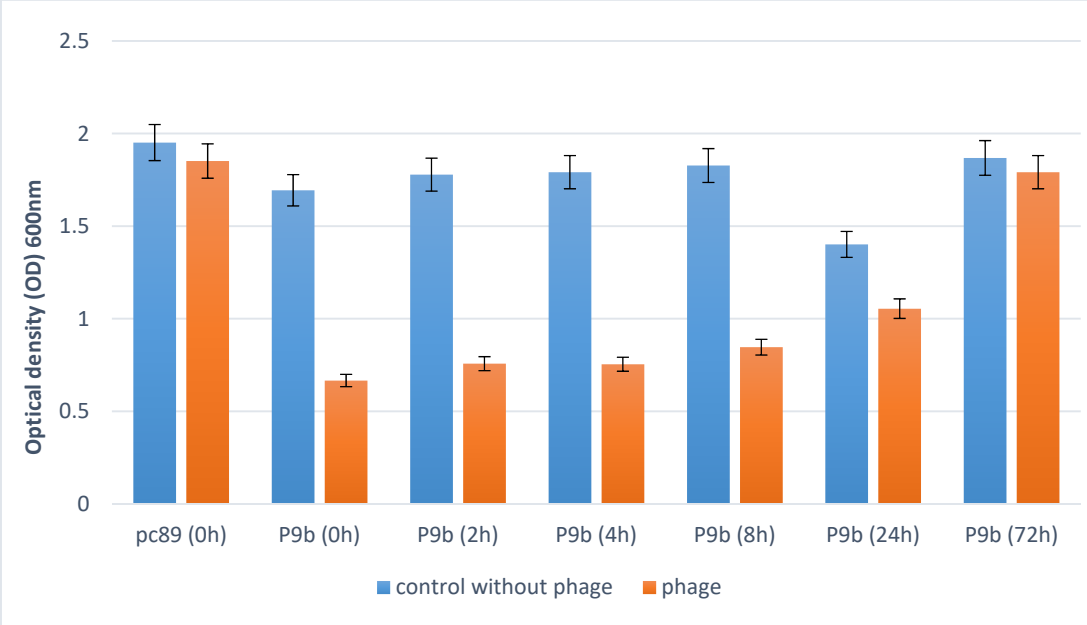

Figure 18: Inhibition of bacteria adhesion of *P. aeruginosa* from P9b phage clone (10^{11}/mL) compared to pC89 phage vector, added at different time and evaluated after 6 day.

The results suggested that this clone could be used only in a prevention of biofilm formation. The combination between its intrinsic inhibition-biofilm action and the possibility to be functionalized in several surfaces without lost its recognition ability could suggested the use as biomaterial in environment and health care.

ES. Experimental Section

ES.1 Phage peptide library

The M13phage library (donated by Professor F. Felici) expressed random peptides, exposed on the pVIII protein, based on the phagemid vector pC89 on which random oligonucleotide sequences were inserted in the region 5' of the VIII gene present in the vector, under the control of the LacZ promoter. The digestion with the restriction enzymes EcoRI and BamHI linearized the vector and allowed the insertion of the oligonucleotides with random sequences which, flanked by the same restriction sites, allow the recircularization of the vector through ligase reaction [Felici et al., 1991; Luzzago and Felici, 1998]. For the selections were used three types of peptide libraries: pVIII-9aa (expressing nine amino acids in the N-termialpVIII), pVIII-12-aa (expressing twelve amino acids in the N-terminal pVIII) and pVIII-12cys-aa (have a cysteine-cysteine constriction expressed in end of the random amino acids sequence, located in the N-terminal pVIII). The amplitude of each library is comprised between 10 and 100 million independent clones.

ES.2 Bacteria and growth media

S. aureus ATCC 29213 obtained from the American Type Culture Collection (ATCC, LGC Promochem, Milan, Italy was propagated in tryptone soya broth (TSB) broth and Mannitol Salt Agar (MSA). *E. coli* TG1 ($lacZ^-$) was used for propagation of phage clones. *P. aeruginosa* ATCC 27853, *S. flexneri* ATCC 12022, *E. coli* ATCC 11303, *S. epidermidis* ATCC 12228, *B. subtilis* ATCC 6633, *L. monocytogenes* ATCC 7644 and nine *S. aureus* clinical isolates, were used in selectivity assessment of phage–bacteria binding. Stock organisms were maintained in LB broth (or TSB, tryptone soya broth, for *S. epidermidis, S. aureus, L. monocytogenes, B. subtilis* and *S. aureus* clinical isolates nine clinical isolates) containing 20% (v/v) glycerol at −80◦C.

ES.3 Phage peptide selection

Firstly, the M13 pVIII-9aa library was pretreatment with the plastic materials. This subtracted library was used to the selection protocol on-binding phage clones for four rounds of affinity selection against *S. aureus* ATCC 29213. 10^{12} phage library was incubated with *S. aureus* cells (OD_{600} 0.5) in 1 mL phosphate-buffered saline (PBS, 137 mM; NaCl,2.7 mM; KCl, 10 mM phosphate buffer, pH 7.4) with gentle agitation for 60’ at room temperature (RT). Bacteria-phage complex were precipitated for 5’ at 16000 ×*g*, and separated from unbound phage in solution by a series of 10 washing and centrifugation steps (16000 ×*g*, 5’) with 1mL TBS/Tween buffer (50 mM Tris–HCl (pH 7.5); 150 mM NaCl, 0.05% (v/v); Tween20) each time. Bound phages were pelleted with cells, eluted with 250 µL of 0.2 M glycine–HCl (pH 2.2) with gentle shaking at RT for 20’, and sonicated in ice bath at 20 KHz for 10’. The solution was neutralized with 25 µL of 1M Tris–HCl (pH 9.1). For each round, eluted phages were used to infect *E. coli* TG1 cells and then the solution plated on LB agar plates containing ampicillin. This cultural condition was used to select bacterial colonies, each containing phage from a single library clone, were randomly selected and propagated using the standard protocols (Manual “Ready-To-Use Phage Display Library” Spring Bioscience).

ES.4 DNA sequencing and peptide analysis

Primers M13–40 reverse (5’- GTTTTCCCAGTCACGAC −3’) and E24 forward (5’− GCTAC-CCTCGTTCCGATGCTGTC −3’) were obtained from Proligo, Sigma (Milan, Italy). 1 µL of the suspended colony (*E.coli* TG1 infected with phage clone) was added to the PCR reaction tube, containing 49 µL of the following PCR mixture:10 × Mg free reaction buffer (Euro Clone, Milan, Italy) (5vol); 50 mM $MgCl_2$ (Euro Clone) (5 vol); Euro-Taq DNA polymerase (5 units

μL^{-1} Euro Clone) (0.5 vol); 2.5 mM dNTPs (Roche) (5 vol); primer M13–40 (10 pmol μL^{-1}) (5 vol); primer E24 (10 pmol μL^{-1}) (5 vol); doubly distilled filter sterilized water (23.5 vol). The PCR was performed by Gene Amp PCR System 2400 (Perkin Elmer, Nor-walk, CT, USA) under the following cycling conditions: one cycle at 94 °C for 5'; 25 cycles at 94 °C for 30'', 52 °C for 30'', 72 °C for 30''; and one cycle at 72 °C for 7'. The PCR products (3 µL) were analyzed by agarose gel electrophoresis (1% wt/vol agarose, Sigma, Milan, Italy) in 1 × TAE buffer. Gel was stained with ethidium bromide, illuminated on a Dark Reader, while DNA bands were visualized by a Kodak imaging system. PCR products were purified by Nucleo Spin PCR Clean-up purification Kit (Macherey-Nagel) and sequenced using the M13–40 reverse primer. The DNA sequences were converted into amino acids by the 'translate' program on the proteomics server of the Swiss Institute of Bioinformatics Expert Protein Analysis System (ExPASy [http://www.expasy.ch/]). The amino acid sequences were aligned by the CLUSTALX sequence alignment program (available at [http://www.ebi.ac.uk/clustalw/]). GeneDoc software (http://www.psc.edu/biomed/genedoc/) was used for visualizing edit and analyze multiple sequence alignments of the peptides. Statistical analysis of the insert composition was performed. A list of the primary amino acid sequences of the variable inserts is then compiled in the FASTA format and submitted to a motif-elucidation bioinformatics algorithm called MEME (multiple expectation-maximization for motif elicitation http://meme.sdsc.edu/meme/intro.html).

ES.5 E.L.I.S.A: test

96-well E.L.I.S.A: plates (Nunc Multisorp) were coated overnight at 4 °C with 100 µL suspensions of $\sim 10^{12}$ phage clone/mL in TBS. Washed 3 times with PBS/0.05% Tween 20 on an automatic plate washer, blocked with 5% non-fat dry milk in PBS/0.05% Tween for 2 h at 37 °C and washed again. 100 µL of *S. aureus* ATCC 29213 cells (OD_{600} 2.0) were added in PBS/1% non-fat dry milk +0,1% Tween 20 for 2 h at RT with shaking; washed again (5 times). Then 100 µL of 1:3000 dilution of mouse anti-Lipotheicoic acid antibody (QED Biosence) added for 1 h in PBS/1% non-fat dry milk +0,1% Tween20, washed again; incubated with a 1:50,000 dilution of goat anti-mouse-HRP (AbCAM ab97023) for 1 h with shaking and washed again. The final reaction with 100 µL of TMB (3,3,5,5-tetramethylbenzidine) liquid substrate for E.L.I.S.A: added in the plate for 45' at RT and stopped with 100 µL of 1 M H_2SO_4 allowed the read at 405 nm in Multiskan Reader, LabSystem. Phage particles bearing no recombinant insert, from superinfection of phagemid vector pC89-containing cells, served as a negative control for evaluation of background from non-specific binding. A similar procedure was used to test the binding capacity of selected phage against nine clinical isolated *S. aureus* and a panel of other Gram positive, *Staphylococcus epidermidis* ATCC12228, *Bacillus subtilis* ATCC 6633, *Listeria monocytogenes* ATCC7644 and Gram negative bacteria *Pseudomonas aeruginosa* ATCC27853, *Shigella flexneri* ATCC 12022, *Escherichia coli* ATCC 11303, in order to assess its selectivity and specificity of binding.

ES.6 Bacterial protein extraction and Western blot

The extraction procedure was performed according to the protocol of George c. Paoli et al. [2007] with minor modification. Two aliquots of 5 mL in PBS of *S. aureus* (OD_{600} =1) were spun down at 3500 ×*g* for 10', washed two times with PBS and unified. The pellet was suspended in 100 µL of extraction buffer (125 mM Tris-HCl, pH 7.0 containing 2% SDS, protease inhibitor cock-tail at 10 µL/mg, 20% glycerol and bromophenol blue) vortexed for 5'. After 45' of incubation at 37 °C in agitation 8 rpm, the cell suspension was centrifuged again, and the supernatant recuperated in a new tube. For Western immunoblot analyses, protein lysate from *S. aureus* were boiled for 5' at 95 °C and separated at 25 mA on Bio-Rad SDS-10% polyacrylamide gel electrophoresis (PAGE). Following electrophoresis, proteins were transferred onto a nitrocellulose membrane (0.45 µm Bio-Rad) by using the Mini-Trans-Blot transfer cell (Bio-Rad) for 16–20 h at 25 mA. The membranes were blocked at RT for 2 h in

blocking buffer (5% non-fat dry milk +0.05% Tween20 in PBS), washed for 5' with PBS/0.05% Tween 20 and then incubated with 10^{12} virions of phage-displayed peptides for 2 h at 37 °C in a gently agitation. After washing in PBS/0.05% Tween 20 for 15', the membranes were incubated with a 1:5000 dilution of anti-M13 peroxidase conjugate antibody in PBS/1% non-fat dry milk +0.1% Tween20 for 1 h. After the membranes were washed as described above, the bands on the immunoblots were detected by DAB (Sigma, Milan, Italy) for 15', dried and preserved in plastic envelop. SDS-PAGE broad-range pre-stained markers (Bio-Rad) were used for size estimation of the bands binding the recombinant phage.

ES.7 Phage-capture E.L.I.S.A: (kinetic reaction)

96-well E.L.I.S.A: plates were coated overnight at 4 °C with 100 µL suspensions of ~10^{12} phage clone/mL in TBS, washed 3 times with PBS/0.05% Tween 20 on an automatic plate washer and blocked with 5% non-fat dry milk in PBS/0.05% Tween for 2 h at 37 °C. Washed again (5 times); put in the reaction 100 µL/well of *S. aureus* ATCC 29213 cells (OD_{600} 2.0) in PBS/1% non-fat dry milk +0,1% Tween20 for different time (15', 30', 60' and 120') at RT with shaking, washed again (5 times). Reacted with 100 µL of 1:3000 dilution of mouse anti-Lipotheicoic acid antibody (QED Biosence) for 1 h in PBS/1% non-fat dry milk +0,1% Tween20, washed again (5 times) and incubated with a 1:50,000 dilution of goat anti-mouse- HRP for 1 h with shaking. Then washed again (5 times). Reacted with 100 µL of TMB for 45' at RT and stopped with 100 µL of 1M H_2SO_4. Wells were then read on a kinetic plate reader at 405 nm.

ES.8 Phage clones

P9b, St.au 9IVS5 and Li5 phage clones were derived from M13-pVIII-9aa phage peptide library previously described affinity-selection processes. The clones display the foreign peptide QRKLAAKLT, RVRSAPSSS and RKILRAGPL, which represent specific and selective probes for *P. aeruginosa* [Carnazza et al., 2008], *S. aureus* [De Plano et al., 2017), and *E. coli* respectively [De Plano et al., 2019]. The specificity and selectivity of probes were tested against different bacteria target as reported in our previous works.

ES.9 Functionalization of Magnetic and Latex Beads

ScreenMAG-Amine superparamagnetic beads (1 µm diameter, Chemicell GmbH (Berlin, Germany) and Carboxyl-polystyrene latex beads (0.8 µm diameter, SERVA Electrophoresis GmbH (Heidelberg, Germany) were functionalized using protocol described previous [Calabrese et al., 2015; Lentini et al., 2016]. Phage suspensions in ultrapure water were functionalized with the ratio about 360 phage clones/magnetic beads or with the ratio w/v of 320 µl of phage (title of $1.3 \cdot 10^{12}$ PFU/mL) and 1 mL of beads (10% w/v in ultrapure water). In order to verify phage coating of the beads, we performed an E.L.I.S.A: test with M13-pVIII antibody. In order to determine maximum capture efficiency, 10^3 *P. aeruginosa* ATCC 27853 cells/mL were incubated for 30' against scalar concentration of phage-coated beads (for latex beads: 5, 7.5, 10 and 12.5% w/v; for magnetic beads: 10^2, 10^4, 10^6 and 10^8 beads). Colony Forming units per millilitre (CFU/mL) counts were determined before and after beads incubation with bacteria and the capture efficiency percentage was calculated. The same capture test was performed with unfunctionalized beads (Blank). Tests were done in triplicate and results were reported as percentage average of capture.

ES.10 Optimization of capture efficiency using M13 phage-coated beads

The capture ability of phage-coated beads was performed in 7 mL of artificially infected blood, captures efficiency was assessed by Standard Plate Count. In details, tests were done incubating 20 μL of M13 phage-coated beads with bacteria target (*P. aeruginosa* ATCC 27853, *S. aureus* ATCC 29213 or *E. coli* LE392) for 15' at RT in a rotation. Dilutions ranging from 10^6 to 10^2 beads/7 mL of each phage-coated bead complex was evaluated in capture-testing vs ten-fold bacterial dilutions ranging from 10^4 to 10 cells/mL; after incubation, the beads were separated from the mixture using a magnetic-particle concentrator (DynalMPCs-S, Invitrogen Dynal AS, Oslo, Norway). Then phage-beads-captured bacteria were resuspended in PBS. Colony Forming Units per mL (CFU/mL) values were determined before and after beads incubation with bacteria and the capture efficiency percentage was calculated by spread on Agar plates, followed by incubation overnight at 37 °C. A capture test was performed with not functionalized beads (Blank). All tests were performed in triplicate and overall results are reported as mean capture percentage. For the assessment of the efficiency of the phage-magnetic separation we used the following relation:

$$\text{Efficiency} = X_{b1} + 3S_{b1}$$

where X_{b1} and $3S_{b1}$ are the mean concentration of the blank and the standard deviation of the blank, respectively (Shrivastava and Gupta, 2011). After the magnetic separation the complexes (phage-beads-captured/bacteria-captured) were incubated with 1 mL Mueller Hinton Broth (MHB) for 4 h at 37 °C in agitation. After, phage coated beads were removed, and bacteria centrifuged at 8000 ×*g* for 10' and resuspended in 10 μL PBS buffer and dropped on to CaF_2 glass over an area of ~1 cm^2. All experiments were conducted in triplicate.

ES.11 Raman spectroscopy analysis

Raman scattering was excited by the 532 nm (2.33 eV) radiation of a diode laser and analyzed by a Horiba XploRa micro-Raman apparatus equipped with an imaging flat field monochromator for use with a CCD camera detector cooled at 77 K and a full optical microscope so that users can also see their samples. An acquisition time of 100 s allowed a good signal/noise (S/N) ratio. Also, in this case, to ensure reproducibility, experiments were performed in triplicate. Multivariate data analyses were carried out with Matlab software. See more details in Ref. [Lentini et al., 2015; Lentini et al., 2016]. To improve Raman analysis, all the spectra were previously subjected to some data treatment. First of all, a continuous baseline correction was performed using the adaptive iteratively re-weighted penalized least square algorithm (airPLS) (Zhang et al., 2010). Corrected spectra were then normalized to their own maximum intensity and slightly smoothed using the Savitzky- Golay smoothing-derivative procedure [Savitzky and Golay, 1964]. The resulting spectra were loaded into rows of a matrix which was used as input for Principal Component Analysis (PCA) and subsequent Hierarchical Cluster Analysis (HCA). The detection by micro-Raman spectroscopy of the bacteria captured by phage magnetic separation (at different concentrations in blood samples) allowed the determination of the limit of detection (LOD).

ES.12 Preparation and characterization of AuNPs

Au nanocolloids were prepared removing material from an 99.9% purity Au target, immersed in distilled water, on which the beam going from a neodymium-doped yttrium aluminum garnet (Nd:YAG) laser (model New Wave Mod. Tempest 300) was focused (532 nm wavelength, 10 Hz repetition rate). During the ablation, the beaker was moved using a rotating support to provide the target fresh surface.

The AuNPs UV-vis optical absorption signal was monitored after the ablation process and the assembly with the phage clone. To this scope, a Perkin Elmer Lambda 750 UV-Vis spectrometer in the 190-1100 nm range was used. The NPs size was estimated by Dynamic Light Scattering (DLS) measurements, using a Horiba Nano Particle Analyzer SZ-100, and

Scanning Transmission Electron Microscopy (STEM), using a Zeiss microscope operating at the acceleration voltage of 30 kV.

ES.13 Phage/AuNPs networks preparation

The phage/AuNPs networks were performed by incubation AuNPs with the phage clone suspended in Phosphate Buffered Saline (PBS) 0.01M, pH 7.18 (final titer of $5 \cdot 10^{11}$ PFU/mL) in a 5:1 ratio at 30 °C in orbital shaking at 240 rpm (KS130 Basic IKA) over night.

The separation of the phage/AuNPs networks from the unbounded phages and free AuNPs, networks were carried out by centrifugation at 2150 *xg* for 40'. Then suspended in 5 mL of PBS. The complexes were stored at 4 °C until utilization.

ES.14 Sample Preparation for Raman analysis

- *Pseudomonas cells:* $4 \cdot 10^9$ cells were put on polylysine (PLL) coated CaF_2 slides and fixed by drying.
- *p9b phage clone:* 50 µL of phage suspension were put on PLL coated CaF_2 slides. The sample was allowed to dry in air.
- *Phage/AuNPs*: 50 µL of phage/AuNPs network suspension were put on PLL coated CaF_2 slides. The sample was allowed to dry in air.
- *Pseudomonas cells + phage/AuNPs:* $4 \cdot 10^9$ cells were put on PLL coated CaF_2 slides fixed by drying. After three washing steps with PBS, cells were incubated with 50 µL of Ag-phage network for 1h at 37°C. After incubation period, sample was washed thrice to remove unbound phage clones and then allowed to dry in air.

Before micro-Raman measurements, all samples were washed twice in PBS, and once in ultrapure water, to remove any crystals of salts after drying.

Micro-Raman spectroscopy measurements were carried out in the 200–1800 cm^{-1} range by the Horiba XploRa spectrometer. The 532 nm (2.33 eV) laser line was used as the excitation source. An acquisition time of 80'' and 3 accumulation times are the optimize parameters adopted to allow a sufficient signal/noise (S/N) ratio, without damaging the bacteria. The experimental reproducibility was assured by carrying out every single analysis in triplicate.

ES.15 Isoelectric point prediction

ExPASy tool (https://web.expasy.org/protparam/) bioinformatics tool was used to presume molecular weight, theoretical pI, amino acid composition, atomic composition, extinction coefficient, estimated half-life, instability index, aliphatic index and grand average of hydropathicity (GRAVY) of the amino acid sequence of the peptide.

ES.16 Binding of Phage to Polymeric Surface and Capture of Bacteria Target

Polymeric surfaces (1cmx1cm) mica, APTES and PEI were functionalized using physisorption protocol described previous work [Carnazza et al., 2008; De Plano et al., 2017]. Phage suspensions in ultrapure water at pH7 and Tris-buffered saline (TBS) (Tris hydrochloride (7.88 g/L) and sodium chloride 140 mM (8.77 g/L) at pI of the bacteriophage, 4.2, 6.3 and 5.4 for pC89 vector, P9b and St.au9IVS5, respectively. The organization of the physisorbed phage layer on the surface was analyzed by AFM analysis. AFM measurements were carried out in tapping mode by using a Nanoscope IIIA-Multi Mode AFM (Digital Instruments, Santa Barbara, CA, USA). A negative control, consisting of surface functionalized with pC89 vector was also analyzed. A culture of *P. aeruginosa* or *S. aureus* in PBS at $\approx 4 \times 10^6$ CFU/mL were pre-labeled with DAPI fluorochrome, then was incubated for 15' at RT with the functionalized surface; washed for three times and observed by fluorescence microscopy (Leica DMRE). Sequential digital images of cell binding were acquired using a CCD camera (LeicaDC300F)

and cells number estimated by Scion Image Software (Windows version of NIH Image Software), in terms of integrated density (I.D.).

ES.17 Inhibition test by phage clones on broth culture

Pseudomonas aeruginosa ATCC27853, was cultured in Mueller Hinton Broth (beef infusion solids 2 g/L; Starch 1.5 g/L; casein hydrolysate 17.5 g/L), a liquid medium for antibiotic susceptibility studies. Minimum Bactericidal Concentration (MBC) was determined increasing aliquots of 20 µL phage clone, ranging between 10^8 vir/mL – 10^{11} vir/mL, in decimal scalar dilutions. Total of 200 µL of semi-exponential cultures, ranging between 10^2 CFU/mL – 10^5 CFU/mL, were deposited in wells of 96-well plate (8 replicates per condition). Each plate was incubated in gentle shaking (100 rpm, orbital shaker KS-15, Edmund Bühler GmbH) at 37 °C for 18 h. In order to verify the possible bactericidal activity, abacteria culture without phage clone, as positive control was prepared in the same conditions. In all cases, bactericidal activity is determined by Colony Forming Unity (CFU) and expressed as bacterial viability percentage, compared to positive control. Briefly, 100 µL aliquots of bacterial suspension were serially diluted in 900 µL aliquots of sterile Phosphate Buffer Saline (PBS). From each dilution, 100 µL were spread on solid medium and incubated overnight at 37 °C. After incubation, colonies in the range 30-300 were considered to determine the number of CFU, which was calculated as follows:

$$\mathrm{CFU} = \frac{(\text{number of colonies})}{\text{volume (0.1 mL)} \times \text{dilution factor}}$$

Statistical analysis: one way ANOVA was used to analyze difference among groups by PRISM software (GraphPad), and difference was regarded significant if $p < 0.05$.

ES.18 Inhibition test by phage clones of bacteria adhesion

The inhibition of biofilm formation was assessed using methods according to [Haney E.F et al 2015]. Briefly, 100 µL of a bacterial suspension (final OD_{600} = 0.01, ranging between 10^4 CFU/mL – 10^5 CFU/mL), prepared by diluting an overnight culture grown in LB broth into the medium of interest, was added to the wells of a 96-well polystyrene microtitre plate, and incubated at 37°C under static conditions to allow for bacterial growth and biofilm maturation. 10 µL of phage clone at MBC value (10^{11}vir/mL), or 10 µL of phage control (pC89 wild-type) were added at times 0, 2, 4, 8, 24 and 72 h after biofilm stimulation. At final 6 days, bacterial growth was quantified by recording OD_{600} of each well using an Epoch Microplate Spectrophotometer (BioTek Instruments Inc., Winooski, VT, USA). The planktonic cells and the spent medium were discarded, and the adhered biomass was rinsed three times with distilled water. The biomass was stained with 0.1% CV solution for 20' and then rinsed three times with distilled water to remove unbound dye. The bound CV dye was resuspended in 70% ethanol with gentle mixing and the OD_{595} was recorded in the same sample plate. The amount of biofilm inhibition was calculated relative to the amount of biofilm that was grown in the absence of phage clones (defined as 100% biofilm) and the media sterility control (defined as 0% biofilm). Results from at least three separate biological replicates were averaged.
Statistical analysis: one way ANOVA was used to analyze difference among groups by PRISM software (GraphPad), and difference was regarded significant if $p < 0.05$.

CHAPTER 3
Amyloid Mimotope from Phage Display: State/Stage Diagnosis and Therapy in Alzheimer's Disease

Alzheimer's disease (AD) is the most common form of dementia and is a leading cause of morbidity and mortality worldwide. In the population of most industrialized countries, AD cases are rapidly increasing with the ageing society, thus there is a crucial need for new methods for early diagnosis and prevention [Jack et al., 2018]. Actually, diagnosis of AD consists in the combination of neuropsychiatric tests and laboratory assay for the positive biomarker identification of both amyloid and pathologic tau in biological samples. These screening is not enough to correct characterization of the AD, due to the false-positive that are associated ad different neurodegenerative disease, such as Parkinson, Scleroses multiple etc. Therefore, the most accurate AD diagnosis remains the identification of AD plaques in the brain *post-mortem* [Petersen, 2018].

For this, many research groups are focused on biomarkers discovery in a non-invasive way, thought the investigation levels of antibodies binding amyloid-β (Aβ) in biological fluids, such as cerebrospinal fluid (CSF), saliva, urine and blood [Thambisetty and Lovestone, 2010; Blennow and Zetterberg, 2009]. However, the results of these studies are contradictory or inconsistent due to several factors affecting the detection of specific Aβ-IgGs such as the circulation of Aβ-autoantibodies both in free and antigen-bound forms and as several structural conformations of Aβ42. In fact, some author reported high levels of anti-Aβ-IgGs in subjects with AD compared to healthy controls [Mruthinti et al., 2004], whereas others, on the contrary, showed a reduction of anti-Aβ-IgGs in AD patients [Qu et al., 2014], or even no difference [Baril et al., 2004].

The Aβ has a plastic structure able to form aggregates of different conformation, indeed, its polymorphism lead to assume several β-sheets conformations [Kodali et al., 2010]. Therefore, it is reasonable to assume that the deposition of diverse misfolded amyloids

can self-assemble and generate new epitopes (e.g. discontinuous or conformational epitopes derived from amyloid-based aggregation), that could induce an immune response. These epitopes, specific for many types of amyloid fibrils can be identified from conformation-dependent antibodies, regardless their amino acid sequence [Kayed et al., 2007; Yoshiike et al., 2008]. These antibodies, although not specific, can likewise recognize other proteins with similar amyloid conformation. Consequently, the detection in AD patients of antibodies against conformational epitopes of the aggregation states of the amyloid fibrils could be very useful, in order to define the state/stage markers of the disease. Since both the antigen and the antibody are unknown, this objective is difficult to fulfill. In this research, the use of phage peptides libraries is advantageous to find antibody ligands with partly or completely structures unlike to the native antigen [Knittelfelder et al., 2009].

In the present chapter is described "double binding" selection approach forisolation of phage clones displaying conformational structures similar to fibrillar Aβ42. The approach consists in a preliminary research and identification of other proteins with region conformational similar to Aβ fibrils by using of bioinformatics tools. From this analysis, an epitopic region of *Yersinia pestis,* F1 capsular antigen, was chosen for the significant structural homology with fibrillar Aβ42. Then mAbYPF19 (**m**onoclonal **a**nti**b**ody anti ***Y****ersinia* ***p****estis* **F1** antigen) were used as primary target to restrict the phage display library to phage clones with peptide mimotope to Aβ42-like structure. Restrict phage display library was, finally, selected against IgGs of a pool of sera from AD patient, in order to select phage clones recognized by both IgG from AD-sera, named IgG AD and mAbYPF19 ("Double Binding" screening).

Among the most reactive selected phage pool, 12III1 phage clone was found to significantly enhance inhibition in vitro of Aβ fibrillation as well as disaggregation of preformed fibrils, compared to wild-type vector pC89 without peptide, in SH-SY5Y

neuroblastoma cell line. Moreover, this phage used in E.L.I.S.A. assay, was found significantly discriminate AD-IgGs levels between sera of AD and in healthy subjects, as well as in AD-IgGs levels to have a good correlation with the state progression of the disease, giving significant impact in the AD state/stage diagnosis.The significant results obtained has led to require a patent of the displayed peptides on the selected phage clones.

3.1 "Double Binding" selection of phages displaying conformational peptides

The bioinformatics planning was performed for the identification of amyloid-like structures "common" to Aβ fibrils. By UniProtKB tool (https://www.uniprot.org/) 47 proteins were found to be Aβ42-like template proteins. However, the next analysis has led to exclude, the proteins uncharacterized, without identified 3D structure, belonging to infectious agents involved in common human diseases or commensal bacteria of human microbiome, then only F1 capsular antigen (Caf1) of *Yersinia pestis* and fibrillar Aβ42 was identify like good template. This identification not surprising because similar amyloid oligomer conformations were found in several bacterial, yeast, human and mammalian proteins, suggesting that they share a common structure, the so-called amyloid oligomer conformation [Yoshiike et al., 2008]. The F1 capsular antigen includes linear fibers of monomers subunits (Caf1) assembled via the chaperone/usher pathway [Zavialov et al., 2003; 2005]. The 2.2 Å resolution crystal structure of the ternary Caf1M:Caf1:Caf1N complex revealed that Caf1 is an incomplete β-sandwich immunoglobulin-like fold [Soliakov et al., 2010; Zavialov et al., 2003]. The final stable fold is the result of replacement of the chaperone parallel β-strand by the "spare" anti-parallel β-strand from the N terminus of the subsequent subunit, thus linking them to form a chain. Similarly, it is known that the 3D structure of the Aβ42 protofilament is

formed by two stacked, intermolecular, parallel, in-register β-sheets that perpetuate along the fibril axis [Lührs et al., 2005]. On the other hand, it is well known that Aβ amyloid exists in several polymorphs with varying width and helical pitch, different cross-section profiles and different interactions between the monomers [Gremer et al., 2007]. F1 antigen (UNIPROT ID: P26948) in 3D protein structure (identify with PDB ID number 1p5u, 1z9s, 3dos, 3dpb, 3dsn) were used to verify the conformational match with Aβ amyloid fibril structures (2NAO).PDB&fold (section in EMBL-EBI tool http://www.ebi.ac.uk/msd-srv/ssm/) showed the alignments distant in amino acids primary sequence but contiguous in the 3D structure. Moreover, RCSB Sequence & Structure Alignment tool (https://www.rcsb.org/pages/analyze_features#Sequence) identify the 3D alignment in immunogenic F1 capsule antigen and different amyloid fibrils. The conformational homology found between the different forms taken by F1 capsular antigen and Aβ42 fibril confirms the non-probability that these are randomly similar (**Figure 1**).

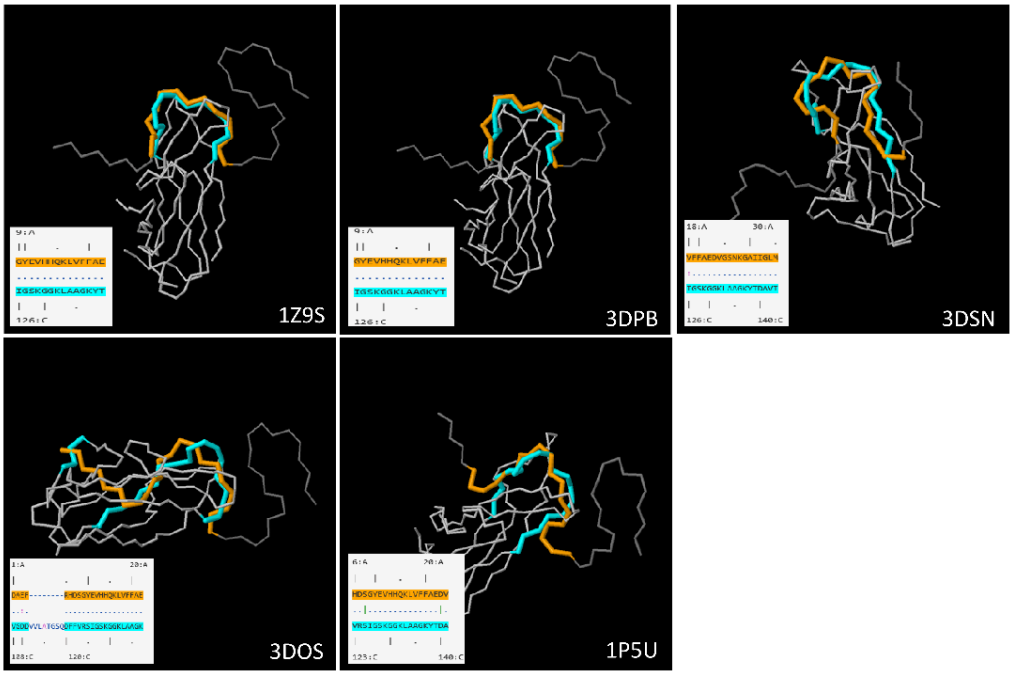

Figure 1. 3D conformational alignments between 2NAO amyloid fibril and different 3D F1 capsule antigen structure identify with PDB ID number 1p5u, 1z9s, 3dos, 3dpb, 3dsn. The chains of 2NAO (chain A: orange) and 3p5u (chains C: light blue) involved in the homologies of the immunodominant region.

In particular, the match between the structures was observed in the immunodominant and highly immunogenic sequences of F1 protein, region 121-144 amino acid position of the chain B and C, which is recognized by a high amount of antibodies raised against the native F1 antigen [Sabhnani,and Rao, 2000]with regions of Aβ42, 1-DAEF--------RHDSGYEVHHQKLVFFAE-22 (with 3dos.C), 9-GYEVHHQKLVFFAE-22 (with 1z9s.C, 3dpb.C) and, 18-VFFAEDVGSNKGAIIGLM-35 (with 1p5u.C, 3dsn.C), comprised in the main Aβ epitopes for immunoglobulins and involved in the formation of proto-filaments (1-16) [Frenkel et al., 1998; 2000] and for "plaque-specific" antibodies inhibiting both Aβ fibrillogenesis and cytotoxicity (4-10) [McLaurin et al., 2002], moreover, the region Aβ(21–37), recognized by "fibril-inhibiting" Aβ-autoantibodies. [Przybylski et al., 2006; Dodel et al., 2018].

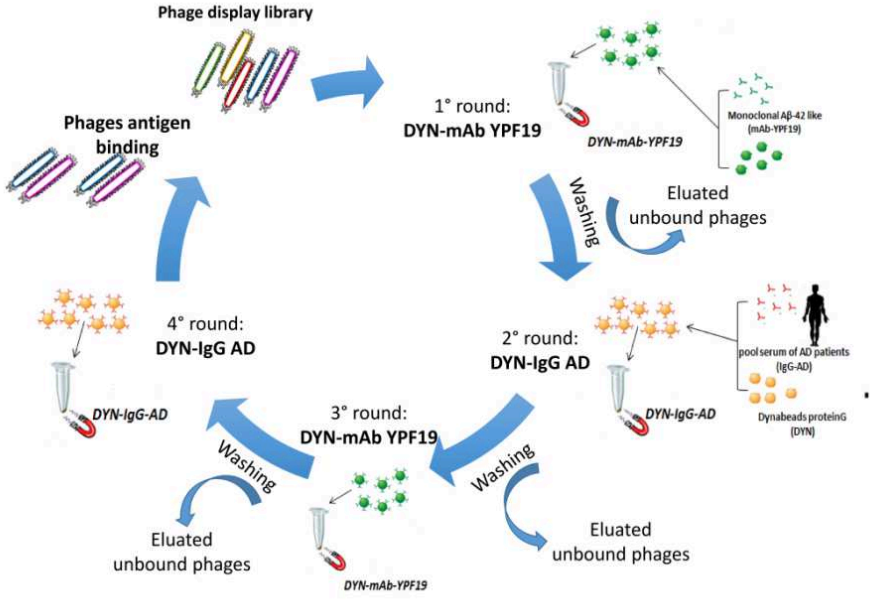

Figure 2. "Double Binding" screening of pVIII-phage display random peptide library IgG-AD andmAbYPF19. Dynabeads, functionalized with IgG-AD (DYN-IgG-AD) or mAbYPF19 (DYN-mAbYPF19) and blocked for with PBS pH 7.4-5%-not fat milk-0.05% Tween 20, were used in "double-blinding" with human sera pool IgG-AD and mAbYPF19 in order to isolate phage expressing common sequences recognized. Briefly, four selection cycles were performed. In the first round, the phage population select were capable of binding the mAb YPF19immobilized on the beads. The eluted phages in this step are used in the second selection round for screening against IgG-AD. In this case, only phage clones which cross react also with mAbYPF19 will have the possibility of binding the target, so as to limit the number of reactive phages to those common to the two antibody classes IgG-AD and mAbYPF19. A third biopanning cycle is then carried out, with the eluted phages from the second selection round, against the mAbYPF19 again, and finally a fourth against IgG-AD, in order to select phage pools having more affinity for the latter.

On the base of these analyses, F1 was considered as protein with amyloid oligomer conformation. Then, M13 pVIII-12-aa and pVIII-12-cys-aa phage random peptide library were screened to find "conformational mimotopes" of Aβ42 fibril able to recognize AD-IgG by circulating antibodies in AD patients. The **m**onoclonal **a**nti**b**ody anti ***Y****ersinia****p****estis***F1**antigen (mAb YPF19) is used in a "double binding" selection as stamp to restrict the libraries at the misfold amyloid-like epitope then pool of five AD sera IgGs is used to select against natural amyloid misfold epitope. In particular four rounds were performed: in the first round, the phage library was screened against mAb YPF19, then eluted phages (restricted Caf1 library), were used in the second selection round against a pool of sera from patients' AD (IgG-AD). A third round was carried out against the mAb YPF19again, and finally with IgG-AD (**Figure 2**).

Antibodies-associated phage isolated by acid elution in each biopanning cycle were separately amplified in *E. coli* strain TG1 and used for subsequent rounds of selection. After each round of selection, the yield of phage eluted from the DYN-antibodies was determined prior amplification (**Table 1**).

ROUND	12aa-cys			12aa		
	IN[a]	OUT[b]	YIELD[c]	IN[a]	OUT[b]	YIELD[c]
I. (against mabYPF19)	3.5×10^{12}	3.3×10^{7}	9.43×10^{-6}	1.5×10^{12}	1.3×10^{7}	8.67×10^{-6}
II. (against AD IgGs)	1.45×10^{13}	4.2×10^{9}	2.9×10^{-4}	1.7×10^{13}	2.65×10^{9}	1.56×10^{-4}
III. (against mabYPF19)	3.6×10^{12}	3.65×10^{8}	1.01×10^{-4}	5.32×10^{12}	8.25×10^{8}	1.55×10^{-4}
IV. (against AD IgGs)	8.75×10^{12}	2.75×10^{9}	3.14×10^{-4}	1.8×10^{12}	1.5×10^{9}	8.33×10^{-4}

Table 1. yields of "double-binding" selection of M13 PVIII-12aa and PVIII-12aa-cys phage display libraries. [a]input quantity of engineered bacteriophages at the start of the biopanning process. [b]quantity of phage recovered at the end of each selection round. [c] input to output ratio to indicate the number of bacteriophages remained bound to the selection target.

Phage clones selected were tested in indirect E.L.I.S.A. assays using both mAb YPF19 and AD sera. All the clones resulted the most reactive compared to the pC89; however, between them 12III1 was significantly reactive, suggesting that displayed peptides likely miming conformational epitopes recognized by circulating IgGs from AD patients but also by the mAb YPF19(**Figure 3**).

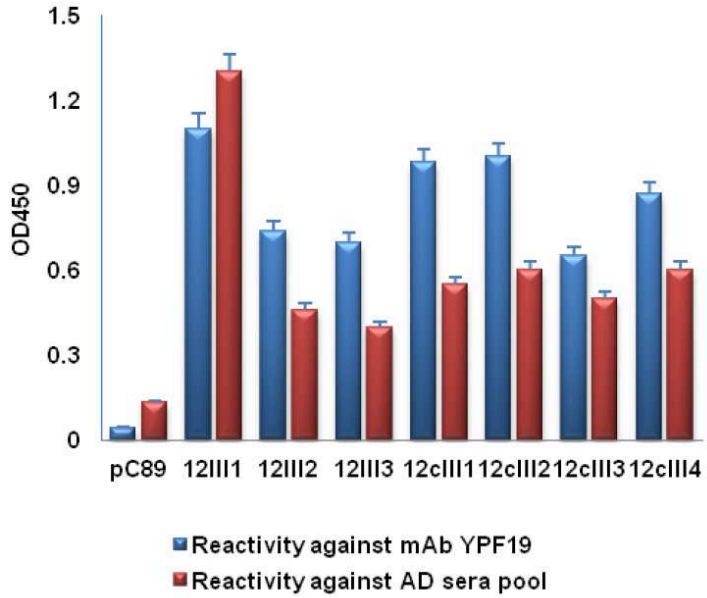

Figure 3. E.L.I.S.A. reactivity of phage clones isolated by "double binding" selection against mAb YPF19 and pool of AD sera.

3.2 *In silico* docking view of selected phage with Aβ-42 fibril

12III1 displays sequence RWPPHFEWHFDD, was verified in the conformational mimotope by three-dimensional alignment using Pepsurf and Mapitope tools. The algorithm for the prediction of epitopes deriving from combinatorial phage-display libraries elaborated a picture with confirms that the best 3D alignment cluster for 12III1 peptide on Aβ fibril is in 3-EFRH-6 (**Figure 4**), region of homology also obtained for Caf1 and Aβ-42.

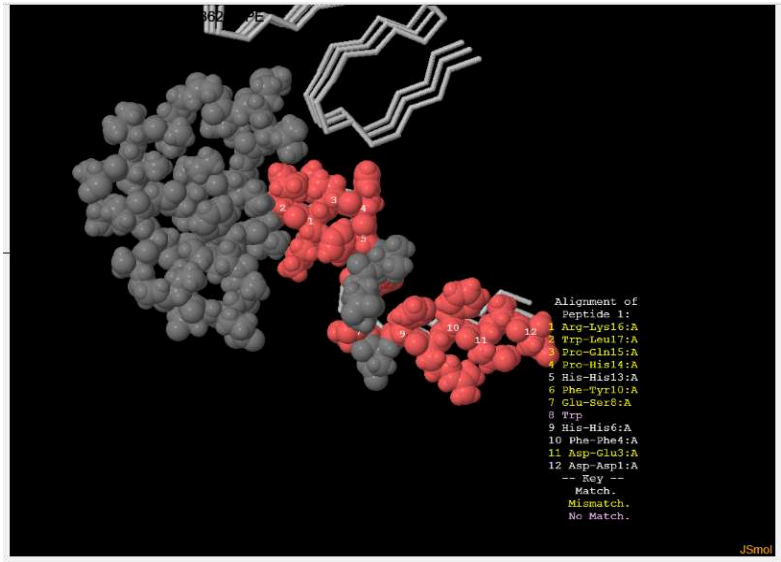

Figure 4. PepSurf analysis results of 12III1 exposed peptide with Aβ42 (PDB ID 2nao chain A, library type. Random _AA) Alignment with highest score 656.675; P-value: 0.00244419.

In the context of the whole phage capsid (model build like described in material and method) the pVIII-displaying peptide RWPPHFEWHFDD was modeled using MODELLER software and used in molecular docking with Aβ42 (PDB ID: 2nao)(used to perform the bioinformatics analysis before the "double binding" phage cycle) (**Figure5**). The probable regions of interaction between the two proteins are better detailed in the **Tables2 and 3**, where are indicated all the amino acid position involved in the contact (**Table 2 and 3**).Also in this view the data confirm that the interaction involved the amino-acids of the region Aβ (21–37), recognized by "fibril-inhibiting" Aβ-autoantibodies and comprised in the main Aβ epitopes for immunoglobulins and involved in the formation of proto-filaments (1-16) like describe above for the interaction involved with the Caf1. Moreover, peptide plays an important role in the interaction acting mainly with the negative amino acids which phenylalanine, proline, tryptophan and glutamic acid; and with positive amino acid histidine and glutamine **(Table 2 and 3).**

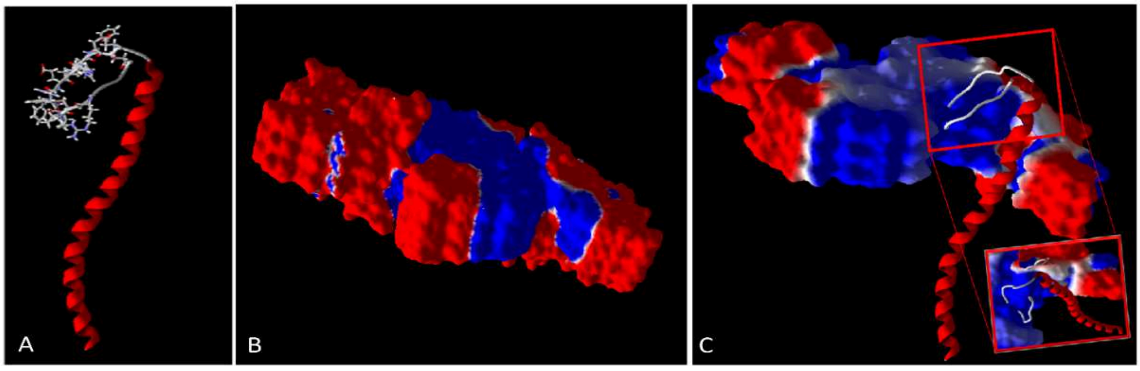

Figure 5. *in silico* models of 3D molecule and docking view.
(A) 3D model of the 12III1 pVIII built using Modeller software in backbones style with highlight the peptides in wireframe style. (B) molecule 3D of the fibril amyloid (2NAO) in surface style (C) the molecular docking view of the fibril amyloid (2NAO) in surface style and the 12III1-pVIII in backbones style. The amino acids involved in the interaction are listed in the **Table 2 and 3.**

Fibril βamyloid Chains	Stearic Interaction	Electrostatic Interaction
Chain A	none	None
Chain B	Phe (11)*	none
Chain C	Trp (7)*, Pro(8)*, Pro (9), His (10)*, Phe (11)*.	none
Chain D	Tyr (35), Ile (36), Tyr (38).	Glu (34).
Chain E	Phe (11)* , Ala (32)	none
Chain F	Pro (9)*, His (10)*, Phe (11)*, Glu (12)*, Trp (13)*, Ala (24), Phe (25), leu (28), Gln (29).	His (10)*, Glu (12)*

Table 2. Amino acids of 12III1-pVIII model involved in the interaction with Fibril βamyloid. *amino acids belonging to peptides displayed in 12III1-pVIII. None: no interaction.

Type of interaction	Chain A	Chain B	Chain C	Chain D	Chain E	Chain F
H-bound	none	none	Gly (37) Gly (38)	none	none	His (14) Gln (15)
Stearic interaction	none	Met (35) Val (36) Gly (37)	Met (35) Gly (37) Gly (38) Val (39) Val (40)	Phe (4) Glu (11) Val (12) His(13) His (14)	Phe (4), His (14)	Phe (4) His (6) His (14) Gln (15) Tyr (10) Lys (16) Leu (17)
Electrostatic interaction	none	none	none	His (14)	none	none

Table 3. Amino acids of fibril βamyloid chains involved in the interaction with designed 12III1-pVIIIl. Interaction between fibril amyloid (2NAO) and the designed 12III1-pVIII, fractionated in H-bound, Electrostatic and Steric interaction. None: no interaction.

3.3 *In vitro* 12III1 inhibition and disaggregation of Aβ42 cytotoxicity

It is showed that highly purified preparations of native M13 potently and broadly mediate binding to and disruption of a variety of misfolded protein assemblies, including Aβ, α-synuclein, tau and yeast prion Sup35 [Krishnan et al., 2014]. Indeed, it has been descripted that filamentous M13 phage can mediate disruption of amyloid assemblies [Dimant et al., 2009; Dimant and Solomon 2010; Messing, 2016] through a bound with the middle and C-terminal residues of the Aβ subunit [Krishnan et al., 2014]. This interaction was considered conformational and not protein primary sequence dependent, because three different amyloid fibers resulted as targets for M13-mediated binding and remodeling. [Messing, 2016]. Phage uses TolA-C binding sequences of pIII to recognize and bind the canonical amyloid fold, inducing binding and disruption of amyloids by its two N-terminal domains as a general amyloid

interaction motif (GAIM). Considering the data reported in the literature, in order to verify the effect of exposed peptide on the pVIII of the engineered 12III1against Aβ42, also phage wild-type, i.e pC89 vector, were used *in vitro* testes. Aβ42 showed in vitro on cell type used in the test a cytotoxicity of about 60%; phage clones by themselves showed no cytotoxicity *in vitro* on SHSY-5Y cells at any time tested (data not shown). In the inhibition of Aβ-amyloid aggregation, the 12III1 phages allowed significantly reduction Aβ42-induced cytotoxicity at all the phage concentrations used. In comparison, wild-type vector pC89 showed a lower inhibition of Aβ42-induced cytotoxicity than 12III1 phage at all the assayed titers (**Figure 6**).

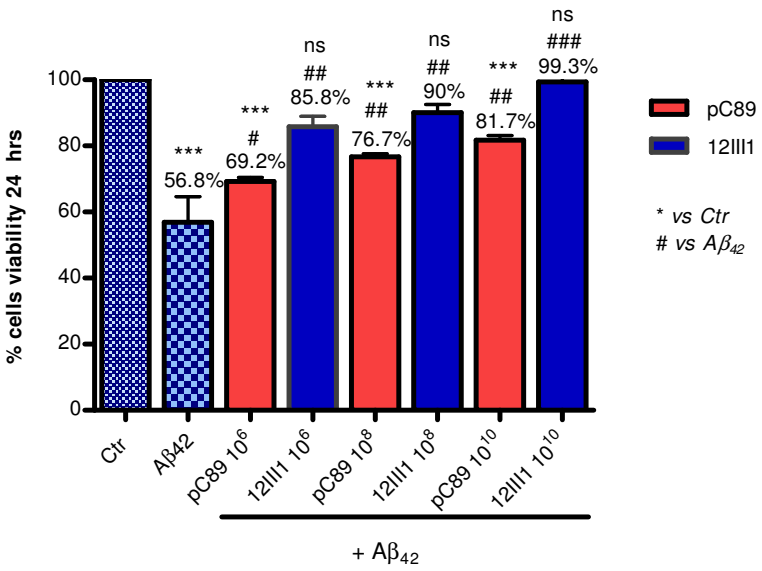

Figure 6. Inhibition of Aβ42-induced cytotoxicity at increasing concentrations of 12III1 recombinant phage clone and wild-type vector pC89, as evaluated in SHSY-5Y cell viability in vitro test.

Moreover, when phages were added after 3h and 6h of the Aβ stimulation, 12III1 phage increased cell survival about 23% after 3h and 6h. Instead, wild-type vector pC89 showed no significant activity after 3h that increase in the cell viability, about 18%, when added after 6h of the Aβ stimulation (**Figure 7**).

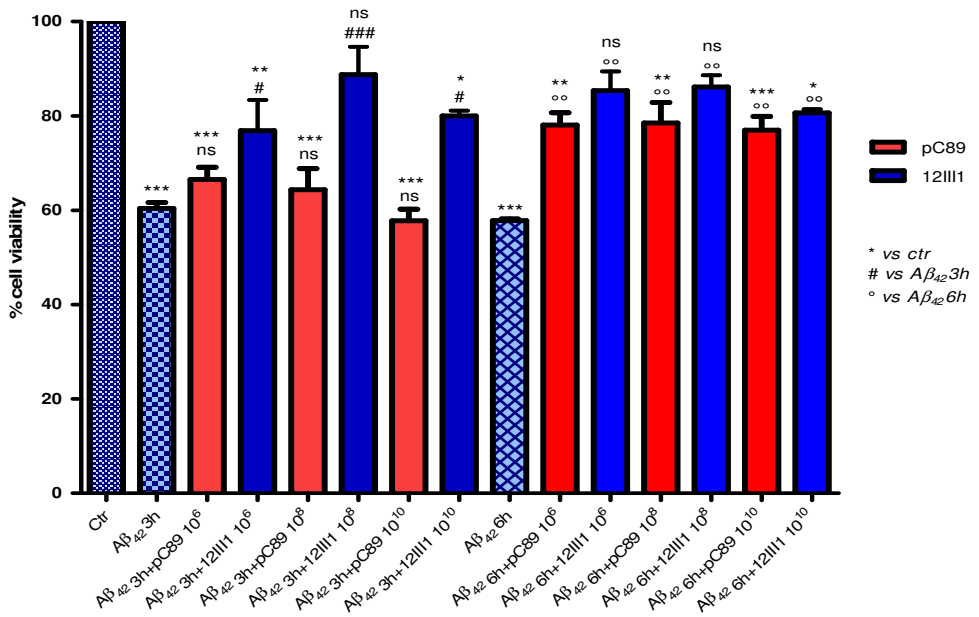

Figure 7. Reduction of Aβ-amyloid cytotoxicity in SHSY-5Y cell viability in vitro test after addition of wild-type vector pC89 and 12III1 recombinant phage clone, at 3h and 6h following Aβ-stimulation.

In any case, 12III1 showed a significant enhancement of activity in both inhibition and disaggregation of Aβ42 amyloid fibrillation. The natural ability of the pIII of wild type phage to interact with Aβ explained the inhibition capacity on Aβ cytotoxicity observed against human SH-SY5Y cells. However, data suggest that 12III1 displaying also peptide in the pVIII able to interact with Aβ increases affinity to Aβ fibrils. Probably, the peptides on pVIII could confer at the phage the ability to interact with Aβ-amyloid fibrils in a different conformational stage then pIII coat protein.

3.4 E.L.I.S.A. diagnostic assay for Alzheimer's biomarkers identification

The selected clone, 12III1, was used like probe for specific IgGs discrimination between AD and healthy human sera samples. The clinical criteria used for diagnosis of AD, without the current possibility to analyze how serum IgG levels were related to biomarkers such as Aβ deposition or tau-mediated neuronal degeneration. Firstly, the E.L.I.S.A. assay was optimized using several phage concentrations (1×10^{12}, 1×10^{11},

1×10^{10}) adsorbed onto 96 microwells E.L.I.S.A. plates and reciprocal sera dilutions at 1:10, 1:50, 1:100 (data not shown), with 12III1 phage clone and wild-type vector pC89. Optimal phage binding was found at 1:50 sera dilution and at 10^{11} phage clone concentration. Therefore, the average of the data obtained with wild-type vector pC89 was used to calculate an arbitrary cut-off value (CO). Sera that showed an absorbance value less to 0.398 (CO= N×3, where N is the average value of pc89) were considered as not responsive for 12III1.

Then, preliminary study on 55 serum samples, 29-AD and 26-CTR, showed that the 12III1 phage clone, as antigen target, was able to discern IgG sera of patients with AD from control group without dementia signs (**Figure 8**).

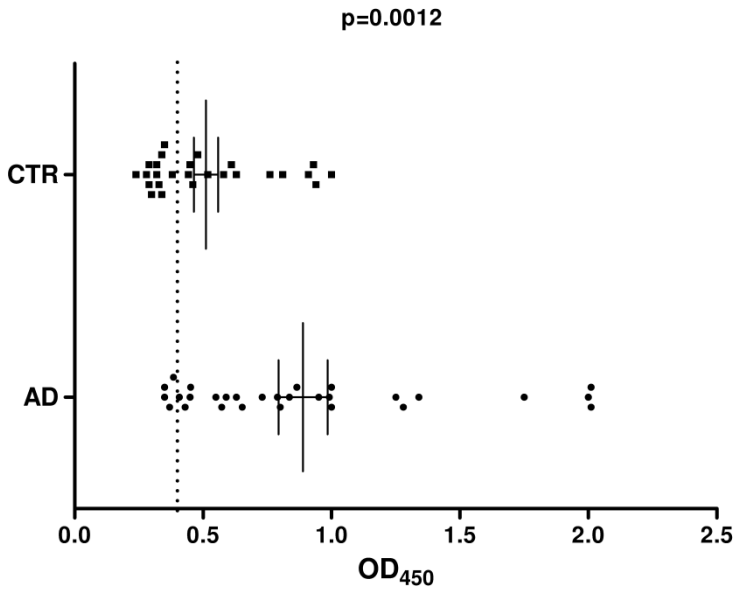

Figure 8. **Antibody binding to 12III1 phage clone in serum samples from patients with AD (n =29), and healthy individuals (CTR) (n= 26).** The dashed line represents the cutoff for positive binding (N×3, where N is the average value of pc89). Data are reported as absorbance at 450 nm.

The data showed IgG levels in AD patients significantly higher than in healthy controls (mean AD=0.89 CTR=0.51, with a p-value=0.0012, R2 0.18), providing a significant level of discrimination between diseased and non-demented subjects. In particular, 25/29 AD sera (86.21%) and 14/26 CTR sera (53.85%) have IgGs recognized by 12III1

phage clone, whereas in 4 AD patients (13.79%) and in 12 control subjects (46.15%), IgG levels were below the wild-type cut off value.

Four of the control subjects, without apparent clinical AD signs, display a relatively high level of antibodies (similar to AD patients). This may represent a possible false positive result, probably due to the cross-reaction of non-AD associated antibodies with this mimotope. In alternative, this could represent pre-symptomatic detection of developing disease. On the other hand, four of AD patients were negative this could be due to an incorrect diagnosis of Alzheimer's disease. In fact, more recent clinical studies have demonstrated biomarker evidence of "suspected non-Alzheimer disease pathophysiology" (SNAP) causing amnestic type cognitive impairment with substantial hippocampal atrophy but lacking detectable ß-amyloid amyloidosis [Caroli et al., 2015]. Indeed, other proteinopathy has been associated with substantial cognitive impairment that mimicked AD clinical syndrome (i.e. limbic-predominant age-related TDP-43 encephalopathy (LATE) [Nelson et al., 2019]. Since a small group of AD patients had IgG titers overlapping to the control subjects, we evaluated the possibility to find a correlation with the disease stage evaluated on the basis of MMSE values **(Figure 9).**

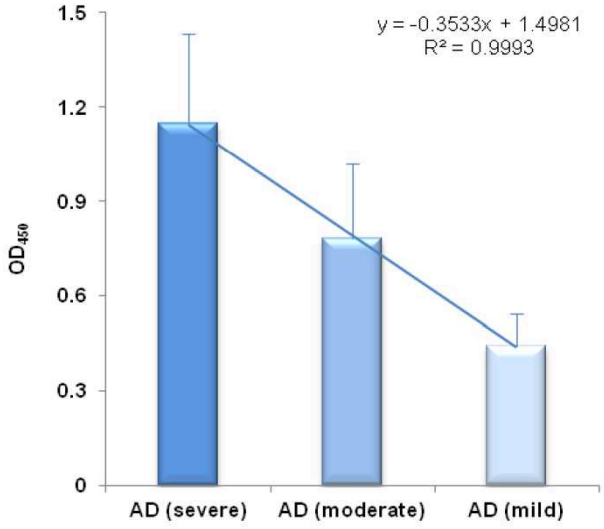

Figure 9. Antibody binding to 12III1 phage clone in serum samples from patients with AD reported as average values of absorbance at 450 nm within three disease stages according MMSE evaluation. Mild dementia: score of 20- 24; Moderate dementia: score 12- 20; Severe dementia: score less than 10. Error bars: standard deviations. The plotted trend line, the regression equation, and the R2 value are showed.

Based on MMSE data, the stratification of AD serum IgGs recognized by 12III1 are low in subjects with mild dementia, while they rise significantly in 88% of patients with moderate AD and they are elevated in all sera with severe Alzheimer, suggesting this phage clone could be used as probe for different Aβ polymorphisms typical of disease progression. It has been reported that serum levels of Aβ-autoantibodies were lower in AD patients than in healthy subjects, [Brettschneider et al., 2005; Qu et al., 2014; Weksler et al., 2002] while others reported either higher values (Mruthinti et al 2004) or no difference [Baril et al., 2004; Hyman et al., 2001]. Our results indicate that IgG levels detected by 12III1 phage clone are significantly higher as the disease progresses, suggesting that these IgG antibodies recognize other epitopes respect to Aβ-autoantibodies detected by several authors (Kayed et al., 2010; Nagele et al., 2010). Similar approach for discovery of IgG serum biomarkers, without prior knowledge of native antigens, and similar results were obtained using the selected synthetic peptoids by Reddy et al (Reddy et al., 2011). These data highlight the ability of this technology to discovery unknown antigen/antibody, mainly requested in self-degenerating disease [Wu and Li]. In fact, the production of high affinity autoantibodies toward targeting self-antigens, mostly belonging to the IgG class, is due to inflammation, then at the successive breakdown of immune tolerance. In the specific, autoantibodies, with unknown role, against a variety of molecules have been associated with AD. Therefore, the increase in knowledge of new unknown epitope conformational could play a key role in the development of more efficient systems in diagnosis than in therapy, as preliminarly confirmed by the results described above.

ES. Experimental Section

ES.1 Bioinformatics analyses

Structural similarity search, to identify Aβ42-like conformational structures, consisted of the following steps:

I. Template selection– using UniProtKB tool (https://www.uniprot.org/). The search was restricted according to the known properties of amyloid oligomer conformations, using settin set: i) field: UniProt KB AC Term: beta strand. ii) field: structure; 3D structure available. iii) field: NOT Homo sapiens (Human) [9606]. iv) field: binary interaction. v) field: NOT function Function CC, enzyme classification, activity regulation, catalytic activity.
II. The 47 proteins identified were screened from the protein that had 3D structures and the proteins not involved in infectious agents, common human diseases or commensal bacteria of human microbiome. Then F1 capsule antigen (UNIPROT ID: P26948) was isolated.
III. Alignments homology were performed between Aβ42and F1 antigen using Clustal X2.11(Gonnet 250 Protein Weight Matrix, Gap opening 10, Gap extend 0.1) and GeneDoc (http://www.psc.edu/biomed/genedoc/) tool to identify similar regions based on physico-chemical properties of side chain amino acids. Then, alignment of 3D protein structure was performed to verify the conformational match of F1 protein with Aβ amyloid structures. The PDB IDs associated to 3D structure of the F1 capsule antigen (1p5u, 1z9s, 3dos, 3dpb, 3dsn) were obtained from Uniprot KB, through the ENTRY code P26948 and excluding which were not in the mature conformation. Then evaluated using PDB&fold (in EMBL-EBI tool) (http://www.ebi.ac.uk/msd-srv/ssm/) and Structure Alignment tool available in https://www.rcsb.org/pages/analyze_features#Sequence, with algorithm JFATCAT rigid in 3D alignment with Aβ amyloid in fibril form (PDB ID 2nao).

ES.2 Human samples

29 sera (15 men and 14 women, mean age 70.7) of patients affected by AD diagnosed according to the criteria of the National Institute of Neurological and Communicative Disorders and Stroke and the Alzheimer's Disease and Related Disorders Association,2 attending the Neurologic Unit of the University Hospital “Policlinico Vittorio Emanuele” in Catania. All AD patients underwent clinical and instrumental evaluations as normal diagnostic workup at the time of their admission. Presence and severity of cognitive impairment was assessed through the Mini-Mental State Examination (MMSE).3 During the admission a serum sample was collected and stored at -80°C. At the time of the admission, patients signed an informed consent allowing further use of the samples for diagnostic or research purposes. 26 healthy controls (12 men and 14 women, mean age 65.3) were recruited from subjects who accompanied patients for hospital check-ups. Healthy controls underwent a standard neurological examination performed by experienced neurologists in order to exclude the presence of neurological disorders and were enrolled in the study only after signed an informed consent. A serum sample was collected at the time of the enrolment and stored at -80°C. The study was approved by the Ethic committee of the Policlinico Vittorio Emanuele of Catania.

ES.3 Functionalization of Dynabeads® Protein G with Antibodies

As source of antibodies directed against possible conformational epitopes of human polymorphic beta-amyloid 1-42 (Aβ42), was use a pool of 5 human sera from patients with AD (IgG-AD) (mean age of 77.4 years, mean value of MMSE = 15.2). The mAb YPF19 (AbDSerotec® A Bio-Rad Company, IgG1-9820-5007) anti-*Yersinia pestis* F1 (reacting to Y. pestis F1 capsular antigen, Uniprot code P26948) was used to screen for putative conformational mimotopes homologous to Caf1 of *Yersinia pestis* which results Aβ42like

conformational structure by bioinformatic analysis. These antibodies were immobilized in Dynabeads® Protein G (Thermo Fischer scientific) super magnetic beads of 2.8 μm. Buffers and reagents were purchased at Sigma Aldrich. 50 μL of Dynabeads® Protein G were washed 3 times with citrate-phosphate buffer under stirring for 10', separated with a magnetic device for 1-2', then incubated with respectively sera pool containing IgG-AD diluted 1:10 and 5 μg of mAbYPF19, for 60' at room temperature (RT) under mild stirring. Dynabeads, functionalized with IgG-AD (DYN-IgG-AD) or mAbYPF19 (DYNmAbYPF19), were separated with a magnetic device for 2', washed 4 times with Conjugation Buffer (20 mM sodium phosphate, 0.15 M NaCl, pH 7-9), separated with a magnetic device for 2' and resuspended in 250 μL of 5 mM BS3 (bis (sulfosuccinimidyl) suberate) at RT for 30'. Crosslinking reaction was blocked by adding 12.5 μL of Quenching Buffer, from 25 mM to 60 mMTris, incubated at room temperature for 15' with inclination/rotation. DYN-IgG-AD and DYNmAbYPF19 were washed 3 times with 200 μL PBST and finally resuspended in 1 mL of storage solution (PBS + 1% BSA + 0.01% Tween 20 pH 7.4). Before using for phage display selection, beads were blocked for 1 h at room temperature with PBS pH 7.4-5%-not fat milk-0.05% Tween 20.

ES.4 Phage peptide library

The M13phage library (kindly donated by Professor F.Felici) expressed random peptides, exposed on the pVIII protein, based on the phagemid vector pC89 on which random oligonucleotide sequences were inserted in the region 5' of the VIII gene present in the vector, under the control of the LacZ promoter. The digestion with the restriction enzymes EcoRI and BamHI linearized the vector and allowed the insertion of the oligonucleotides with random sequences which, flanked by the same restriction sites, allow the recircularization of the vector through ligase reaction. [Felici et al., 1991; Lugazzo and Felici, 1998]. For the selections were used three types of peptide libraries: pVIII-9aa (expressing nine amino acids in the N-termialpVIII), pVIII-12-aa (expressing twelve amino acids in the N-terminal pVIII) and pVIII-12cys-aa (have a cysteine-cysteine constriction expressed in end of the random amino acids sequence, located in the N-terminal pVIII). The amplitude of each library is comprised between 10 and 100 million independent clones.

ES.5 "Double binding" phage display selection

Then M13 pVIII-12aa and pVIII-12cys-aa phage libraries (1×10^{12} viral particles) were pretreatment with 50 μL of Dynabeads® Protein G and resuspended in 190 μL of TBS-Tween 0.1%. After 30' incubation, separate with a magnetic device for 1-2'; the supernatant is recovered and used to carry out again the two preceding steps twice before the use of the library for the selection. The restricted libraries were used in four selection rounds. In the first round, 500 μL of DynabeadsmAb YPF19 were incubated with phage libraries for 3-4 h at room temperature under mild stirring. The beads were washed 3 times in PBS-0.05%Tween 20 and separate with a magnetic device for 1-2' and selected phage clones eluted from antibodies with 500 μL of eluting buffer, 0.2 M of glycine-HCl (pH 2.2) + 0.1% BSA, neutralized immediately with 1 M Tris–HCl pH 9.6. Biopanning affinity selection was repeated in the second round against Dynabeads IgG-AD, then in the third round against DynabeadsmAb YPF19 again, and finally a fourth selection round was carried out with Dynabeads IgG-AD, in order to select phage pools having more affinity for the latter. For each round, the eluted phage pools were amplified by infecting TG1 *E. coli*, purified twice by PEG and used for the next round (**Figure 10).**

ES.6 E.L.I.S.A. binding specificity of the phage clones for the mAb YPF19 and the IgG-AD of the AD pool.

Firstly, filamentous the M13 wild-type, in vector pC89 form (containing no insert) was tested against antibodies used as bait in "double binding" phage display selection. It showed no reactivity against mAb YPF19 (mean 0.045, as the negative control in E.L.I.S.A. assay at every phage titer tested) and a mild reactivity against AD-sera pool (mean 0.1326 in E.L.I.S.A. assay at 10^{11} phage/well) that was used to calculate the cut-off value in serum platforms of E.L.I.S.A. assays with recombinant phage clones obtained by selection. Phage clones at concentration of 10^{12}virions/mL were added in duplicate 100 µL/well into a 96-well microtiter plate (Multisorp, Nunc, Roskilde, Denmark). Plates were left overnight at 4°C, blocked for 2 h at room temperature with blocking buffer (PBS - Tween 20 0.05% - 6% Not Fat milk), and washed in PBS-0.05% Tween 20. 100 µL of mAb YPF19 diluted 1:100 in dilution buffer (PBS - Tween 20 0.1% - 1% Not Fat milk) or 100 µL of AD sera pool diluted 1:50 in dilution buffer were added in duplicate into wells and incubated 1 h at 37 °C under stirring. The plates were washed 10 times as described above and exposed to (HRP)-conjugated anti-human IgG (IgG Fc AP113P) diluted 1:15000 in dilution buffer, or anti-mouse diluted 1:50000, for 1 h at 37 °C under stirring. The plates were washed 5 times as described above and developed with TMB substrate, incubating in the dark for 30'-45' at room temperature, and stopped with 100 µL of 1N HCl. Optical absorbance was recorded at 450 nm (Labsystem Multiskan Bichromatic).

ES.7 *In silico* analysis: Sequence determination and epitope conformation

The most reactive phage clones in E.L.I.S.A. were amplified and their DNA sequenced to determine the amino acid sequences of the displayed peptides. Briefly, the sequencing primers M13–40 reverse (5'- GTTTTCCCAGTCACGAC –3') and E24 forward (5'– GCTAC-CCTCGTTCCGATGCTGTC –3') were obtained from Proligo, Sigma (Milan, Italy). 1 µL of the suspended colony (*E.coli* TG1 infected with phage clone) was added to the PCR reaction tube, containing 49 µL of the following PCR mixture:10 × Mg free reaction buffer (Euro Clone, Milan, Italy) (5vol); 50 mM MgCl2 (Euro Clone) (5 vol); Euro-Taq DNA polymerase (5 units μl^{-1} Euro Clone) (0.5 vol); 2.5 mM dNTPs (Roche) (5 vol); primer M13–40 (10 pmol μL^{-1}) (5 vol); primer E24 (10 pmol μl^{-1}) (5 vol); doubly distilled filter sterilized water (23.5 vol). The PCR was performed by GeneAmp PCR System 2400 (Perkin Elmer, Nor-walk, CT, USA) under the following cycling conditions: one cycle at 94 °C for 5'; 25 cycles at 94 °C for 30 s, 52 °C for 30 s, 72 °C for 30 s; and one cycle at 72 °C for 7'. The PCR products (3 µl) were analyzed by agarose gel electrophoresis (1% wt/vol agarose, Sigma, Milan, Italy) in 1 × TAE buffer. Gel was stained with ethidium bromide, illuminated on a Dark Reader, while DNA bands were visualized by a Kodak imaging system. PCR products were purified by NucleoSpin PCR Clean-up purification Kit (Macherey-Nagel) and sequenced using the M13–40 reverse primer. The DNA sequences were translated into amino acids by the 'translate' program on the proteomics server of the Swiss Institute of Bioinformatics Expert Protein Analysis System (ExPASy [http://www.expasy.ch/]). The amino acid sequences were aligned by the CLUSTALX sequence alignment program (available at [http://www.ebi.ac.uk/clustalw/]).
GeneDoc software (http://www.psc.edu/biomed/genedoc/)was used for visualization edit and analyze multiple sequence alignments of the peptides. Statistical analysis of the insert composition was performed. A list of the primary amino acid sequences of the variable inserts is then compiled in the FASTA format and submitted to a motif-elucidation bioinformatics algorithm called MEME (multiple expectation-maximization for motif elicitation http://meme.sdsc.edu/meme/intro.html).
The epitope mapping algorithm, PepSurf (http://pepitope.tau.ac.il/), was used to map 12III1 peptide onto the three-dimensional protein structure of F1 capsular antigen (chain C of the relative PDB IDs) and Aβ42 (chain A of PDB ID 2nao), and the algorithm Mapitope to map the selected peptide flanked by the sequence of exposed pVIII protein. The GRANTHAM matrix was used since it is based on physico-chemical properties, such as side chain composition, polarity, and molecular volume. The gap penalty accounting for unmatched peptide residues

was set to the default value of -0.5. Library type is random amino acid and the stop codon UAG is read as glutamine (in TG1 bacterial strain this function is encoded by the gene supE which suppresses the UAG stop codon inserting a tRNA-amino acid instead).

ES.8 Building 3D models and molecular docking

Engineered pVIII Protein Structure Modeling was performed using MODELLER9.20 (https://salilab.org/modeller/) a computer program for comparative protein structure modeling. The user provides an alignment of a sequence (target) to be modeled with known related structures (template) and MODELLER automatically calculates a model containing all non-hydrogen atoms. The models were built as reported previously [Webb and Sali, 2014]. Briefly, PDB structure of pVIII protein (PDB ID: 2mjz) was downloaded for M13 phage. In the context of the whole virus particle of 2mjz, pVIII proteins, Chain [1a] have been chosen for modelling the pVIII engineered protein. The pVIII proteins were kept like single pVIII protein in a PDB-format, namely chain A then used like template. The amino acid sequences of engineered pVIII proteins of phage clone, with foreign peptide inside of fourth/fifth amino acids of the pVIII wild-type (more 2 extra residues of Phenylalanine and Glutamine, encoded by the EcoRI site as reported in Felici et al. [1991]) were written in FASTA format and then converted in ALI format.

i) ^{1}AEGDDPAKAAFNSLQASATEYIGYAWAMVVVIVGATIGIKLFKKFTSKAS^{50} for wild-type vector pC89;

ii) ^{1}AEGEF**RWPPHFEWHFDD**GDPAKAAFNSLQASATEYIGYAWAMVVVIVGATIGIK LFKKFTSKAS^{64} for 12III1 (in bold the foreign amino acid sequence).

The scripts of the computer program were modified with the name of the engineered protein and with ID of the molecule template then a target-template alignment is constructed. Successively, MODELLER calculates several 3-D models of the target in PDB format. The best model was selected picking the model with the lowest value of DOPE, which value indicates the construction energy. For each engineered pVIII proteins were obtained the model of the chain A in the capsid context PDB ID: 2mjz.

Molecular docking was performed using Z-DOC online tools. The 12III1-pVIII model was upload like ligand-template, and the PDB ID 2nao (corresponding to the 3D model of the Aβ fibril) upload like template of protein. Then the tool ran, and the output obtained in pdb format.

ES.9 Inhibition test by 12III1 and pc89 on β-amyloid cytotoxicity

Unless otherwise stated, all compounds were obtained from Sigma-Aldrich. All other chemicals were of the highest commercial grade available. All stock solutions were prepared in non-pyrogenic saline (0.9% NaCl, Baxter, Milan, Italy). Aβ1-42was purchased from Tocris Bioscience and was dissolved 1 mg/mL in sterile water. SH-SY5Y cells were purchase from ATCC (CRL-2266™).

SH-SY5Y cells are a cloned sub-line of SK-N-SH cells originally established from a bone marrow biopsy of a neuroblastoma patient with sympathetic adrenergic ganglialorigin.10 SH-SY5Y neuroblastoma cells can be differentiated into neuron-like cells displaying morphological and biochemical features of mature neurons. Furthermore, these cells display axonal expression of mature tau protein isoforms. In the light of this, we found the best overall neuronal differentiation was achieved using retinoic acid (RA) pretreated SH-SY5Y cells as previously described.11 Human neuroblastoma SH-SY5Y cells were obtained from American Type Culture Collection (ATCC CLR-2266) and were grown to monolayer in a culture medium containing Dulbecco's Minimal Essential Medium (DMEM) and Ham's F12, modified with 2 mM L-glutamine, 1.0 mM sodium piruvate, supplemented with fetal bovine serum (FBS) to 10%, streptomycin 50 mg/mL. SH-SY5Y cells were maintained at 37 °C and 5% CO2.

For cell viability tests, 3×104 cells were plated in 96-well plates (Corning Cell Culture) in a volume of 150 μL and differentiated with RA (100 nM) for 24h. In order to test the inhibition of Aβ-amyloid aggregation, different titers (10^{6}, 10^{8} and 10^{10} TU/mL) of 12III1 phage clone or

wild-type vector pC89 were added simultaneously to $A\beta_{1-42}$ peptide 1 μg/mL, and cell viability was assayed after 24h incubation. For evaluation of cytotoxicity inhibition by phages on preassembled Aβ-amyloid, differentiated SH-SY5Y cells were stimulated with $A\beta_{1-42}$ peptide 1 μg/mL for 3, 6 or 12 hours and then, at each time, incubated with the different titers of 12III1/pC89 phage for other 24h.
Cell viability was evaluated by using the mitochondria-dependent dye 3-(4,5-dimethylthiazol-2-yl)-2,5-diphenyltetrazolium bromide (MTT) colorimetric assay as previously described,[12] expressed as % viability *versus* control cells grown in normal culture medium (Ctr). Cultures pre-treated with increasing concentrations of the test compound were incubated at 37°C with MTT (0.2 mg/mL) for 1 h. Medium was removed and the cells lysed with dimethyl sulfoxide (100 μl). The extent of reduction of MTT to formazan was quantified by measurement of optical density at 550 nm with a microplate reader.
Statistical analysis: one way ANOVA was used to analyze difference among groups by PRISM software (GraphPad), and difference was regarded significant if $p < 0.05$.

ES.10 E.L.I.S.A. assay of 12III1 phage clone against single AD and healthy (CTR) subjects sera

29 patients affected with AD with a MMSE index comprised between 22 and 6.8 and 26 healthy non-demented control individuals were recruited, and the samples were tested according to a phage E.L.I.S.A. assay as follows. Indirect E.L.I.S.A. test was standardized for 12III1 clone and pC89 vector, adsorbing on the bottom of the wells logarithmic scale dilutions of phage (1×10^{12}, 1×10^{11}, 1×10^{10} phage final concentrations) and then using 1:10, 1:50 and 1:100 dilutions of sera. The procedure showed to give maximal phage specific binding for all sera used with phage concentration at 1×10^{11} TU/well and serum dilution at 1:50.
Phage preparations were added in duplicate 100 μL/well into a 96-well microtiter plate (Multisorp, Nunc, Roskilde, Denmark). Plates were left overnight at 4°C, blocked for 2 h at room temperature with blocking buffer (PBS - Tween 20 0.05% - 6% Not Fat milk), and washed in PBS-0.05% Tween 20. 200 μL of 1:50 AD/CTR-sera were added and incubated 2 h at 37°C. The plates were washed 10 times as described above and exposed to (HRP)-conjugated anti-human IgG (IgG Fc AP113P) diluted 1:15000 in dilution buffer for 1 h at 37°C. The plates were washed 5 times as described above and developed with TMB substrate, incubating in the dark for 30'-45' at room temperature, and stopped with 100 μL of 1N HCl. Optical absorbance was recorded at 450 nm (LabsystemMultiskanBichromatic). The TBS was used as a negative control for the evaluation of the non-specific binding background. The cut-off value (CO= 0.398) was calculated as $CO = N \times 3$ where N is the average of the data obtained with wild-type vector pC89.
Statistical analysis: one way ANOVA was used to analyze difference among groups by PRISM software (GraphPad), and difference was regarded significant if $p < 0.05$.
No unexpected or unusually high safety hazards were encountered.

Chapter 4
Phage Display for direct detection of Leukemia/Mieloma Cells

Cancer has become the number one cause of death amongst in the World. It can exist in several forms, and can be separated in two macro-classes, liquid and solid tumors. For both of them there is a relative high risk to form chemo-resistant cells and/or to have cytotoxicity for the healthy cells due to chemo-drugs used to kill carcinogenic cells themselves. Therefore, prominent priority in medicine is the necessity to find different approaches for the development of novel methods of early and not invasive detection and/or effective treatments of cancer diseases. In this prospective, identification of tumor-specific ligands is a growing area of research. Tumor-specific binding agents can be used as probe for tumor cell phenotype identification for both diagnosis and therapy applications. However, the choice of binding agents is central for the success of targeting applications.

The use of phage clones, selected by phage-display libraries, not only, could ensure affinity and specificity for the targets of interest, but also be advantageous thanks to the exposition of more receptor binding peptides in one probe (phage-probe), compared to the antibodies, or synthetic peptides [Brown, 2010]. Moreover, the resistance and ductility of the phages could make them useful in the functionalization with biocompatible and conductive materials for the identification of last residue cell in the monitoring of minimal residual disease, often found in neoplasia and disorder in blood. For example, chronic lymphocytic leukemia (CLL), which is characterized from accumulation of neoplastic B cells in the peripheral blood (PB), bone marrow (BM) and lymph nodes (LN), is one the most cause of mortality for its asymptomatic course [Chiorazzi et al., 2005]. However, the knowledge has undergone remarkable changes during the past decade, highlighting that the neoplastic clonal cells exhibit marked

heterogeneity, and that your outgrowth is the major causes of disease progression in CLL (Landau et al, 2013]. These evidences can also relate to other neoplases associated with blood disorders, such as multiple myeloma (MM) that is a cancer of plasma cells characterized by accumulation of clonal plasma cells (PCs). Low levels of CD45 expression, a regulator involved in antigen-mediated signaling and activation of lymphocytes, have been found in myeloma patients with advanced disease, bone lesions and high-grade angiogenesis [Kumar et al., 2005].

These characteristics make difficult to find peptides useful for several "cancer patients" using traditional selection methods.

In this chapter is described:

- An alternative approach "Promiscuous selection", to identify phage clone from peripheral blood mononuclear cells (PBMC) of two patients affected by chronic lymphocytic leukemia (CLL), was performed. The selected clone was analyzed *in silico* comparing the amino-acids sequences of the displayed peptide, for mimotopic homology with known proteins hematological neoplasm-associated.
- Then phage clone was labeled with silicon nano-particles (SiNPs), and Fluorescein isothiocyanate (FITC). The fluorescent phage-complexes obtained were verified in the recognition of the PBMCs targets.
- Finally, *ex-vivo* diagnostic system was proposed using FITC-labeled-phage as probe to detect leukemia cells in whole blood from patients affected by CLL and the bound detected by fluorescent microscopy.
- By same experimental design, other phage clones have been selected for their ability to bind/discriminate myeloma cells from non–myeloma cell.

4.1 "Promiscuous selection" against PBMCs from CLL patients

The heterogeneity of the cells and clones neoplastic of CLL is the first cause of disease progression. In order to find peptide useful for several "cancer patients", able to identify a common, always expressed receptor leukemia-associated, a new scheme of selection was performed.

pVIII-9-aa M13 phage-display peptide library was used in a "promiscuous selection" against peripheral blood mononuclear cells (PBMCs). Firstly, the library was subtracted again the PBMCs from healthy patients, then the depressed library was used to four affinity rounds selection against PBMCs from two patients affected by chronic lymphocytic leukaemia (CLL) (**Figure 1**).

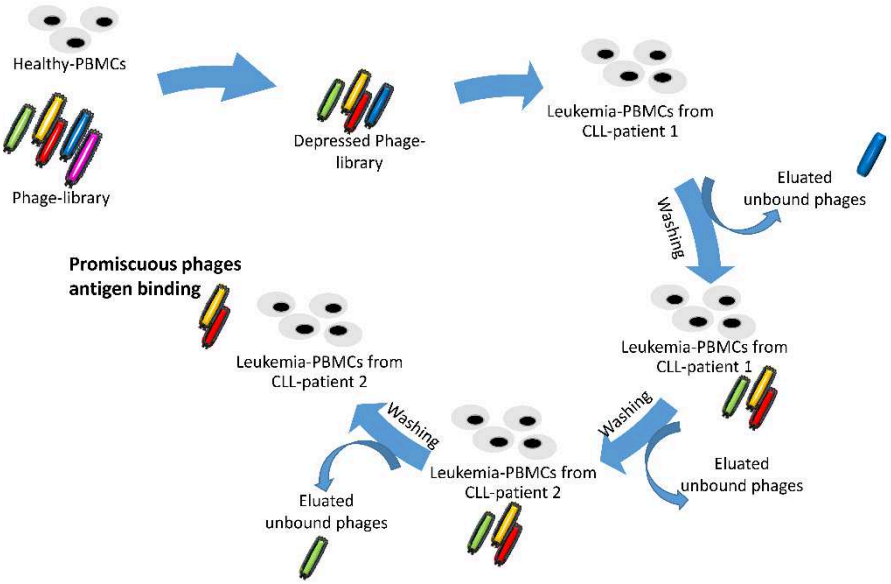

Figure 1. Promiscuous selection. The schema shows the promiscuous selection of pVIII-9-aa M13 phage-display peptide library against leukemic PBMCs. Firstly, the library was subtracted again the PBMCs from healthy patients, then the depressed library was used to four affinity rounds selection against PBMCs from two patients affected by chronic lymphocytic leukaemia (CLL).

The phage clone, named CLL-1, shown the most reactive specific bound with leukemic PBMCs-binding in E.L.I.S.A. assay (data not shown). Therefore, the displayed peptide, ARKMNPPAG, on the pVIII-phage coat were determined from DNA sequencing and translated in the amino-acid sequences, then *in silico* analysed. The primary sequence of the peptide compared to homo sapience sequences collected in BLAST server, show a

statistically significant (about 100% identity in the amino acid sequence query covered) with motif of 182 KDa tankyrase 1-binding protein (**Figure 2**). This data was conferment in the identity of homology by CLUSTALX 2.1 alignment tool (**Figure 3**).

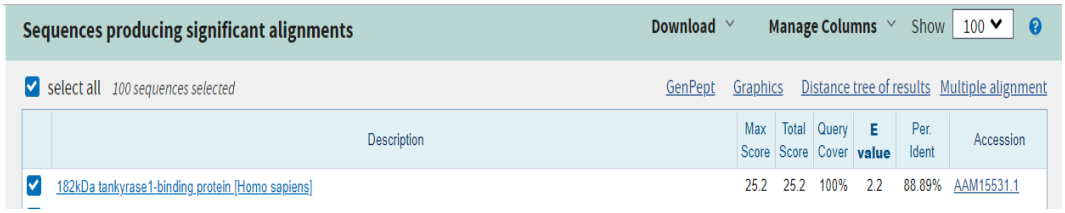

Figure 2. BLAST analysis of the peptides ARKMNPPAG, displayed on the CLL1. The match was performed choose in sequences set: Not-redundant protein sequences; and Humo sapient (taxid: 9606).

Figure 3. CLUSTALX 2.1 alignment. The peptides ARKMNPPAG, displayed on the CLL1, almost entirely aligns with 182KDa tankyrase 1-binding protein (TAB 182).

Tankyrase is a protein, belonging to the ankyrin protein family, with several functions in both the nucleus and the cytoplasm where the majority of tankyrase molecules can be found [Smith et al., 1998; Chi and Lodish, 2000]. The predict target could interacts with several Bcl-2 family proteins in the modulation of apoptosis pathway of the leukemic cells and neoplastic cells. Consequently, it is possible to think that the clones CLL1 could identify neoplastic cells coming from several CLL-patents.

The in vitro ability of the phage to detect CLLs-PBMCs of different samples was described in the next paragraph after the functionalization of the phage with fluorescent markers.

4.2 Fluorescent functionalization of phage-probes

Fluorescence imaging remains the simultaneous real-time technique most used in diagnostic imaging because fast and cheap. The strength is the use of labelled probes,

which permit the development of non-invasive, early, and accurate identification system of biomarkers disease in biological samples such as biologic fluid, serum and blood. In this prospective, the optimization of fluorescent phage-probes has been performed using biocompatible and self-fluorescent silica nanoparticles (SiNPs) and traditional chemical-fluorcrome as Fluorescein isothiocyanate (FITC).

4.2.1 One-step production of phage–SiNPs

Promising candidate to create new biocompatible devices with longer fluorescence lifetime, photo-stability and high resistance to metabolic degradation is silica [Walling et al., 2009]. SiNPs have the potential to permit fluorescence imaging techniques in real-time and noninvasive tests, due to their intrinsically light emission. An "one-step" approach for bio-functionalization of SiNPs based on pulsed laser ablation (PLAL) was exploited [De Plano et al., 2018]. In particular, silicon plate ablation was performed in Tris-buffer-solution (TBS) without phages (**Figure 4)** and with phages **(Figure 5**).

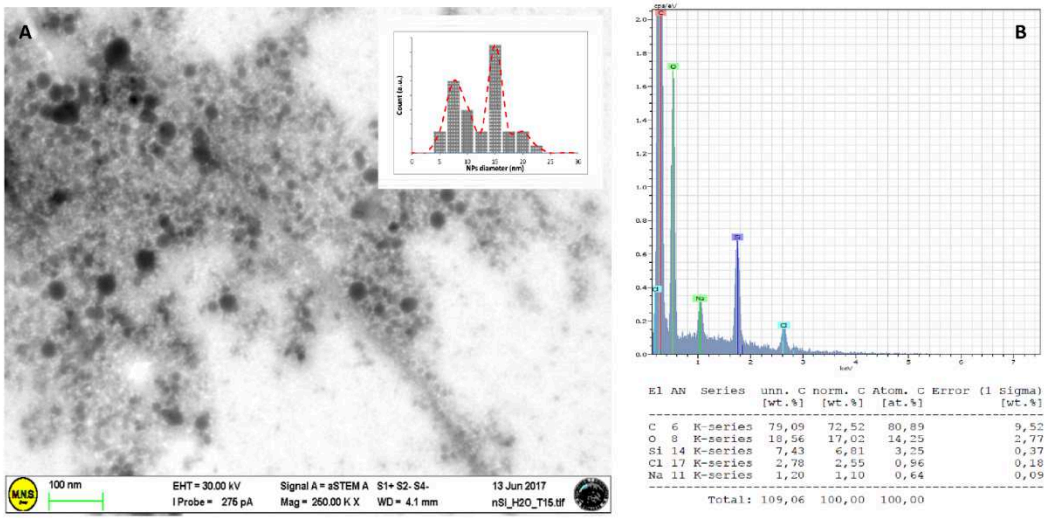

Figure 4. **PLAL of Si in TBS**. (A) Bright-field STEM (BF-STEM) image obtained at 30,000 kV, shows SiNPS obtained from PLAL of Si plate in TBS, and the relative range of size distribution (in the inset) showing the mean diameter of ~ 8 nm and ~ 15.1 nm. (B) EDX analysis of SiNPs.

The broad range of size distribution, between ~8 nm and ~ 15.1 nm (insert **Figure 4**), obtained in PLAL in TBS was due to ions present in the buffer, which exceeding 6 mM NaCl, led to the attractive between nanoparticles then at their aggregation [Chewchinda

et al., 2016]. The consistent presence of oxygen (O) shown in EDX analysis presupposed that the SiNPs performed could be found as amorphous silica (SiOx) (figure 4 B). It was probable because when the temperature is high (above 1050 °C), silicon was brought at the full oxidation [Ulusoy Ghobadi et al., 2016]. Indeed, the temperature in the silicon bulk reached the same temperature during the PLAL, therefore, the oxidation occurred when formed SiNPs and water/ions entered in contact, leading at the formation of the observed amorphous SiOx, as also demonstrated Intartaglia et al. [2012]. Despite the high temperature generated during the process, phage maintained its structure. Indeed, the phage degradation occurs at 1.34×10^5 J/mol [Brigati and Petrenko, 2005], therefore, most of the phage population complexed with SiNPs maintains intact its structure as shown in SEM image (**Figure 5**). The obtained complexes CLL1 and SiNPs clearly show the arrangement of the SiNPs on the capsid proteins of the phage filaments.

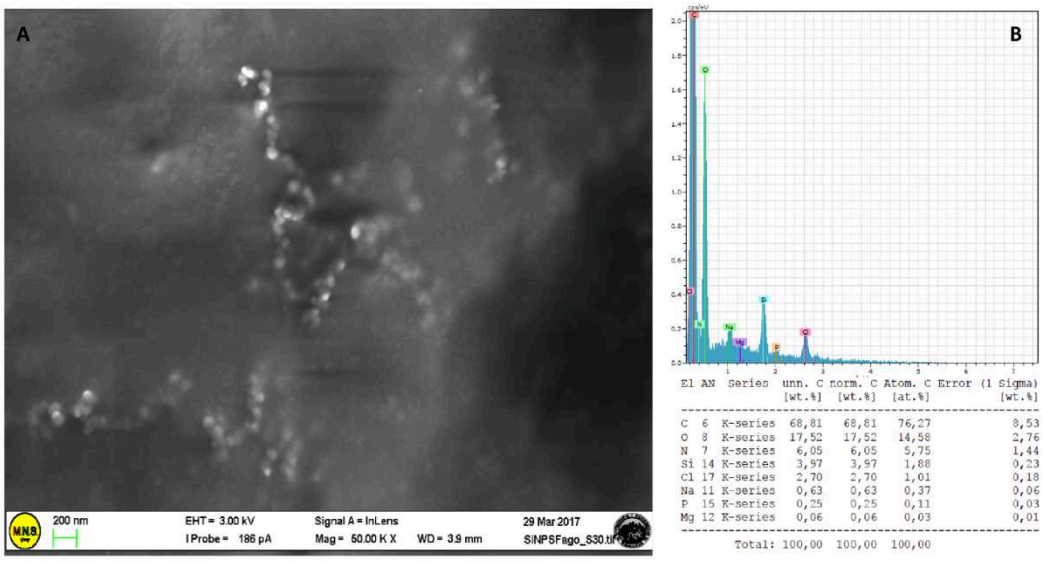

Figure 5. **PLAL of Si in TBS with CLL1 phage**. (A) SEM image obtained at 3.00 kV shows phage-SiNPS obtained from PLAL of Si plate in TBS with CLL1. SiNPs clearly cover the surfaces of the CLL1. (B) EDX analysis of phage–SiNPs.

The phage appeared decorated of SiNPs probable due to both the electrostatic interaction between charges of SiNPs' surface and pVIII coat protein of phage, and by the ions present in TBS buffer, which formed salt bridges between SiNP and phages

[Coen et al., 2001]. Moreover, EDX analysis confirmed the bond between SiNPs and CLL1 phage, for the presence of nitrogen (N), atomic species typical relate to the protein presented on the phage surface. The successive, Ultraviolet (UV)–visible absorption spectra of SiNPs (black line) and phage–SiNPs (red line), also, revealed the presence of centered peak at 550 nm, ascribable to the silicon for both the spectra; moreover, another peak, around 269 nm presented by SiNP–phage spectra, was attributed to aromatic residues of phage (**Figure 6A**) [Schmid, 2005]. CLL1 phage appeared as a template where the SiNPs could be stratified. The SiNPs on the phage surface were aggregates (around 50 nm) or as single particles of few nm (~8 and ~ 15.1 nm likewise the values obtained in the insert **Figure 6A**). Photoluminescence (PL) spectrum showed different peaks of less intensity at 438,454, 485, 495 nm and an intense band around 465 nm (**Figure 6B**) and, confirming the presence of the different size of the SiNPs and different states of SiOx as reported from Ulusoy Ghobadi et al. [2016]. The PL values were indicative of yellow-green light emission of the SiNPs due to the size and different oxidation state (SiOx).

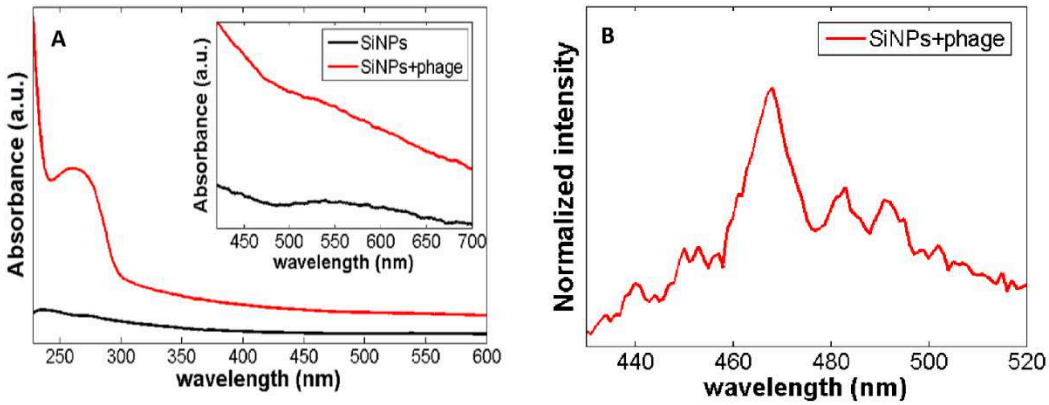

Figure 6. UV-vis and PL spectra. (A) The UV–Vis absorption spectra of SiNPs (black line), SiNPs–phage (red line) obtained by PLAL on a Si plate in TBS with and without phage. (B) The PL spectrum of phage–SiNPs.

After the characterization of the CLL1-SiNPs complexes, Leukemia-PBMCs cells were incubated with SiNPs alone, and with CLL1-SiNPs complexes to evaluate ability and specificity of the complexes to bind targets. After reaction, the bright fluorescence on

the Leukemia-PBMCs indicated that CLL1–SiNPs was able to effectively bind the cells target, thanks to CLL1 phages, and due to the presence of SiNPs yellow-green fluorescent cover the PBMCs (**Figure 7A**). This did not happen with SiNPs alone (**Figure 7 B**). Moreover, from these data, it can deduce, also, that the CLL1 complexed with SiNPs maintained the ability to recognize the cells target.

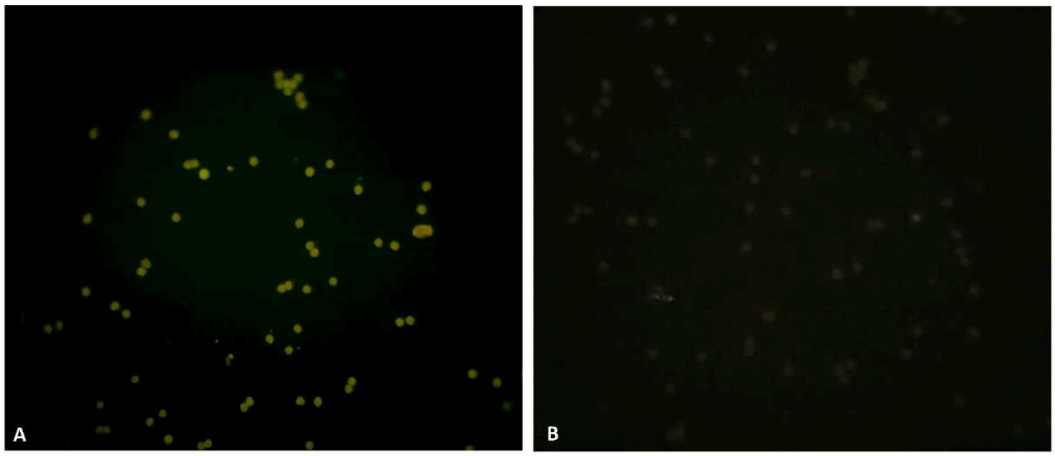

Figure 7. Leukemia-PBMCs after reaction with and without CLL1-SiNPs. (A) The yellow-green fluorescence due to the CLL1-SiNPs complexes on the leukemia-PBMC cells confirmed the interaction by fluorescent microscopy. In particular, phage–SiNPs was able to effectively bind the cellular target, thanks to CLL1 phage, in addition, due to the presence of SiNPs a yellow-green fluorescence is observed on PBMC cells. (B) Never fluorescence was observed in the leukemia-PBMC after reaction with SiNPs alone.

4.2.2 FITC-labelled phage

The use of the chemical- fluorochrome had permitted to obtain another phage-fluorescent complex. In this case, FITC was used to label CLL1. Between the advantages in the use of labelled phage there are the lung time stability and resistant to temperature, pH, organic solvents, but also, in this context, the possibility to bring on the cells target more than one fluorescent molecule, acting as amplifier. Indeed, 2/3 molecules of FITC stained the phage coat in its amino-groups exposed in the N-teminal of pVIII major coat protein, as demonstrated by Jaye et al [2004].

The CLL1 maintained the ability to recognize the target after conjugation with FITC, as was showed in the interaction CLL1-FITC with leukemic-PBMCs by fluorescence microscopy (**Figure 8A**). Moreover, the specificity of recognition was observed

comparing the fluorescence on the leukemic-PBMCs due to the CLL1 with pC89 wild-type vector (phage without the specific peptide). The bright green fluorescent, due to the FITC, stained only the leukemic-PBMCs placed in reaction with CLL1 (**Figure 8B**).

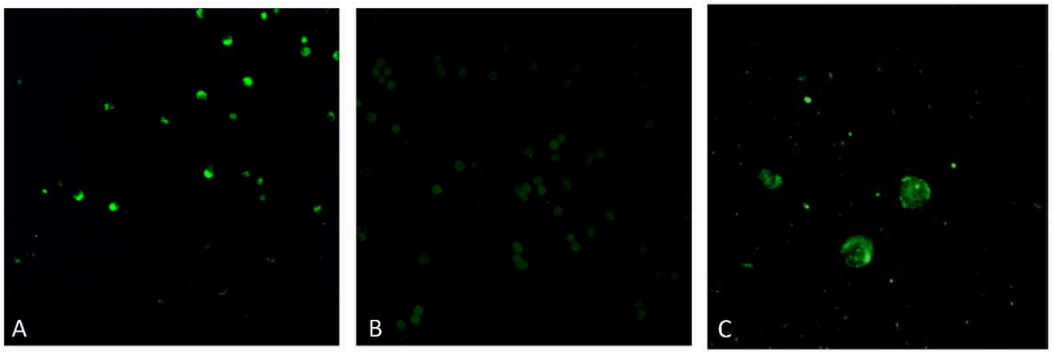

Figure 8. PBMC targeting by FITC-labelled CLL1 (A), compared to pC89 wild-type (phage without specific peptide) (B) (magnification 40x). Microscopy observations revealed bright green fluorescent stained leukemic PBMC cells due to CLL-1 FITC-labelled. On the contrary, only background fluorescence was observed in leukemic PBMC by using FITC-labelled pC89 (insert-less phagemid), confirming leukemic PBMC specificity by E.L.I.S.A. test of the peptide expressed by CLL-1. (C) Specific localization of FITC-labelled CLL-1in leukemic PBMC subcellular sites (magnification 63×).

In some cells that had reacted with CLL1-FITC, green fluorescence seemed localized in subcellular sites (**Figure 8C**) according to bioinformatics results, and as descripted from Chang et al. about the distribution of tankyrase 1 in multiple subcellular sites [Chang et al., 2005]. However further studies should be carried out to confirm the hypothesis of interaction between the tankyrase 1 and CLL-1.

4.3 Single Drop Biosensor based on FITC-labelled phage for fluorescent imaging

Therefore, Single Drop Biosensor based on phage-labelled as probes to directly detect leukaemia cells in blood from patients affected by chronic lymphocytic leukaemia (CLL) has been performed. The schematized design of system is described in **Figure 9**.

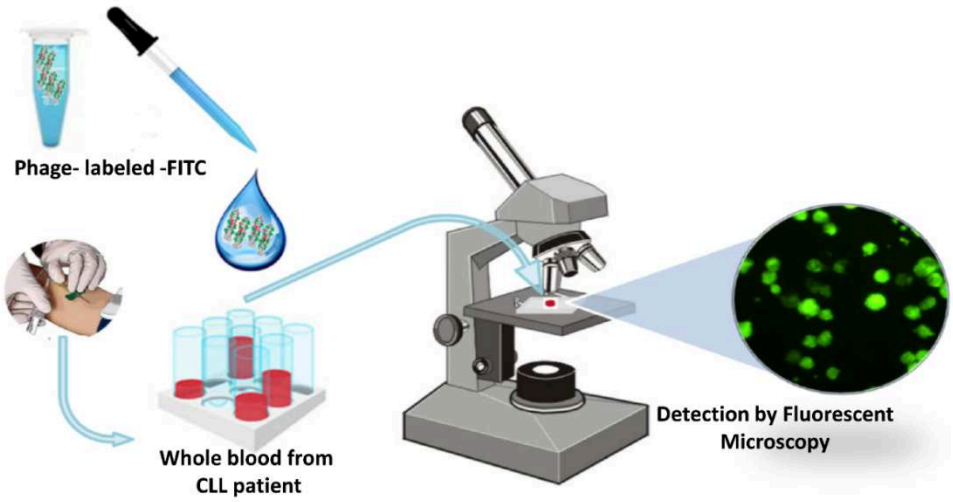

Figure 8: **Single Drop Biosensor Based on phage-labeled** probes to detect leukemia cells in blood from patient affected by CLL.

Ex-vivo diagnosis of whole blood from patients affected by CLL was placed to reach with CLL1-labeled-FITC. The time-lapse performed at 30', 1 h and 2 h incubation times, showed that the complexes were not influenced by the presence of other blood elements (erythrocytes, thrombocytes and other elements of leukocytes), then maintain the ability to recognition the cells target, already after 30' (**Figure 9).**

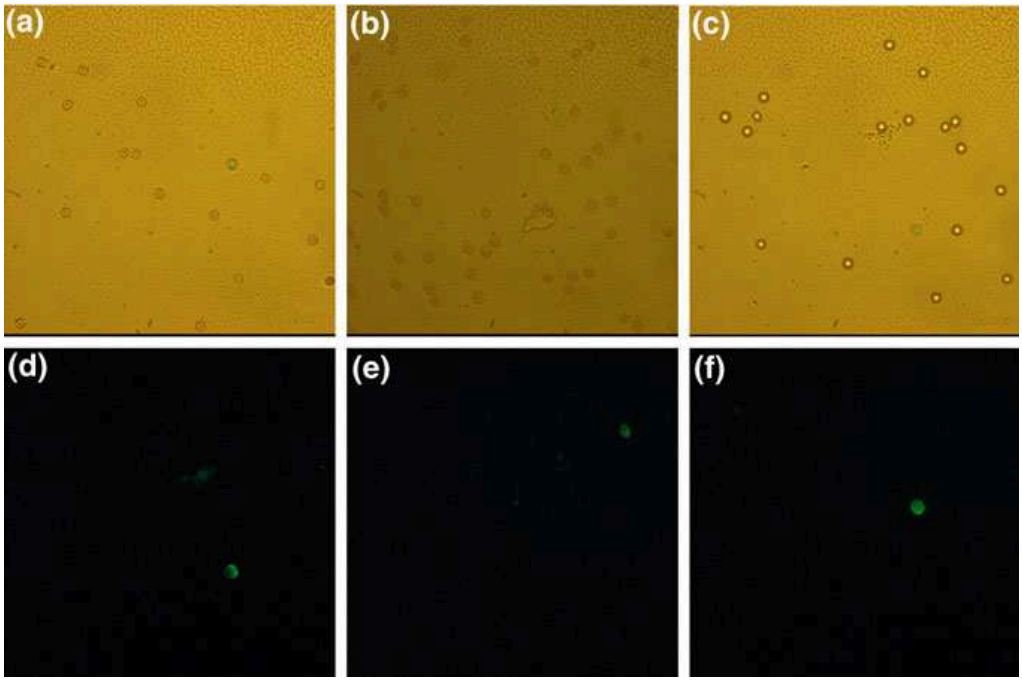

Figure 9. Time-lapse of whole blood from CLL patients in reaction with CLL1-labeled-FITC. Light phase contrast (a, b and c) and fluorescence (d, e and f) of blood blood from patient affected by CLL in reaction with CLL1- labelled FITC in at 30' (a and d), 1 h (b and e) and 2 h (c and f) incubation times (magnification 20×). The bring fluorescence due to FITC was present only in Leukaemia-PBMCs cell, target of CLL1.

Detection of circulating cancer cells in the blood is very useful in order not only to characterize leukaemia typologies but also for the monitoring of therapy, the control of treatment efficacy and, after the therapy, the detection of the minimal residual disease. The "proofs of concept" proposed demonstrated good selectivity and high reliability for measurements in real-time of blood samples, which may find potential applications in chronic lymphocytic leukaemia control.

4.4 Fluorescent probes from phage display for myeloma molecular mapping

Same approach and experimental design are used to select three other phage clones, named CLL-IV, EIII-14 and EIII-10, have been found for their ability to bind/discriminate myeloma cells from non–myeloma cell, discriminated for the cluster differentiation CD45, CD38 and CD138. This approach validates use of Phage Display for an antigenic mapping of cells from hematological neoplasm.

CLL-IV phage clone displays a foreign peptide with the amino acid sequences RRANNPSPQ. By Blast-p analysis, we deduced a significant alignment with chains A and B of several proteins, including the Thrombospondin (TSP) type 1. Particularly, we found that the amino acid motif NNPSPQ of foreign peptide align in two different protein portions (regions 30-35 and 87-92) with a degree of identity of 83%, namely 5/6 amino acids (**Figure 10**)

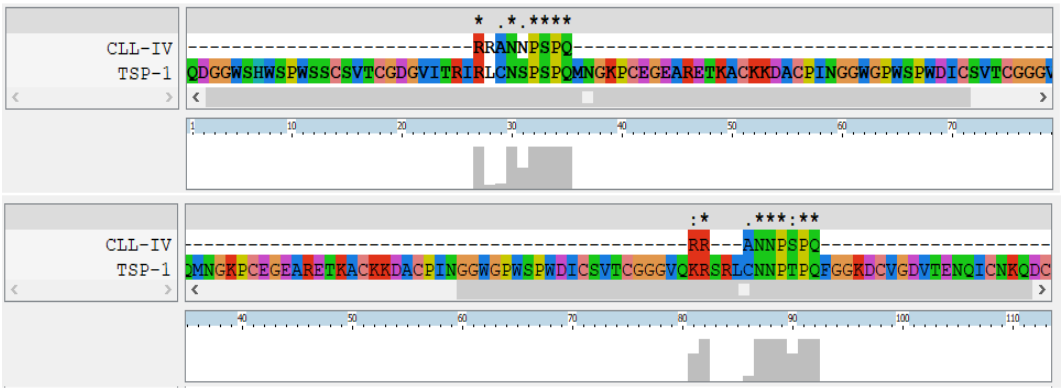

Figure 10. Alignment of foreign peptide displayed by CLL-IV phage clone with several regions of TSP-1 by using CLUSTALX 2.1. Dashes indicate gaps used to maximize the alignment.

Expression levels of TSP type 1 and 2, along with high levels of CD47, have been found in plasma cells cultures from bone marrow of MM patients compared to healthy subjects [Rendtlew Danielsen et al., 2007]. At this purpose, it has been hypothesized that CD47 and TSP-1 and -2 are involved in the progression from Monoclonal Gammopathy of Undetermined Significance (MGUS) to Myeloma Multiple (MM) and subsequently in interaction of MM plasma cells with the microenvironment [Rendtlew Danielsen et al., 2007]. By including the Blast-p analysis to insertion amino acids, namely EF (N-terminus) and D (C-terminus), a significant alignment to integrin αXβ2 (regions 186-93) were deduced for the amino acid motif EFRRANNP of foreign peptide with a degree of identity of 75%, namely 6/8 amino acids (**Figure 11**)

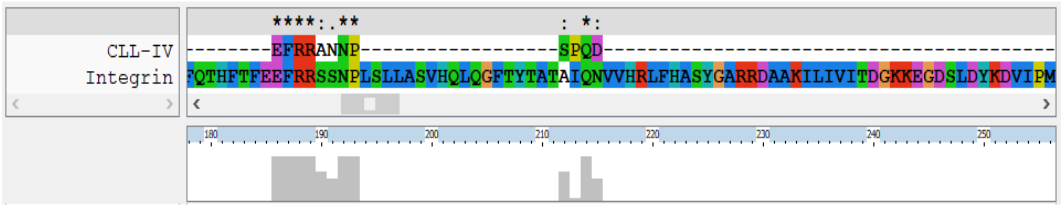

Figure 11. Alignment of foreign peptide, including insertion amino acids, displayed by CLL-IV phage clone with integrin αXβ2 by using CLUSTALX 2.1. Dashes indicate gaps used to maximize the alignment.

β2-integrins are trans-membrane receptors involved in the biology of many human pathologies. Specifically, integrin αXβ2 seems to be involved, as well as also αMβ2, in phagocytosis, migration and cellular adherence during inflammation and antimicrobial responses [Jawhara et al., 2017]. It's known that integrins αDß2, αMß2 and αXß2 also show interaction with ICAM-1, making them possible alternative binding partners that tumor cells could make use of to accomplish adhesion [Humphries et al., 2006]. Moreover, αXβ2 is most expressed on tumor-infiltrating dendritic cells that mediate an anti-tumor immune response [Harjunpää et al., 2019; Leone et al., 2017].

These findings could be directed to other types of tumors, in addition to what has been described for myeloma plasma cells [Wang et al., 2015].

About EIII-14, phage clone displays a peptide with the amino acids sequences RRYTHPNNS. By Blast-p analysis, we deduced that the foreign peptide shows a significant alignment with the inhibitor of nuclear factor kappa-B kinase subunit beta (IKK-β, or more commonly IKK2). Particularly, we found that the amino acid motif RRYTHPN of foreign peptide align with a protein portions of both A and B chains (region 66-72 for chain A and 72-78 chain B) with a degree of identity of 86%, namely 6/7 amino acids (**Figure 12**)

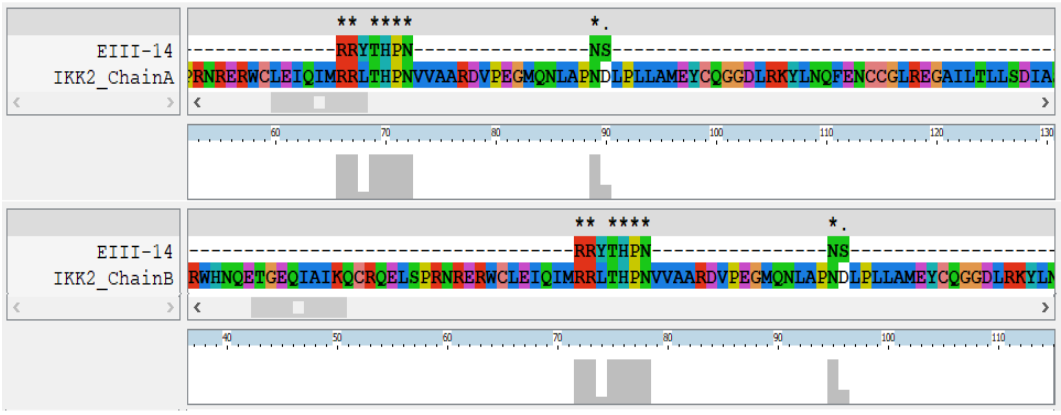

Figure 12. Alignment of foreign peptide, including insertion amino acids, displayed by EIII-14 phage clone with chain A and B of IKK2 by using CLUSTALX 2.1. Dashes indicate gaps used to maximize the alignment.

This enzymatic complex regulates the activity of the nuclear factor kappa-light-chain-enhancer of activated B cells (NF-κB) by phosphorylation of IκBα (inhibitor of kappa B) [Karin, 1998; Frelin et al., 2005]. Deregulated activity of NF-κB has been implicated in the pathogenesis of multiple myeloma, promoting proliferation, survival and drug-resistance of myeloma cells [Mazzera et al., 2013; Roy et al., 2018].

In our case study, experimental data of fluorescent imaging show that both CLL-IV and EIII-14 phage clones were able to bind CD45-/38+/138+ plasma cells, as indicated by the presence of green fluorescence, but not CD45+/38+/138- (**Figure 13**).

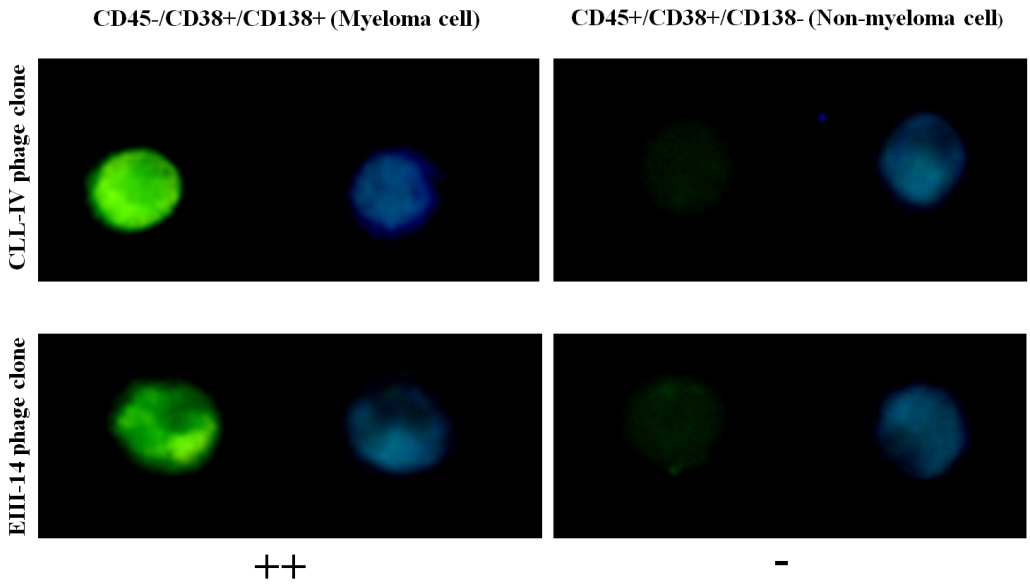

Figure 13. CD45-/38+/138+ and CD45+/38+/138- targeting by FITC-labelled CLL-IV and EIII-14 phage clones (green) and staining by DAPI (blue). Magnification 100x

By the comparison with the non-specific marking of the nucleus from the DAPI coloring, we observed that FITC-labeled phage was homogeneously distributed on the whole cell surface for CLL-IV phage clone and specifically localized in subcellular sites, identified as nuclear, for EIII-14 phage clone (**Figure 13**). These findings are in according with deductions from the Blast-p analysis that would assume a selectively recognition of foreign peptides displayed by phage clones in different sub-cellular sites of CD45-/38+/138+ plasma cells and not present in the other plasma cells tested.

Regarding EIII-10 phage clone, displayed peptide has the amino acid sequence KKAHPGGSP. By Blast-p analysis, we deduced that the foreign peptide shows a significant alignment with the chain A of Netrin-1. Particularly, we found that the amino acid motif KKAHP of foreign peptide aligns with the protein regions 62-66 of Netrin-1 with a degree of identity of 100%, namely 5/5 amino acids (**Figure 14**).

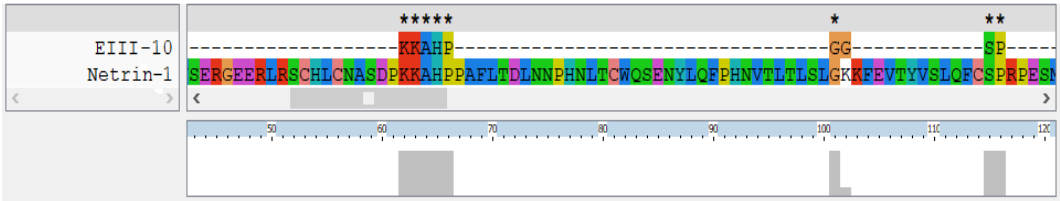

Figure 14. Alignment of foreign peptide displayed by EIII-10 phage clone with Netrin-1 by using CLUSTALX 2.1. Dashes indicate gaps used to maximize the alignment.

Netrin-1 receptor is involved in the osteoblast/osteoclast differentiation and tumor suppression by preventions of cell growth [Sato et al., 2017; Nagoshi et al., 2015]. Although loser o decrease of expression of gene encoding a netrin-1 receptor has been associated to progression of solid tumor and hematologic malignancies, its role in MM is still unknown. However, it has been supposed an involvement in the MM refractory patient as consequence of the modulation of osteoclast activity [Mediero et al., 2015].

Experimental data of fluorescent imaging for EIII-10 phage clone shows a reversal of the recognition trend with respect to what has been described for the other two phage clones (**Figure 15**).

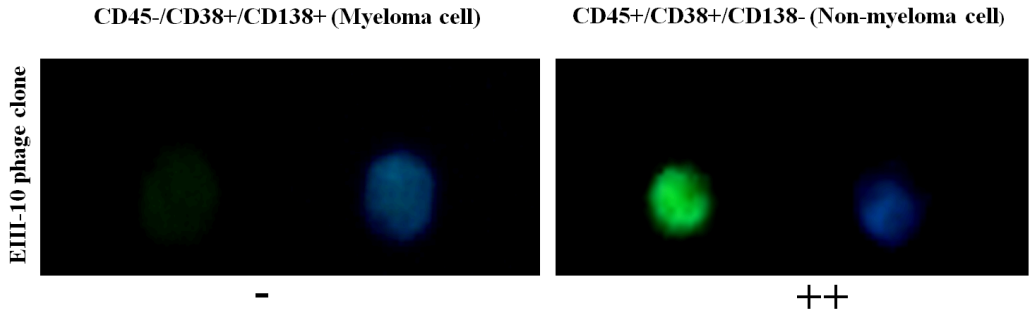

Figure 15. CD45-/38+/138+ and CD45+/38+/138- targeting by FITC-labelled phage clone (green) and staining by DAPI (blue). Magnification 100x.

The recognition of plasma cells by EIII-10 phage clone would seem to follow the expression alterations of Netrin-1 and its associated receptors, generally reduced in the presence of neoplastic conditions.

By described approach, three different phage peptides have been identified for their ability to bind/discriminate myeloma cells from non–myeloma cell, discriminated for the cluster differentiation CD45, CD38 and CD138. The phage peptides displayed by phage clones named CLL-IV and EIII-14, showed fluorescence positivity to myeloma cells CD45-/CD38+/CD138+, while that by EIII-10 phage clone showed fluorescence positivity toward non-myeloma cells CD45+/CD38+/CD138-.

Based on these findings, it was possible to construct a simplified phage array for the distinction of myeloma cells from non-myeloma cells.

Phage Clone	Blastp Structural homology	Myeloma cell	Non-myeloma cell	Cluster of differentiation (CD) CD45	CD38	CD138
CLL-IV	***TSP type 1;* Integrin *αXβ2***	**++**	**-**	**-**	**+/-**	**+**
EIII-10	***Netrin-1;* pp-GalNAc**	**-**	**++**	**+**	**+/-**	**-**
EIII-14	***IκB kinase***	**+/++**	**+/-**	**+/-**	**+/-**	**+**

Table 1. Simplified phage array for myeloma/non myeloma discrimination

Preliminary results from the three phage clones, labeled with a fluorescent dye, had allowed to discriminate the two different types of plasma cells.

ES. Experimental Section

ES.1 "Promiscuous selection" against PBMCs from CLL patients

The M13 pVIII-9aa phage library was used in the selection against whole peripheral blood mononuclear cells (PBMC) provided by from Messina University Hospital. Firstly, the 10^{12} phage library was subtracted by pretreatment with 2×10^5 cells PBMCs from healthy patients, then it was used to the selection protocol-binding phage clones for four rounds of affinity selection against 2×10^5 cells PBMCs from two patients affected by chronic lymphocytic leukemia (CLL), two for each one, according to our previous work [Lentini et al., 2015; De Plano et al., 2018, Franco et al., 2018]. The most reactive phage clones showing a specific leukemic PBMCs binding were amplified and their DNA was sequenced to determine the amino acid sequences of the displayed peptides (like describe previous chapter 2). Sequence similarity searching was carried out by BLAST, an algorithm for comparing primary biological sequence information, then sequences were treated with Epitope-Mediated Antigen Prediction (E-MAP) tools to predict epitopes.
The same selection protocol, described above, has been used against model cell lines of leukemia and myeloma and applied for the discovery of the phage clones with ability to bind/discriminate myeloma cells from non–myeloma cell.

ES.2 Phage labelling with FITC

Phage labelling with FITC was carried out according to the procedure described by Herman et al [2007] and adapted to experimental condition of the present study. 1×10^{13} phage clones were resuspended in 200 µL Buffer $Na_2CO_3/NaHCO_3$ (pH 9.2) with 5 µL of fluorescein isothiocyanate (FITC, 5mg/mL). Clones were incubated for 2 h in the dark on rotator (8 rpm) at Room Temperature (RT) to allow reaction with fluorochrome. Sample was incubated at 4 °C overnight with 200 µL of PEG/NaCl and then centrifuged at 15300 ×*g* at 4 °C for 1 h. The supernatant was discarded, and the pellet resuspended in 100 µL of Tris Buffered Saline [TBS, (7.88 gr/L Tris-HCl, 8.77 gr/L NaCl)]. Labelled clones were stored in the dark at 4 °C until utilization.

ES.3 Sample Preparation for fluorescence imaging

100 µL of 2×10^5 cells were incubated with 25 µL FITC-labelled phage clone stocks solution (titer 10^{11} PFU/mL, cell/phage ratio 1:5000) for 2 h at 37 °C. After incubation, cells were washed three times with Phosphate-buffered saline (PBS) to remove excess unbinding phage and then put on glass slides. Wild-type vector pC89 (phage without foreign peptide) served as negative control for evaluation of background from nonspecific binding. The samples were analysed by fluorescence microscope (Leica DMRE).

ES.4 One-step synthesis of phage–SiNP Bioconjugates

Phage–SiNP bioconjugates were prepared by pulsed laser ablation in liquid (PLAL) of a high-purity (99.99%) monocrystalline silicon plate immersed in a glass vessel filled with 2.5 mL of phage suspension in TBS at the concentration 8×10^{11} PFU/mL. The ablation process was performed using the second harmonic (532 nm) of a neodymium-doped yttrium–aluminum–garnet (Nd:YAG) laser (model New Wave Mod. Tempest 300), operating at 10 Hz repetition rate with a pulse width of 5 ns [Fazio et al., 2013]. The silicon target was irradiated at the laser fluence of 7.5 J cm^{-2} and for an ablation time of 30'. Contextually, an ablation with the same parameters was performed on a silicon target immersed in TBS, as a control sample. To separate the networks were purified by centrifugation at 20800 ×*g* for 30'. The complex was resuspended in 100 µL of TBS and stored at 4 °C until utilization.

ES.5 SiNPs and the phage–SiNP conjugates Samples characterization

The UV–Vis absorption response of the SiNPs and the phage–SiNP conjugates was investigated immediately after the ablation process by means of a Perkin-Elmer Lambda 750 UV–Vis spectrometer in the 190–1100 nm range. Photoluminescence (PL) measurements were performed at room temperature by means of a Horiba Jobin Yvon spectrometer (Fluoromax-4) arranged in T-shaped geometry with excitation energy of 3.1 eV (400 nm). The spectra of the prepared colloidal solutions were recorded, using quartz cells with a 10 mm optical path length. Morphology of samples was investigated by a scanning electron microscopy (SEM), a scanning electron microscopy operating in transmission mode (STEM) and energy-dispersive X-ray analysis (EDX) was carried out using a Quantax EDX spectrometer. Analyses were performed by a ZEISSMerlin with Gemini II column field emission scanning electron microscope, operating at 30 kV in STEM configuration, equipped with multi-scan CCD camera for digital imaging. To carry out STEM measurements, few drops of each solution were casted on carbon-coated copper grids. The particles size distribution was determined by STEM using image analysis software. The Z-potential was analysed using a Horiba Nano Particle Analyzer SZ-100 (range 0.3 nm–8 μm). phage–SiNPs from the unbounded phage and free SiNPs, network was purified at 20800 $\times g$ for 30'. The complex was stored a 4 °C after suspension in 100 μL of TBS.

CHAPTER 5
Novel paradigm of programmed, self-navigating phage particles – from *in vitro* to *in vivo*

This study was performed under the guidance of Professor Valery A. Petrenko in the Phage Display Laboratory at the College of Veterinary Medicine, Auburn University, Alabama, USA.

Cancer is one of the major causes of death in the World, as described in the previous chapter. Tumor heterogeneity associated with a poor delivery performance of actively targeted nanomedicines, which increased tissue accumulation by only 0.7% of the ID, is a recognized problem, debilitating clinical performance of targeted anti-cancer nanomedicines. Low efficacy in controlling tumor growth by traditional tools, requires novel nanotechnology strategies to increase the success of treatments such as reduction of off-target cytotoxicity, improved pharmacokinetic profiles to increase drug exposure, active targeting to delivery drugs specifically to the site of disease, etc. Due to these limitations, a new concept for the analysis of phage-peptides was suggested based on the theory of "elementary binding units". Biological processes often involve many interactions between proteins and/or other molecules mediated by amino acids. Several studies have revealed that "Core motifs" (CorMs), composed of three-four amino-acids, play a major role during initial protein interactions in many cellular processes encoding the majority of affinity and specificity of binding [Khazanov and Carlson, 2013; Mészáros et al., 2009; Kinjo and Nakamura, 2012; Davey et al., 2012]. They are initiators in the formation of short linear motifs (SLiMs), which control dynamic networks of activities through reversible interactions with several proteins due to the naturally low affinity of these interactions. This characteristic of SLiMs allowed us to propose them as potential programming modules for development of self-navigating molecules. Recently, the rapid expansion and interest in studying SLiMs, has led to

establishment of collections of discovered SLiMs in the eukaryotic linear motif (ELM) server that helps reveal new candidate SLiMs in protein sequences.

In this chapter, we describe a new algorithm for analysis of phage peptides populations based on the concept that longer peptides evolve through the accumulation of multiple elementary binding units (EBUs) with increasing biological function/fitness:

- Phage peptides, obtained through screening of f8/8 and f8/9 landscape phage libraries against MDA-MB-231 human breast cancer cells *in vitro*, were analyzed using publically available bioinformatics tools and databases for the discovery of peptides enriched with previously identified SLiM domains. Several motifs, containing multiple CorMs, were identified within the same peptide to form more biologically active SLiMs. We validated the ability of candidate phage particles to move, or "migrate", inside of the target cells using confocal microscopy.
- Next, we performed an *in vivo* evaluation of the tissue distribution of the landscape phage library f8/9 in a nude mouse xenograft model of the human breast cancer cell line, MDA-MB-231. Phage DNA previously extracted from mouse tissues and tumor samples permitted us to evaluate the pharmacokinetics of phage tissue distribution by quantification of phage genomes using qPCR and subsequently identify the displayed peptide sequences using Next Generation Sequencing (NGS). Preliminary data of phage-displayed peptides indicate that phages were identified that home specifically to the tumor or other tissues. These peptide structures will be analyzed, as in our *in vitro* study and by novel approaches to find "self-navigating phage particles programmed" for specific and selective migration to each tissue.

5.1 Discovery and analysis of CorMs and SLiMs enriched following *in vitro* selection of phage-displayed peptides

Previously, the multibillion clone landscape phage libraries f8/8 and f8/9 were screened against the human metastatic breast cancer cell line MDA-MB-231 *in vitro* to isolate phage peptides with high selectivity. The human metastatic breast cancer cells MDA-MB-231, are an ideal model for this study, because they demonstrate triple negative (ER^-, PR^-, and $HER2^-$), highly aggressive phenotype and poor clinical prognosis [Cailleau et al., 1974]. After depletion of the naïve library against plastic, serum and phenotypically normal breast epithelial cells [Gross et al., 2016; Fagbohun et al., 2012; Gillespie et al., 2015; 2016] the library was used for positive selection of clones. Following the final round of selection, hundreds of phage clones from the eluate and lysate fractions were randomly chosen to determine the peptide primary structure by Sanger sequencing. Results from a phage capture assay were used to evaluate both specificity of selected phages (in comparison with non-related phage, VPEGAFSS, and their selectivity towards target cancer cells in comparison with other breast cancer cell lines [Petrenko et al., 2019]. Using the Multiple EM Motif Elicitation (MEME) program, in MEME suite tools, *in silico* analysis was performed to reveal linear, non-gaped, trimer CorMs found within the selected peptides (**Table 1**). The structural origins of SLiMs behavior were deduced by identification of interactions with corresponding protein domains on/in cancer cells using the Eukaryotic Linear Motif (ELM) resource [Gouw, et al., 2018](**Table 1**).

Partner Domain		Function [Location]	CorM	SliM[a]	Phage
A	**Atg8[b]**	LC3-interacting region (LIR) mediates binding to Atg8 ubiquitylated proteins [membrane]	**STL, AEY VND ESW, SWD DYD EYG, GES, VNA, SVN**	**EYSTL EYNMV DFSTP DYDMI GESVNA**	**ADHAEYSTL DFEYNMVND DFSTPESWD VDYDMIGDQ AEYGESVNA**
B	**PDZ**	Autophagy-related [membrane-associated complexes]	**EYG, GES, VNA, SVN SVD**	**VNA QSSVDA**	**AEYGESVNA GDYQSSVDA**

C	**WD40** domain of **WDR5**	Mediate assembly of histone modification complexes [nucleus]	**VDV** **SVD** **PPT, APE**	**DYVDV** **QSSVDA** **PTAP**	**DYVDVSIND** **GDYQSSVDA** **DFPPTAPED**
D	**SUMO** membrane protein	Sorting and internalization signal	**LLN, LNE** **LLN, LNE**	**DTIALL** **ELEHLLN**	**DDTIALLNE** **EELEHLLNE**
E	nuclear receptors	Expression of specific genes, development, homeostasis, and metabolism	**LLN, LNE**	**ELEHLLN**	**EELEHLLNE**
F	**LEV**	Nucleus, ESCRT-I complex[c] [cytosol]	**DFP, FPP, PPT, APE**	**PPTAPE**	**DFPPTAPED**
G	**SH3**	Signal transduction, traffic, cytoskeleton and organelle organization [cytosol]	**DFP, FPP, PPT, APE** **DSF, FVN, VNA**	**DFPPTAP** **DSFVNAP**	**DFPPTAPED** **DSFVNAPED**
H	**mu subunit** Adaptor Protein **AP**	Proteins directing traffic within the endosomal and the secretory pathways	**DYD** **VND**	**DYDMI** **YNMV**	**VDYDMIGDQ** **DFEYNMVND**
I	**MYND** zinc	gene regulation, cancers	**DFPPTAP** **DSFVNAP**	**PPLEP**	**GPPLEPGQ**
J	**MATH**[d]	deubiquitinating protease **USP7**[c]**;** substrate recognition, nuclear localization	**DSY** **DDS, DSY**	**PLDSY** **PDDSY**	**GTGPLDSYD** **VHPDDSYSD**
k	**BIRf** motif in **IAP**[e] Proteins	involved in regulation of apoptosis	**DAD, DPS**	**DADPS**	**VPSYDADPS**

Table 1. Target domains identified from selected phages. [a] Short Linear Motifs (SLiMs) discovered using the Eukaryotic Linear Motif (ELM) resource (Gouw, et al., 2018); [b]Atg8 - Autophagy-related protein; [c]USP7 - ubiquitin specific protease 7; [d]MATH - Meprin And TRAF-Homology (MATH) domain; [e]IAP - Inhibitor of Apoptosis Proteins; [f]BIR - Baculovirus Inhibitor of apoptosis protein Repeat

For example, the phage clone displaying the DSFVNAPE peptide, exhibited the greatest selectivity toward MDA-MB-231 (~10-fold in comparison with normal breast epithelial cells) [Petrenko et al., 2019], revealed the combination of five CorMs (DSF, FVN, VNA, APE, PED), which evolved into two functional SLiMs (DSFVNAP and VNAPEDP). These in turn, were responsible for interaction of the fusion peptide with a SRC Homology 3 (SH3) domain [Teyra et al., 2017; Saksela and Permi, 2012]. SH3 domains are present in all eukaryotes cells and are restricted to intracellular proteins involved in regulation of cellular signaling pathways, substrate recognition and membrane localization [Kurochkina and Guha]. Based on these predictions, phage DSFVNAPE may be found either extracellularly and/or intracellularly. In fact,

DSFVNAPE phages were found internalized in MDA-MB-231 cells after 1 h and demonstrated perinuclear localization as round, green spots (Figure 1A), as visualized by confocal florescent microscopy.

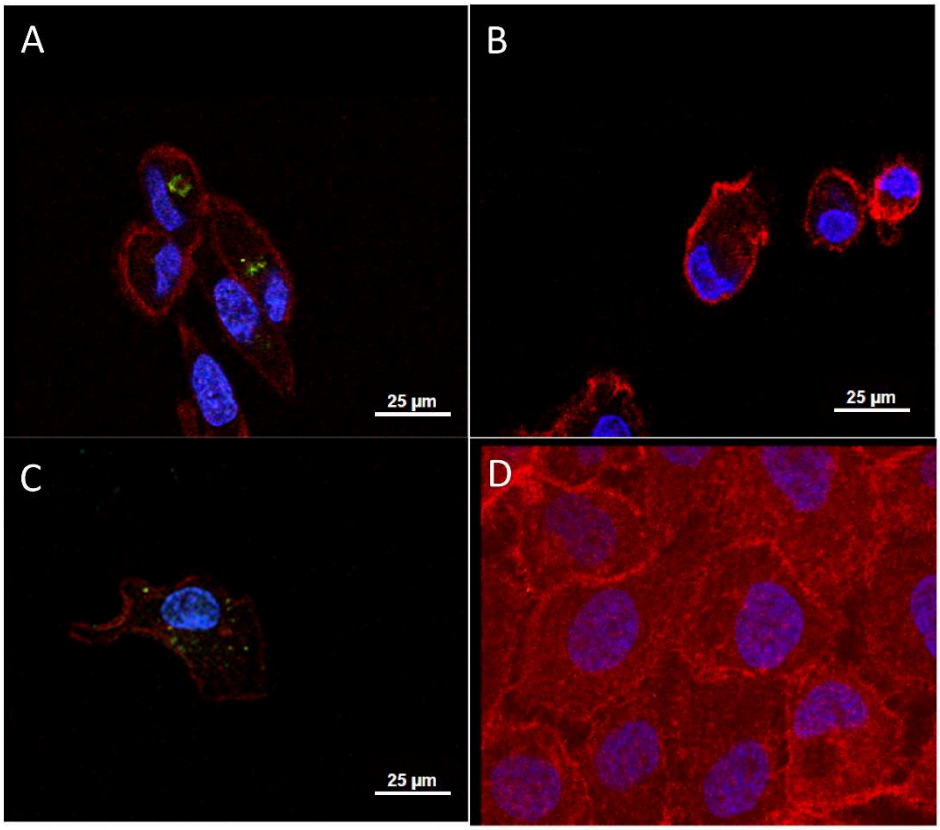

Figure 1: **Immunofluorescence analysis of phages towards breast cancer cells *in vitro***. Phage particles (~10^{10} virions) displaying the breast cancer cell-specific (A) DSFVNAPE peptide or (C) DRDDSFMND peptide; or (B) VPEGAFSS peptide, an unrelated peptide structure were incubated with MDA-MB-231 breast cancer cells for 1 h and visualized at 60× magnification using confocal microscopy. (D) Phage displaying the DSFVNAPE peptide was incubated with MCF-10A cells for 1 h as a negative control for specificity. Phages were revealed using a rabbit anti-fd IgG primary antibody and an AlexaFluor® 488-conjugated goat anti-rabbit IgG secondary antibody (green), actin was identified using AlexaFluor® 546-labeled phalloidin (red) and nuclei were identified by DAPI staining (blue). DSFVNAPE and DRDDSFMND phages were found internalized as green round spots. Phages bearing, VPEGAFSS, were not found interacting with the cells under the same conditions. Finally DSFVNAPE phages were not found interacting with the phenotypically normal breast epithelial cell line, MFC-10A, under the same conditions.

Moreover, four other phage clones isolated from the f8/9 landscape phage library: ELHSDQAWD, DRDDSFMND, DVETHHIND and DYVDVSIND, demonstrated a selectivity of 14-fold, 20-fold, 26-fold, and 18-fold for MDA-MB-231 cells compared to MCF-10A cells, respectively. We identified one potential CorM (DQA) from phage ELHSDQAWD and no enrichment for any SLiMs; four CorMs (DRD, RDD, DDS,

DSF) and one SLiM (RDDSFMN) for DRDDSFMND; two CorMs (DVE, IND) and one SLiM (VETHHIN) for DVETHHIND; and two CorMs (VDV, IND) and one SLiM (DYVDV) enriched in the DYVDVSIND peptide. Potential target binding domains for these SLiMs are summarized in **Table 1**. In particular the SLiM RDDSFMN identified in the peptide DRDDSFMND, hypothesized to interact with a polo-box domain (PBD) found in Polo-like kinase 1 (Plk-1) and Polo-like kinase 4 (Plk-4), may be involved in controlling division of eukaryotic cells through the regulation of cell cycle, chromosome segregation and cytokinesis [Lee et al., 2014]. As expected, this phage was found dispersed throughout the cytoplasm environment of the cancer cells (**Figure 1C**). Usually, aberrant expression of Plk-1 is associated with development of many types of cancer including breast cancers [Kumar et al., 2016]. Consequently, selective inhibition of Plk-1 has been suggested as a potential therapeutic target for development of future chemotherapies [Lee et al., 2014].

This new algorithm permits us to find smart phage proteins that could be used in the new vision of "programmed, self-navigating phage particles"- peptide-bearing phages that can migrate from target-specific cell surface molecules to intracellular antigens.

5.2 Biodistribution of f8/9 landscape phage library in a nude mouse xenograft model of human triple negative breast cancer

There are many reports describing peptides able to recognize a range of different human antigens, including cell surface-expressed tumor antigens, thanks to selection against purified antigens or whole tumor cells using phage display libraries *in vitro*. However, clinical application of these tumor-specific peptides depends on their ability to specifically target the tumor *in vivo*, which in many cases, does not match with *in vitro* data. Consequently, *in vivo* phage display emerged as an important technique that allows identification of peptides that recognize biologically relevant *in vivo* tumor

targets. For successful application of *in vivo* selection for the isolation of tumor-specific peptides, a basic understanding of the pharmacokinetics of phage display landscape libraries is required. For this, the first step for *in vivo* characterization of the f8/9 landscape library was the study of phage biodistribution. Previously, female athymic (NCR *nu/nu*) mice, with (tumor mouse) or without (healthy mouse) a small tumor fragment of MDA-MB-231 human breast cancer xenograft implanted in the rear flank, were injected intravenously with different doses of phage library; a high dose (ID ~4×10^{10} phages) and a medium dose (ID dose ~4×10^{9} phages) were administered in 0.2 mL of physiological solution. Libraries were allowed to circulate for 1 h or 24 h before mice were sacrificed. In all cases, blood was collected prior to perfusion with saline solution for isolation of serum. Following perfusion, tissue samples including brain, heart, liver, spleen, kidneys, lungs, pancreas and tumor were collected and stored at -80 ºC. Tissue fragments of approximately 100 mg were homogenized and total DNA extracted. Phage DNA and mammalian genomic DNA were quantified distinctly using amplicon-specific qPCRs.

Consequently, the accumulation of landscape phage library in each organ of the mice was measured to determine its biodistribution *in vivo* (**Figure 2 and 3**). The quantity of the phages determined by titering in bacteria (not shown) was 10-100 times lower than measured by qPCR in each sample, in accordance with the literature [Dias-Neto et al., 2009]. As expected, following injection of phage libraries with medium ID, the amount of collected phage particles was lower by ~10-100X then observed when mice were injected with higher IDs in all conditions studied (**Figure 2 and 3**).

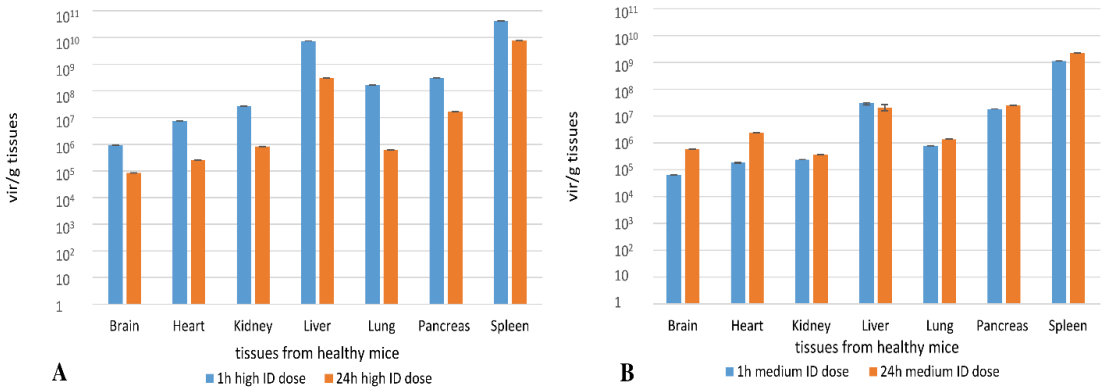

Figure 2: **Quantification of phages in tissues of healthy mice**. The graphic shows the data obtained in the tissues of healthy mice when high (A) or medium (B) doses of f8/9 phage library were injected and left to circulate for 1 h or 24 h. Standard deviations were obtained from technical replicas of the tested samples.

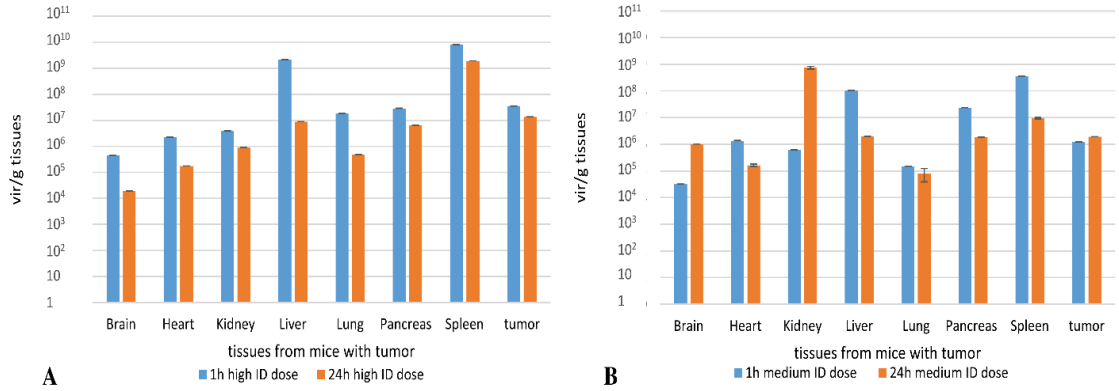

Figure 3: **Quantification of phages in tissues of mice with inducted tumor.** The graphic shows the data obtained in the tissue of mice with inducted tumor when high (A) or medium (B) doses of f8/9 phage library were injected and left to circulate for 1h or 24h. Standard deviations were obtained from technical replicas of the tested samples.

To determine the quantity of the phage able to home and persist within the tissues, we determined phage accumulation amid different times of incubation: 1h or 24h. It was found that at the high concentration of the phage library, after 1h, all tissues bind "saturating" amounts of virions, that decreases ~10 times after 24 h incubation (**Fig.2A**). Surprisingly, at the medium ID in healthy mice the accumulation of phage in some tissues is higher after 24h library circulation, than after 1h (**Figure 2B**). A similar pattern was observed in mice with induced tumors for the brain, kidney and tumor mass

(**Figure 3B**). However, we noticed that the quantity of collected phages in the tumor mass are similar amid 1h and 24 h time points, highlighting the probably that phages at the medium concentration, saturate the binding sites in some tissues (brain, heart) not as fast as at high concentration, and reach the maximum past 1 hour treatment.

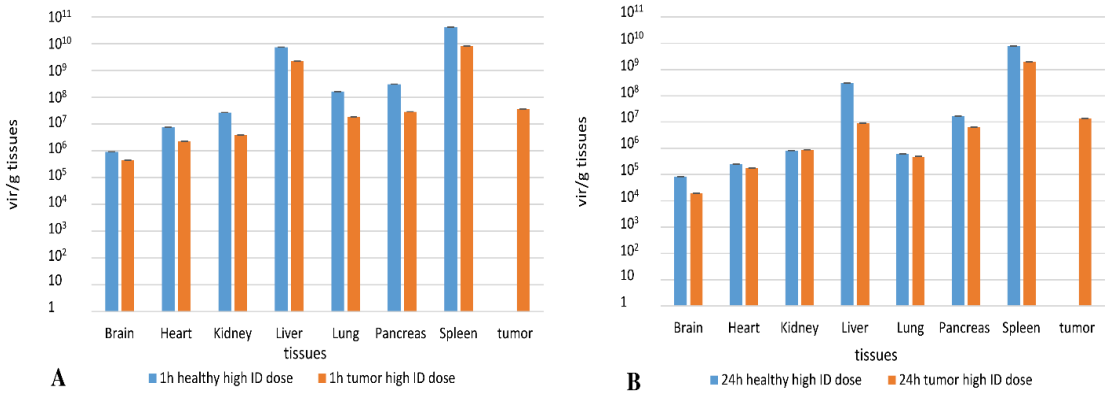

Figure 4. Comparison phage quantity found in tissues of healthy and tumor mice after injection of high ID of f8/9 phage library after 1h (A) or 24h (B) of circulation time. Standard deviation is obtained from technical replicas of the tested samples.

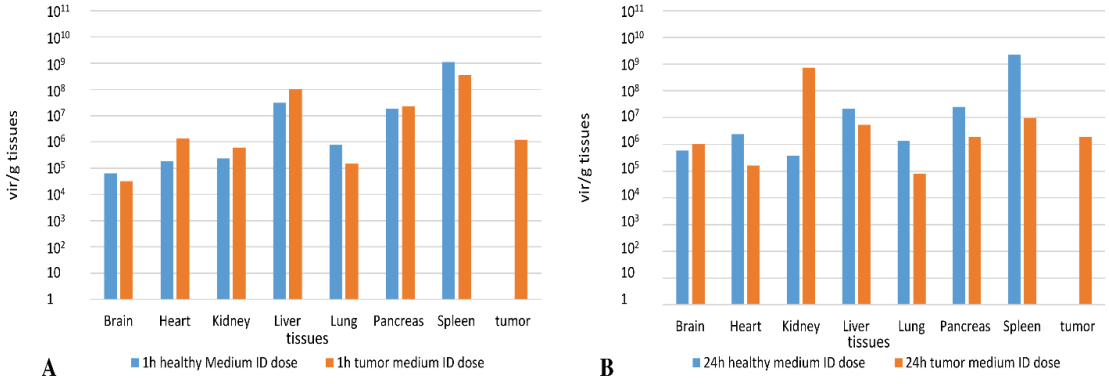

Figure 5. Comparison phage quantity found in tissues of healthy and tumor mice after injection of medium ID of f8/9 phage library after 1h (A) or 24h (B) of circulation time. Standard deviations are obtained from the technical replicas of the tested samples.

The total quantity of phage collected from the tumor-bearing mice are higher compared to the phage quantity in healthy mice for each tissues following injection of the high library dose (**Figure 4).** This suggests that the tumor mass may play an important role in the uptake of the phage library at both time points (**Figure 4**). In particular, after 1h of incubation, the amount of the phages collected in tissues from healthy mice were 1 logarithm higher compared with corresponding tissues from tumor-bearing mice in

kidney, lung and pancreas, closer to the 1/2 logarithm higher for the other tissues (**Figure 4A**). However, no significant difference in phage accumulation at 24h incubation was observed in heart, kidney and lung, while in brain, liver, pancreas and spleen the quantity of collected phages in healthy mice were higher compared with corresponding tissues from mice with tumor (**Figure 4B**). At the medium ID (**Figure 5**), effect of the tumor on the biodistribution of the phage library in mice after 1 h and 24 h is rather inconsistent and requires more detailed study, using selected tissue specific landscape phage clones.

Purified phage p8 amplicons obtained from brain, heart, liver, pancreas, kidney, lung, spleen, serum and tumor after injection of high ID of the phage library with 1h circulation were sent to the Massachusetts General Hospital (MGH) for Next Generation Sequencing (NGS) to determine the amino acid sequences of peptides enriched in each tissue (**Figure 6**).

Sample	Target	Library	Time (Hrs)	Raw Total Reads	Corrected Total Reads	Total Unique Nucleotide	Unique Nucleotide Q>33	Unique Peptides Total	Unique Peptides Q>33
1	Brain	f8/9	1	1,391,930	773,829	41,682	3,093	31,565	1,907
2	Heart	f8/9	1	1,876,833	1,459,809	113,528	17,568	85,991	12,238
3	Kidney	f8/9	1	1,882,594	1,500,643	116,547	12,300	90,357	8,488
4	Liver	f8/9	1	2,114,754	1,736,711	307,404	96,676	253,738	78,645
5	Lung	f8/9	1	1,341,366	1,073,051	108,023	25,765	82,750	18,409
6	Pancreas	f8/9	1	2,110,750	1,476,437	59,616	1,707	42,319	930
7	Spleen	f8/9	1	1,843,436	1,607,490	301,142	102,886	252,724	86,911
8	Tumor	f8/9	1	1,277,600	1,048,030	113,256	22,516	86,617	15,836
9	Serum	f8/9	1	1,608,775	1,379,259	218,582	63,836	177,636	50,073
10	Tumor	f8/9	24	2,448,655	2,028,291	245,213	52,008	193,593	38,305
Average				1,789,669	1,408,355	162,499	39,836	129,729	31,174
Stdev.S				382,429	364,131	97,348	37,247	82,788	31,289
Total				17,896,693	14,083,550	1,624,993	398,355	1,297,290	311,742

Figure 6. Summary of peptide populations by NGS. Summary of nucleotide sequences and amino acid sequences derived from each tissue sample. Numbers show both unfiltered and filtered for quality score (Q>33).

Following NGS and processing through the bioinformatics workflow, generated files containing nucleotide structures, which were then translated in their corresponding amino-acid sequence:

- One file per sample contains a list of all unique peptide sequences in FASTA file format not filtered for quality score. These files have been removed of duplicate peptide sequences generated from different nucleotide coding sequences and have been cleaned of sequences with bad translations; for example, sequences containing a stop codon in the middle of the sequence.
- One file per sample contains a list of all unique peptide sequences in FASTA file format which could be filtered for quality score (Q) > 33 for each base. The quality score was evaluate considering a compromise between the accuracy of the sequencing technique and the recovery of the most possible structurally unique peptides for each sample. Low quality scores can lead to increased false-positive variant calls, resulting in inaccurate conclusions. Bases scoring Q30 and above are ideal for clinical research.

We next analyzed the occurrence of trimer motifs (sequences of three amino acids) within each identified peptide sequence recovered from each tissue. Using these occurrences, we prepared a hierarchically-clustered heatmap of trimers recovered from each tissues from the high ID of library after 1 hour. Some motifs are very common across all tissues and are non-selective for any particular tissues. However, several clusters of motifs were unique or occurred more often in specific tissues (**Figure 7**).

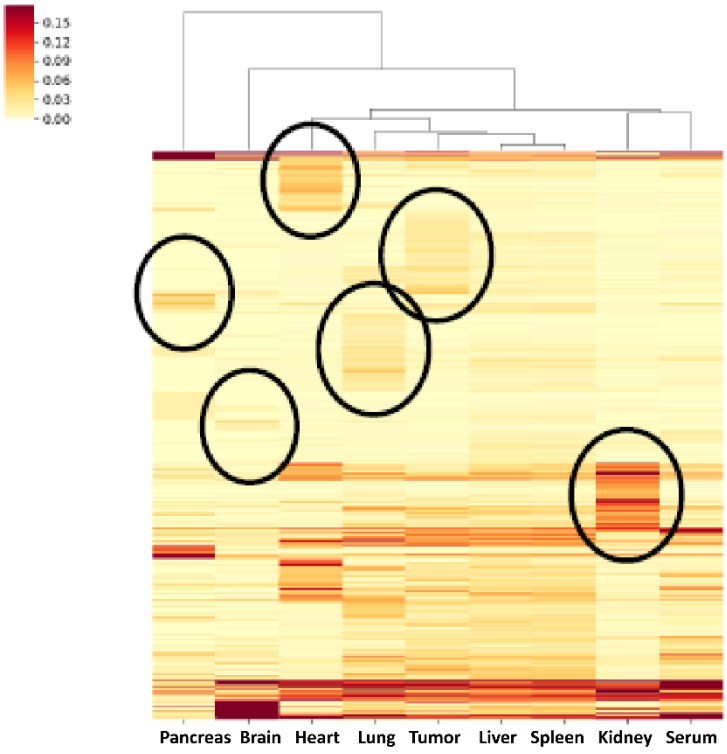

Figure 7: Heatmap of trimer motifs. Heatmap shows the occurrence of each amino acid trimer motif sequenced within each tissue (from 1 hour mouse w/ MDA-MB-231 xenograft). The hierarchically-clustered represent the trimers map into the tissues. In particular, each row represent a unique motif (based on trimers) with a percent occurrence <0.0125% identified in overlapping with the total sequences found in the tissue, in turn represented in column. The circles highlight clusters of motifs that were unique or occurred more often in specific tissues.

Some tissues, like liver and spleen, have similar motif distributions as may be expected for their non-selective processing of phages due to the biological flow and/or degradation activity of these tissues. However, tissues such as kidney, brain, pancreas and tumor contain populations with significant variation in motif distributions than other tissues, suggesting selection of tissue-selective enrichment of peptide structures has occurred. These preliminary data formed the basis for identification of peptide sequences that selectively home to specific tissues, including a tumor xenograft of human breast cancer cells. Identified sequences will be further analyzed using the algorithm presented above (Chapter 5.1), in order to identify and/or create novel mosaic proteins based on short Linear Motifs (SLiMs). These identified peptide structures would allow a phage, or other nanomedicine delivery systems, to extravasate from the local blood stream at the tumor site. By mimicking the mechanisms of neutrophil

extravasation, phage clones could migrate through several molecular/cellular barriers surrounding tumors, penetrate into the tumor mass and attack the diverse tumor cell population.

The advantage of this novel paradigm of “self-navigating programmed phage particles” could allow the rational design of multi-motif phage proteins able to target multiple cellular receptors. Moreover, it is possible to hypothesize that mosaic phage proteins or composed mosaic proteins from the association of CorMs and SLIMs, discovered through migration selection, can be used as molecular programs for cancer cell-targeted, tumor-targeted or tissue-targeted therapeutics. In order to develop novel tissue-specific probes for targeted imaging, anti-cancer preparations, and medications for the precise and personalized medicine, amplifying the potential of delivering drugs to a specific point in the body.

ES. Experimental Section

ES.1 Cells and cell culture

Human cell lines used in these studies were purchased from American Type Culture Collection (ATCC, Manassas, VA, USA): MCF-10A (Phenotypically normal breast epithelial cells; ATCC® CRL-10317™), and MDA-MB-231 (ATCC® HTB- 26™). All cells were maintained as sub-confluent monolayers in 25-cm^2 polystyrene flasks in the respective complete growth medium for each cell type, as recommended by ATCC, and grown in a water-jacketed incubator at 37 °C with 5% CO_2. A comparison of genome copy number and transcriptional profiles for the cell lines with those measured for primary breast tumors is available from [Neve et al, 2006].

ES.2 Computational Analysis

The list of fusion peptides displayed on the phage proteins (peptide inserts) was converted into FASTA files using Excel, and analyzed by MEME Suite (Motif-based sequence analysis tools v.5.0.5 [Bailey et al, 2009]; http://meme-suite.org/) to discover non-degenerate, non-gapped, tri-peptide motifs. The likely range of SLiMs, and Domain Motif Interactions (DMIs) they mediate, were identified using the Eukaryotic Linear Motif (ELM) resource [Gouw et al., 2018], http://elm.eu.org/. Biopanning Data Bank BDB [He et al., 2018], http://immunet.cn/bdb/index.php, a manually curated, publicly accessible database of peptides, selected from random phage display libraries, was used for identification of conserved structural motifs within short peptides, and for their comparison to the latest released version of the database. For prediction of protein functional activity, classifying peptides into families and predicting domains and important sites, we used InterPro—a single searchable resource that combines protein signatures from multiple databases [Mitchell et al., 2019], http://www.ebi.ac.uk/interpro/. For annotation of functional attributes that can be assigned to a genome, based on the presence of a defined set of protein family markers within that genome, we used an annotation system "Genome properties (GP)" [Richardson et al., 2019], https://www.ebi.ac.uk/interpro/genomeproperties/.

ES.3 Immunofluorescence Analysis of Phages

Individual representative phage clones, listed in paper Petrenko et al 2019, interacting with the human MDA-MB-231 breast cancer cell line, were propagated and purified, as described previously [Brigati et al., 2008], and verified for binding interactions in cell-association assays [Jayanna et al., 2010; Fagbohun et al., 2012]. Interactions of isolated phage clones with MDA-MB-231 breast cancer cells were analyzed as previously [Fagbohun et al., 2013]. Briefly, MDA-MB-231 cells were seeded into 4-well chamber slides (~50,000 cells/well in L15 medium w/ 10% FBS) and incubated in a 37 °C incubator with 5% CO_2 until cells were ~70% confluent. Cells were washed 3 times with 1X PBS, pH 7.4 for 5 minutes at room temperature. Next, cells were incubated with ~1.0×10^{10} virions of an isolated phage clone in serum-free L15 culture medium for 15 minutes or up to 24 hours at 37°C. Cells were washed with 1X PBS, pH 7.4 and fixed with 4% paraformaldehyde in PBS for 15 minutes at room temperature. After an additional 3 washes, cells were permeabilized with 0.1% Triton X-100 in PBS for 10 minutes at room temperature and blocked with 1% BSA for 30 minutes at room temperature. Cells were treated with a 1:1000 dilution of 3.3 mg/mL rabbit anti-fd bacteriophage antibodies [Smith et al., 1998] in blocking buffer (1% BSA in 1X PBS, pH 7.4) for 1 hour at room temperature. Cells were washed with 1X PBS and treated with a 1:500 dilution of AlexaFlour® 488 goat anti-rabbit IgG and 0.022 μM AlexaFlour® 546 phalloidin for 1 hour at room temperature in the dark. After washing, slides were cover slipped with VECTA shield mounting medium with DAPI (Vector Laboratories). Slides were visualized with a Nikon A1 laser module coupled to a

Nikon Eclipse C1 2000-E confocal microscope and z-stacks captured using the Nikon Elements software package at 0.150 µm/step with representative slices shown.

ES.4 qPCR of phage-DNA extracted from mouse tissues

On hundred microliters of homogenized tissues samples were mixed with 1 mL of DNAzol (Invitrogen). After thorough mixing, 500µL of 100% ethanol was added to each sample to precipitate the DNA. After centrifugation at ~6,000×g for 5 minutes the supernatant was removed, and the precipitated DNA washed twice with 800 µL of 75% ethanol. Precipitated DNA was dissolved in 100 µL of 8 mM NaOH and neutralized with 2.3 µL of 1 M HEPES (final solution pH ~7.2). Extracted DNA was quantified by qPCR by QuantStudio 3 Real-Time PCR System (Thermo Fisher Scientific).
The sequencing primers reverse (5'- AATGACAACAACCATCGCCC –3') and forward (5'– CAAAGCCTCCGTAGCCGTTG –3') were drawn to permit the amplicons of 160 pb (able to work with fd derived phage clones).

The study of correlation necessitated the use of the UC33 primers to identify the PTBP2 ultra-conserved gene in tissues, which translated for polypyrimidine tract binding protein, to quantify the cell DNA [forward 5' – AACTTGCCCCAATTAACCGC -3' and reverse 5'-AGACTTTGGGGCGTAACCAT – 3']. Consequently, two standard curves were obtained using the known quantities of phages DNA range (~1.0 – 10^9 vir/µL), and MCF-7 gDNA range (0.00731 - 73.1 ng/uL) in DNase-free H_2O. 2 µL of the DNA-template sample (cellular extracted DNA or known phage suspension) was added to the PCR reaction tube, containing 20 µL of the following qPCR mixture: 7 µL DNase-free H_2O; 10 µL 1X PerfeCTa SYBR Green FastMix (2×); 0.5 µL (250 nM (0.25 pmol/ µL)) forward; 0.5 µL (250 nM (0.25 pmol/ µL)) reverse. The qPCR was performed by Quant Studio 3 machine under the following cycling conditions: one cycle at 95 °C for 180'' (×1); 40 cycles at 95 °C for 10'', 60 °C for 30''; 72 °C for 5' (×1); and 1 cycle at 72-95 °C for 10''. The qPCR products (4 µL) were analyzed by agarose gel electrophoresis (1% wt/vol agarose, Sigma, Milan, Italy) in 1× TBE buffer. Gel was stained with of 3X gel green dye, illuminated on a Dark Reader, while DNA bands were visualized by a Kodak imaging system. qPCR products were purified by Qiagen PCR Clean-up purification kit and eluted in DNase-free H_2O. Purified amplicons were sent to the Massachusetts General Hospital Next Generation Sequencing (MGH NGS) core facility for massively parallel sequencing on an Illumina MiSeq platform.

After the translation of the received nucleotide sequences in amino-acid sequences, the calculation of the occurrence of each trimer motif (sequences of three amino acids) in each sequences within each tissue was performed, using a custom Python 3 script. Take each peptide sequences, of each tissue set, and count the number of overlapping trimers into a Python dictionary, then calculate the percent occurrence of each motif in the tissue as: ((motif count)/(total motif count)) x 100. Export the data from each into a csv file containing the motif, motif count, and the motif percent occurrence. Transform the percent occurrence data into a data frame with each row representing each possible AA trimer and each column representing a tissue. Filter and exclude each row (motif) with a percent occurrence <0.0125% (1/8,000 x 100, where 8,000 are the possible trimer combinations considering the combination of 20amino-acid (AA) disposed at 3AA) in all rows. Using the cluster map function from the sea born library (v0.9.0), construct a hierarchically-clustered heat map using Ward's clustering method. (Kolonin MG et al 2006).

CONCLUSIONS

The public health costs and the proper allocation of resources are among the most important world's problems. Bloodstream infections associated to the continue increase of antibiotic resistant strains are become the most cause of mortality, as well as the heterogeneity, intra and inter patient, of the cancer disease. Also, the population ageing, which leads to the increase of the neurodegenerative diseases, such as Alzheimer disease, implies expenditure for the public health.

Innovative biotechnologies when adequately assembled play a pivotal role in development of cheap, easy, and fast diagnostic and therapeutic systems applicable in public health. Moreover, the advancement of personalized nanomedicine, has increase the necessity to draw smart material targeting the disease.

An innovative contribution at diagnostic and targeted-therapeutic systems is given by phage display technology, which is powerful tool to discovery pathology specific-peptides.

In this work, the polyvalent ability of phage engineered clones has been applied in several fields (infectious, neoplastic and neurodegenerative disease) of diagnosis and targeted therapy.

In particular:

- For infectious disease:
    - Target-specific peptides able to selectively bind bacteria surface were selected;
    - Selected phage clones were used as probes in functionalization of polymeric platform and in micro-beads of different nature for applications in biosensor devises;

- The combination of phage-magnetic-separation and Raman Spectroscopy permitted the detection of bacteria, *S. aureus*, *P. aeruginosa* and *E. coli*, in a blood, with an efficiency of 10 bacteria/7mL.

- For Alzheimer disease:
  - Conformational phage clones were selected by innovative "double binding";
  - The conformational peptides discovered was able to discriminate sera of AD and healthy patients by E.L.I.S.A.. Moreover, levels of identified IgG in AD patient showed good correlation with the progression of the pathology, making the phages biomarkers of state/stage in Alzheimer's disease (AD). A patent has been accepted;
  - Moreover, the phages permitted inhibition and disaggregation *in vitro* of amyloid β42-induced cytotoxicity in SH-SY5Y neuroblastoma cell lines.
- For leukemia/multiple myeloma disease:
  - Phages, displaying promiscuous peptides able to detect common marker of inter-specific leukemia/myeloma disease were selected;
  - Selected phages were used in production fluorescent phage–probes for discrimination of leukemic/myeloma cells.
- For "new targeted medicine":
  - New concept of "self-navigating phage particles programmed" was introduced;
  - New algorithm was applied in phage population, specific for bound of breast cancer cell, to find smart "mosaic peptides" based of CorMs and SLIMs;
  - Bio-distributed landscape phage library f8/9 in nude mice harboring human breast cancer cell, allowed to study the pharmacokinetic of the phage library;
  - Preliminary data of phage-peptides home-tumor and home-tissues were obtained by sequencing in next generation sequencing.

Acknowledgements and Collaborations

This activity was partially funded by Italian Ministry of Education, University and Research (MIUR) by means of the national Program PON R&C 2007–2013, project HIPPOCRATES – Development of Micro and Nano-Technologies and Advanced Systems for Human Health (PON02_00355_29641931) and project.

This activity was partially supported by Associazione pro Bambini e Adulti Leucemici (A.B.A.L.) onlus Messina (Italy) (http://www.abalmessina.it).

My sincere thanks goes to Prof. Dr. Petrenko V.A., who provided me an opportunity to join his team as intern. His precious support and his guidance helped me in all the time of research activity at Auburn University, improving my knowledge in phage-nano-biotechnology application.

This activity was carried out in collaboration with:

Prof. Dr. V. A. Petrenko, Dr. J. Gillespie and Dr. Liping Yang of Department of Pathobiology, College of Veterinary Medicine, Auburn University, Auburn, AL 36849, USA.

Prof. S. Conoci and Dr. S. Petralia of Distretto Tecnologico Micro e Nano Sistemi Sicilia, Strada VII-Zona Industriale, 95121 Catania, Italy.

Prof. S. Cuzzocrea, Prof. E. Esposito and Dr M. Campolo of Department of Chemical, Biological, Pharmaceutical and Environmental Sciences, University of Messina, Viale F. Stagno D'Alcontres 31, 98166 Messina, Italy.

Prof. E. Fazio and Professor F. Neri Department of Mathematical and Computational Sciences, Physical Science and Earth Science (MIFT), University of Messina, Italy.

Doctor S. Trusso Institute of Chemical-Physical Processes (IPCF)-CNR Messina, Italy.

Prof. G. Marletta and Prof. G. M. G. Messina of Laboratory for Molecular Surfaces and Nanotechnology (LAMSUN), Department of Chemical Sciences, University of Catania and CSGI, Viale A. Doria 6, 95125 Catania, Italy.

Professor A. M. Mezzasalma of Department of Mathematical and Computational Sciences, Physical Science and Earth Science (MIFT), University of Messina, Italy.

Professor C. Musolino and Dr A. Allegra of Division of Hematology, Department of General Surgery, Pathological Anatomy and Oncology, University of Messina, Italy.

REFERENCES

Aghebati-Maleki L, Bakhshinejad B, Baradaran B, Motallebnezhad M, Aghebati-Maleki A, Nickho H, Yousefi M, Majidi J. **Phage display as a promising approach for vaccine development**. J Biomed Sci 2016, 23(1):66.

Bagga K, Barchanski A, Intartaglia R, Dante S, Marotta R, Diaspro A, Sajti CL, Brandi F. **Laser-assisted synthesis of Staphylococcus aureus protein-capped silicon quantum dots as bio-functional nanoprobes**. Laser Phys Lett 2013, 10(6): 065603

Bailey TL, Boden M, Buske FA, Frith M, Grant CE, Clementi L, Ren J, Li WW, Noble WS. **MEME SUITE: tools for motif discovery and searching.** Nucleic Acids Res. 2009, 37(Web Server issue): W202-8.

Bakhshinejad B, Zade HM, Shekarabi HS, Neman S. **Phage display biopanning and isolation of target-unrelated peptides: in search of nonspecific binders hidden in a combinatorial library**. Amino Acids 2016, 48(12):2699-2716.

Barbas CF 3rd, Kang AS, Lerner RA and Benkovic SJ. **Assembly of combinatorial antibody libraries on phage surfaces: the gene III site**. Proc Natl Acad Sci USA 1991, 88:7978-7982.

Baril L, Nicolas L, Croisile B, Crozier P, Hessler C, Sassolas A, McCormick JB, Trannoy E. **Immune response to Abeta-peptides in peripheral blood from patients with Alzheimer's disease and control subjects**. Neurosci Lett. 2004, 355(3):226-30.

Bass S, Greene R and Wells JA. **Hormone phage: An enrichment method for variant proteins with altered binding properties**. Proteins 1990, 8:309-314.

Bentley DR. **Whole-genome re-sequencing.** Curr Opin Genet Dev, 2006, 16(6):545-52.

Bentley DR, Balasubramanian S, Swerdlow HP, Smith GP, Milton J, Brown CG, Hall KP, Evers DJ, Barnes CL, Bignell HR, Boutell JM, Bryant J, Carter RJ, Keira Cheetham R, Cox AJ, Ellis DJ, Flatbush MR, Gormley NA, Humphray SJ, Irving LJ, Karbelashvili MS, Kirk SM, Li H, Liu X, Maisinger KS, Murray LJ, Obradovic B, Ost T, Parkinson ML, Pratt MR, Rasolonjatovo IM, Reed MT, Rigatti R, Rodighiero C, Ross MT, Sabot A, Sankar SV, Scally A, Schroth GP, Smith ME, Smith VP, Spiridou A, Torrance PE, Tzonev SS, Vermaas EH, Walter K, Wu X, Zhang L, Alam MD, Anastasi C, Aniebo IC, Bailey DM, Bancarz IR, Banerjee S, Barbour SG, Baybayan PA, Benoit VA, Benson KF, Bevis C, Black PJ, Boodhun A, Brennan JS, Bridgham JA, Brown RC, Brown AA, Buermann DH, Bundu AA, Burrows JC, Carter NP, Castillo N, Chiara E Catenazzi M, Chang S, Neil Cooley R, Crake NR, Dada OO, Diakoumakos KD, Dominguez-Fernandez B, Earnshaw DJ, Egbujor UC, Elmore DW, Etchin SS, Ewan MR, Fedurco M, Fraser LJ, Fuentes Fajardo KV, Scott Furey W, George D, Gietzen KJ, Goddard CP, Golda GS, Granieri PA, Green DE, Gustafson DL, Hansen NF, Harnish K, Haudenschild CD, Heyer NI, Hims MM, Ho JT, Horgan AM, Hoschler K, Hurwitz S, Ivanov DV, Johnson MQ, James T, Huw Jones TA, Kang GD, Kerelska TH, Kersey AD, Khrebtukova I, Kindwall AP, Kingsbury Z, Kokko-Gonzales PI, Kumar A, Laurent MA, Lawley CT, Lee SE, Lee X, Liao AK, Loch JA, Lok M, Luo S, Mammen RM, Martin JW, McCauley PG, McNitt P, Mehta P, Moon KW, Mullens JW, Newington T, Ning Z, Ling Ng B, Novo SM, O'Neill MJ, Osborne MA, Osnowski A, Ostadan O, Paraschos LL, Pickering L, Pike AC, Pike AC, Chris Pinkard D, Pliskin DP, Podhasky J, Quijano VJ, Raczy C, Rae VH, Rawlings SR, Chiva Rodriguez A, Roe PM, Rogers J, Rogert Bacigalupo MC, Romanov N, Romieu A, Roth RK, Rourke NJ, Ruediger ST, Rusman E, Sanches-Kuiper RM, Schenker MR, Seoane JM,

Shaw RJ, Shiver MK, Short SW, Sizto NL, Sluis JP, Smith MA, Ernest Sohna Sohna J, Spence EJ, Stevens K, Sutton N, Szajkowski L, Tregidgo CL, Turcatti G, Vandevondele S, Verhovsky Y, Virk SM, Wakelin S, Walcott GC, Wang J, Worsley GJ, Yan J, Yau L, Zuerlein M, Rogers J, Mullikin JC, Hurles ME, McCooke NJ, West JS, Oaks FL, Lundberg PL, Klenerman D, Durbin R, Smith AJ. **Accurate whole human genome sequencing using reversible terminator chemistry.** Nature. 2008, 456(7218):53-9.

Bertrand N, Wu J, Xu X, Kamaly N, Farokhzad OC. **Cancer nanotechnology: the impact of passive and active targeting in the era of modern cancer biology.** Adv Drug Deliv Rev 2014, 66:2-25.

Blanco E, Hsiao A, Mann AP, Landry MG, Meric-Bernstam F, Ferrari M. **Nanomedicine in cancer therapy: innovative trends and prospects**. Cancer Sci. 2011, 102(7):1247-52.

Blennow K, Zetterberg H. **Cerebrospinal fluid biomarkers for Alzheimer's disease**. J Alzheimers Dis. 2009, 18(2):413-7.

Braga PAC, Tata A, dos Santos VG, Barreiro JR, Schwab NV, dos Santos MV, Eberlina MN, Ferreira CR. **Bacterial identification: from the agar plate to the mass spectrometer**. RSC Adv. 2013, 3: 994–1008.

Bratkovic T. **Progress in phage display: evolution of the technique and its application**. Cell Mol Life Sci 2010, 67(5):749-67.

Brettschneider S, Morgenthaler NG, Teipel SJ, Fischer-Schulz C, Bürger K, Dodel R, Du Y, Möller HJ, Bergmann A, Hampel H. **Decreased serum amyloid beta(1-42) autoantibody levels in Alzheimer's disease, determined by a newly developed immuno-precipitation assay with radiolabeled amyloid beta(1-42) peptide**. Biol Psychiatry. 2005, 57(7):813-6.

Brigati JR, Petrenko VA. **Thermostability of landscape phage probes**. Anal Bioanal Chem. 2005, 382(6):1346-50.

Brigati JR, Samoylova T, Jayanna PK, Petrenko VA. **Phage display for generating peptide reagents.** Curr Protoc Protein Sci. 2008, Chapter 18:Unit 18.9.

Brown KC. **Peptidic tumor targeting agents: the road from phage display peptide selections to clinical applications**. Curr Pharm Des. 2010, 16(9):1040-54.

Bruckman MA, Kaur G, Lee LA, Xie F, Sepulveda J, Breitenkamp R, Zhang X, Joralemon M, Russell TP, Emrick T, Wang Q. **Surface modification of tobacco mosaic virus with "click" chemistry**. Chembiochem 2008, 9(4):519-23.

Bussel JB, Kuter DJ, George JN, McMillan R, Aledort LM, Conklin GT, Lichtin AE, Lyons RM, Nieva J, Wasser JS, Wiznitzer I, Kelly R, Chen CF, Nichol JL. **AMG 531, a thrombopoiesis-stimulating protein, for chronic ITP.** N Engl J Med 2006, 55(16):1672-81.

Butler JC, Angelini T, Tang JX, Wong GC. **Ion multivalence and like-charge polyelectrolyte attraction.** Phys Rev Lett. 2003, 91(2):028301.

Caberoy NB, Zhou Y, Jiang X, Alvarado G, Li W. **Efficient identification of tubby-binding proteins by an improved system of T7 phage display.** J Mol Recognit 2010, 23(1):74-83.

Cailleau R, Young R, Olivé M, Reeves WJ Jr. **Breast tumor cell lines from pleural effusions**. J Natl Cancer Inst. 1974, 53(3):661-74.

Calabrese F, Carnazza S, De Plano LM, Lentini G, Franco D, Guglielmino SPP. **Phage coated paramagnetic beads as selective and specific capture system for biosensor applications**. 2015. XVIII AISEM Annual Conference 1-4.

Cao B, Yang M, Zhu Y, Qu X, Mao C. **Stem cells loaded with nanoparticles as a drug carrier for in vivo breast cancer therapy.** Adv Mater. 2014, 26(27):4627-31.

Carnazza S, Foti C, Gioffrè G, Felici F, Guglielmino S. **Specific and selective probes for Pseudomonas aeruginosa from phage-displayed random peptide libraries**. Biosens Bioelectron. 2008, 23(7):1137-44.

Cardó-Vila M, Zurita AJ, Giordano RJ, Sun J, Rangel R, Guzman-Rojas L, Anobom CD, Valente AP, Almeida FC, Lahdenranta J, Kolonin MG, Arap W, Pasqualini R. **A ligand peptide motif selected from a cancer patient is a receptor-interacting site within human interleukin-11.** PLoS One, 2008, 3(10): e3452.

Caroli A, Prestia A, Galluzzi S, Ferrari C, van der Flier WM, Ossenkoppele R, Van Berckel B, Barkhof F, Teunissen C, Wall AE, Carter SF, Schöll M, Choo IH, Grimmer T, Redolfi A, Nordberg A, Scheltens P, Drzezga A, Frisoni GB; Alzheimer's Disease Neuroimaging Initiative. **Mild cognitive impairment with suspected nonamyloid pathology (SNAP): Prediction of progression.** Neurology. 2015, 84(5):508-15.

Chan WC, Maxwell DJ, Gao X, Bailey RE, Han M, Nie S. **Luminescent quantum dots for multiplexed biological detection and imaging**. Curr Opin Biotechnol. 2002, 13(1):40-6.

Chan JW, Taylor DS, Zwerdling T, Lane SM, Ihara K, Huser T. **Micro-Raman spectroscopy detects individual neoplastic and normal hematopoietic cells.** Biophys J. 2006 Jan 15;90(2):648-56.

Chang W, Dynek JN, Smith S. **NuMA is a major acceptor of poly(ADP-ribosyl)ation by tankyrase 1 in mitosis.** Biochem J. 2005, 391(Pt 2):177-84.

Chen CL, Rosi NL. **Peptide-based methods for the preparation of nanostructured inorganic materials.** Angew Chem Int Ed Engl 2010, 49(11):1924-42.

Cheng WT1, Liu MT, Liu HN, Lin SY**. Micro-Raman spectroscopy used to identify and grade human skin pilomatrixoma**. Microsc Res Tech. 2005 Oct;68(2):75-9.

Chewchinda P, Odawara O, Wad H. **Silicon Nanoparticles Prepared by Laser Ablation in Electrolyte Solution.** CheM 2016, 3:81-86.

Chi NW, Lodish HF. **Tankyrase is a golgi-associated mitogen-activated protein kinase substrate that interacts with IRAP in GLUT4 vesicles.** J Biol Chem 2000, 275(49):38437-44.

Chiorazzi N, Rai KR, Ferrarini M. Chronic lymphocytic leukemia. N Engl J Med. 2005, 352(8):804-15.

Choo-Smith LP, Edwards HGM, Endtz HP, Kros JM, Heule F, Barr H, Robinson J S Jr, Bruining HA, Pupells GJ. **Medical applications of Raman spectroscopy: From proof of principle to clinical implementation**. Biopolymers 2002, 67:1–9.

Chung WJ, Lee DY1, Yoo SY2. **Chemical modulation of M13 bacteriophage and its functional opportunities for nanomedicine.** Int J Nanomedicine 2014, 9:5825-36.

Clackson T, Hoogenboom HR, Griffiths AD, Winter G. **Making antibody fragments using phage display libraries.** Nature 1991, 352(6336):624-8.

Cochran R, Cochran F. **Phage display and molecular imaging: expanding fields of vision in living subjects.** Biotechnol Genet Eng Rev 2010, 27:57-94.

Coen MC, Lehmann R, Gröning P, Bielmann M, Galli C, Schlapbach L. **Adsorption and Bioactivity of Protein A on Silicon Surfaces Studied by AFM and XPS.** J Colloid Interface Sci. 2001, 233(2):180-189.

Davey NE, Van Roey K, Weatheritt RJ, Toedt G, Uyar B, Altenberg B, Budd A, Diella F, Dinkel H, Gibson TJ. **Attributes of short linear motifs**. Mol Biosyst. 2012, 8(1):268-81.

Demidova-Rice TN, Hamblin MR, Herman IM. **Acute and impaired wound healing: pathophysiology and current methods for drug delivery, part 2: role of growth factors in normal and pathological wound healing: therapeutic potential and methods of delivery**. Adv Skin Wound Care 2012, 25(8):349-70.

De Plano LM, Carnazza S, Messina GML, Rizzo MG, Marletta G, Guglielmino SPP**. Specific and selective probes for Staphylococcus aureus from phage-displayed random peptide libraries**. Colloids Surf B Biointerfaces 2017, 157:473-480.

De Plano LM, Scibilia S, Rizzo MG, Crea S, Franco D, Mezzasalma AM, Guglielmino SPP. **One-step production of phage–silicon nanoparticles by PLAL as fluorescent nanoprobes for cell identification.** Applied Physics A 2018, 124:222

De Plano LM, Franco D, Rizzo MG, Crea S, Messina GML, Marletta G, Guglielmino SPP. **M13 Bacteriophages as Bioreceptors in Biosensor Device**. In: Andò B. et al. (eds) Sensors. CNS 2018. Lecture Notes in Electrical Engineering, vol 539. Springer, Cham.

De Plano LM, Fazio E, Rizzo MG, Franco D, Carnazza S, Trusso S, Neri F, Guglielmino SPP**. Phage-based assay for rapid detection of bacterial pathogens in blood by Raman spectroscopy**. J Immunol Methods. 2019, 465:45-52.

Derfus AM, Chan WCW, Bhatia SN. **Probing the Cytotoxicity Of Semiconductor Quantum Dots.** Nano Lett. 2004, 4(1):11-18.

Dias-Neto E, Nunes DN, Giordano RJ, Sun J, Botz GH, Yang K, Setubal JC, Pasqualini R, Arap W. **Next-generation phage display: integrating and comparing available molecular tools to enable cost-effective high-throughput analysis**. PLoS One. 2009, 4(12):e8338.

Dimant H, Sharon N, Solomon B. **Modulation effect of filamentous phage on alpha- synuclein aggregation**. Biochem. Biophys Res Commun. 2009, 383:491–6.

Dimant H, Solomon B. **Filamentous phages reduce alpha-synuclein oligomerization in the membrane fraction of SH-SY5Y cells**. Neurodegener Dis 2010, 7:203–5.

Dodel R, Bacher M, Przybylski M, Stefanescu R, Manea M. **Diagnosis of Alzheimer's disease and other neurodementing disorders**. Patent International Application No.: PCT/IB2008/000456, Pub. No.: WO/2008/084402, European Patent Office 2018

Endemann H, Model P. **Location of filamentous phage minor coat proteins in phage and in infected cells.** J Mol Biol 1995, 250(4):496-506.

Fack F, Hügle-Dörr B, Song D, Queitsch I, Petersen G, Bautz EK. **Epitope mapping by phage display: random versus gene-fragment libraries.** J Immunol Methods 1997, 206(1-2):43-52.

Fagbohun OA, Bedi D, Grabchenko NI, Deinnocentes PA, Bird RC, Petrenko VA. **Landscape phages and their fusion proteins targeted to breast cancer cells.** Protein Eng Des Sel 2012, 25(6):271-83.

Fagbohun OA, Kazmierczak RA, Petrenko VA, Eisenstark A. **Metastatic prostate cancer cell-specific phage-like particles as a targeted gene-delivery system.** J Nanobiotechnology. 2013, 11:31.

Fazio E, Cacciola A, Mezzasalma AM, Mondio G, Neri N, Saija R. **Modelling of the optical absorption spectra of PLAL prepared ZnO colloids.** J. Quant. Spectro. Rad. Trans. 2013, 295:119-127.

Fazio B, D'Andrea C, Foti A, Messina E, Irrera A, Donato MG, Villari V, Micali N, Maragò OM, Gucciardi PG. **SERS detection of Biomolecules at Physiological pH via aggregation of Gold Nanorods mediated by Optical Forces and Plasmonic Heating.** Sci Rep. 2016, 6:26952.

Felici F, Castagnoli L, Musacchio A, Jappelli R, Cesareni G. **Selection of antibody ligands from a large library of oligopeptides expressed on a multivalent exposition vector**. J Mol Biol. 1991 Nov 20;222(2):301-10.

Fillmore CM, Kuperwass C. **Human breast cancer cell lines contain stem-like cells that self-renew, give rise to phenotypically diverse progeny and survive chemotherapy.** Breast Cancer Res. 2008, 10(2): R25.

Foddai A, Elliott CT, Grant IR. **Maximizing capture efficiency and specificity of magnetic separation for Mycobacterium avium subsp. paratuberculosis cells**. Appl Environ Microbiol 2010, 76(22):7550-8.

Franco D, De Plano LM, Rizzo MG, Crea S, Fazio E, Bonsignore M, Neri F, Allegra A, Musolino C, Ferlazzo G, Trusso S, Guglielmino SPP. **FITC-Labelled Clone from Phage Display for Direct Detection of Leukemia Cells in Blood.** In Andò B. et al. (eds) Sensors. CNS 2018. Lecture Notes in Electrical Engineering, vol 539. Springer, Cham.

Franco D, De Plano LM, Rizzo MG, Scibilia S, Lentini G, Fazio E, Neri F, Guglielmino SPP, Mezzasalma AM. **Bio-hybrid gold nanoparticles as SERS probe for rapid bacteria cell identification**. Spectrochim Acta A Mol Biomol Spectrosc. 2019, 224:117394.

Frelin C, Imbert V, Griessinger E, Peyron AC, Rochet N, Philip P, Dageville C, Sirvent A, Hummelsberger M, Bérard E, Dreano M, Sirvent N, Peyron JF. **Targeting NF-kappaB activation**

via pharmacologic inhibition of IKK2-induced apoptosis of human acute myeloid leukemia cells. Blood. 2005, 105(2):804-11.

Frenkel D, Katz O, Solomon B. **Immunization against Alzheimer's beta -amyloid plaques via EFRH phage administration.** Proc Natl Acad Sci U S A. 2000, 97(21):11455-9.

Frenkel D, Balass M, Solomon B. **N-terminal EFRH sequence of Alzheimer's beta-amyloid peptide represents the epitope of its anti-aggregating antibodies**. J Neuroimmunol. 1998, 88(1-2):85-90.

Geysen HM, Rodda SJ, Mason TJ. **A priori delineation of a peptide which mimics a discontinuous antigenic determinant**. Mol Immunol 1986, 23(7):709-15.

Gillespie JW, Wei L, Petrenko VA. **Selection of Lung Cancer-Specific Landscape Phage for Targeted Drug Delivery**. Comb Chem High Throughput Screen 2016, 19(5):412-22.

Gillespie JW, Gross AL, Puzyrev AT, Bedi D, Petrenko VA. **Combinatorial synthesis and screening of cancer cell-specific nanomedicines targeted via phage fusion proteins**. Front Microbiol. 2015, 6:628.

Gouw M, Michael S, Sámano-Sánchez H, Kumar M, Zeke A, Lang B, Bely B, Chemes LB, Davey NE, Deng Z, Diella F, Gürth CM, Huber AK, Kleinsorg S, Schlegel LS, Palopoli N, Roey KV, Altenberg B, Reményi A, Dinkel H, Gibson TJ. **The eukaryotic linear motif resource - 2018 update.** Nucleic Acids Res. 2018, 46(D1): D428-D434.

Gremer L, Schölzel D, Schenk C, Reinartz E, Labahn J, Ravelli RBG, Tusche M, Lopez-Iglesias C, Hoyer W, Heise H, Willbold D, Schröder GF. **Fibril structure of amyloid-β(1-42) by cryo-electron microscopy.** Science. 2017, 358(6359):116-119.

Gross AL, Gillespie JW, Petrenko VA. **Promiscuous tumor targeting phage proteins**. Protein Eng Des Sel. 2016, 29(3):93-103.

Haney EF, Mansour SC, Hilchie AL, de la Fuente-Núñez C, Hancock RE. **High throughput screening methods for assessing antibiofilm and immunomodulatory activities of synthetic peptides.** Peptides. 2015, 71:276-85.

Hansenová Maňásková S, van Belkum A, Endtz HP, Bikker FJ, Veerman EC, van Wamel WJ. **Comparison of non-magnetic and magnetic beads in bead-based assays.** J Immunol Methods. 2016, 436:29-33.

Harjunpää H, Llort Asens M, Guenther C, Fagerholm SC. **Cell Adhesion Molecules and Their Roles and Regulation in the Immune and Tumor Microenvironment**. Front Immunol. 2019, 10:1078.

Harmsen M, Yang L, Pamp SJ, Tolker-Nielsen T. **An update on Pseudomonas aeruginosa biofilm formation, tolerance, and dispersal**. FEMS Immunol Med Microbiol 2010, 59(3):253-68.

He B, Jiang L, Duan Y, Chai G, Fang Y, Kang J, Yu M, Li N, Tang Z, Yao P, Wu P, Derda R, Huang J. **Biopanning data bank 2018: hugging next generation phage display.** Database (Oxford). 2018, 2018.

Hemminga MA, Vos WL, Nazarov PV, Koehorst RB, Wolfs CJ, Spruijt RB, Stopar D. **Viruses: incredible nanomachines. New advances with filamentous phages.** Eur Biophys J 2010, 39(4):541-50.

Herman RE, Makienko EG, Prieve MG, Fuller M, Houston ME Jr, Johnson PH. **Phage display screening of epithelial cell monolayers treated with EGTA: identification of peptide FDFWITP that modulates tight junction activity**. J Biomol Screen. 2007, 12(8):1092-101.

Hill HR, Stockley PG. **Phage presentation.** Mol Microbiol, 1996, 20(4):685-92.

Hiraga K, Soga I, Dansereau JT, Pereira B, Derbyshire V, Du Z, Wang C, Van Roey P, Belfort G, Belfort M. **Selection and structure of hyperactive inteins: peripheral changes relayed to the catalytic center.** J Mol Biol. 2009, 393(5):1106-17.

't Hoen PA, Jirka SM, Ten Broeke BR, Schultes EA, Aguilera B, Pang KH, Heemskerk H, Aartsma-Rus A, van Ommen GJ, den Dunnen JT. **Phage display screening without repetitious selection rounds.** Anal Biochem. 2012, 421(2):622-31.

Hoogenboom HR. **Overview of antibody phage-display technology and its applications**. Methods Mol Biol 2002, 178:1-37.

Hoogenboom HR. **Selecting and screening recombinant antibody libraries.** Nat Biotechnol 2005, 23(9):1105-16.

Huang JX, Bishop-Hurley SL, Cooper MA. **Development of anti-infectives using phage display: biological agents against bacteria, viruses, and parasites**. Antimicrob Agents Chemother 2012, 56(9):4569-82.

Huang S, Yang H, Lakshmanan RS, Johnson ML, Chen I, Wan J, Wikle HC, Petrenko VA, Barbaree JM, Cheng ZY, Chin BA. **The effect of salt and phage concentrations on the binding sensitivity of magnetoelastic biosensors for Bacillus anthracis detection.** Biotechnol Bioeng. 2008, 101(5):1014-21.

Humphries JD, Byron A, Humphries MJ. **Integrin ligands at a glance.** J Cell Sci. 2006,119(Pt 19):3901-3.

Hyman BT. **Molecular and anatomical studies in Alzheimer's disease.** Neurologia. 2001, 16(3):100-4.

Intartaglia R, Bagga K, Genovese A, Athanassiou A, Cingolani R, Diaspro A, Brandi F. **Influence of organic solvent on optical and structural properties of ultra-small silicon dots synthesized by UV laser ablation in liquid**. Phys Chem Chem Phys. 2012, 14(44):15406-11.

Jack CR Jr, Bennett DA, Blennow K, Carrillo MC, Dunn B, Haeberlein SB, Holtzman DM, Jagust W, Jessen F, Karlawish J, Liu E, Molinuevo JL, Montine T, Phelps C, Rankin KP, Rowe CC, Scheltens P, Siemers E, Snyder HM, Sperling R; Contributors. **NIA-AA Research Framework: Toward a biological definition of Alzheimer's disease.** Alzheimers Dement. 2018, 14(4):535-562.

Javadpour MM, Juban MM, Lo WC, Bishop SM, Alberty JB, Cowell SM, Becker CL, McLaughlin ML. **De novo antimicrobial peptides with low mammalian cell toxicity**. J Med Chem. 1996, 39(16):3107-13.

Jawhara S, Pluskota E, Cao W, Plow EF, Soloviev DA. **Distinct Effects of Integrins αXβ2 and αMβ2 on Leukocyte Subpopulations during Inflammation and Antimicrobial Responses**. Infect Immun. 2016, 85(1):pii: e00644-16.

Jaye DL, Geigerman CM, Fuller RE, Akyildiz A, Parkos CA. **Direct fluorochrome labeling of phage display library clones for studying binding specificities: applications in flow cytometry and fluorescence microscopy.** J Immunol Methods. 2004, 295(1-2):119-27.

Javadpour MM, Juban MM, Lo WC, Bishop SM, Alberty JB, Cowell SM, Becker CL, McLaughlin ML. **De novo antimicrobial peptides with low mammalian cell toxicity**. J Med Chem. 1996, 39(16):3107-13.

Jayanna PK, Bedi D, Deinnocentes P, Bird RC, Petrenko VA. **Landscape phage ligands for PC3 prostate carcinoma cells.** Protein Eng Des Sel. 2010, 23(6):423-30.

Jehlička J, Edwards HG, Oren A. **Bacterioruberin and salinixanthin carotenoids of extremely halophilic Archaea and Bacteria: a Raman spectroscopic study**. Spectrochim Acta A Mol Biomol Spectrosc. 2013, 106:99-103.

Ju Z, Sun W. **Drug delivery vectors based on filamentous bacteriophages and phage-mimetic nanoparticles.** Drug Deliv. 2017, 24(1):1898-1908.

Karin M. **How NF-kappaB is activated: the role of the IkappaB kinase (IKK) complex**. Oncogene. 1999, 18 (49): 6867–74.

Kast RE, Serhatkulu GK, Cao A, Pandya AK, Dai H, Thakur JS, Naik VM, Naik R, Klein MD, Auner GW, Rabah R. **Raman spectroscopy can differentiate malignant tumors from normal breast tissue and detect early neoplastic changes in a mouse model**. Biopolymers. 2008, 89(3):235-41.

Kay BK, Kasanov J, Yamabhai M. **Screening phage-displayed combinatorial peptide libraries**. Methods 2001, 24(3):240-6.

Kayed R, Head E, Thompson JL, McIntire TM, Milton SC, Cotman CW, Glabe CG. **Common structure of soluble amyloid oligomers implies common mechanism of pathogenesis.** Science. 2003, 300(5618):486-9.

Kehoe JW, Kay BK. **Filamentous phage display in the new millennium**. Chem Rev 2005, 105(11):4056-72.

Khazanov NA, Carlson HA. **Exploring the composition of protein-ligand binding sites on a large scale**. PLoS Comput Biol. 2013, 9(11): e1003321.

Kinjo AR, Nakamura H. **Composite structural motifs of binding sites for delineating biological functions of proteins**. PLoS One. 2012, 7(2): e31437.

Kloß S, Kampe B, Sachse S, Rösch P, Straube E, Pfister W, Kiehntopf M, Popp J. **Culture independent Raman spectroscopic identification of urinary tract infection pathogens: a proof of principle study**. Anal Chem 2013, 85(20):9610-6.

Knittelfelder R, Riemer AB, Jensen-Jarolim E. **Mimotope vaccination – from allergy to cancer. Expert Opin. Biol. Ther**. 2009, 9(4):493–506.

Kodali R, Williams, Chemuru, Wetzel R. **Abeta(1-40) forms five distinct amyloid structures whose beta-sheet contents and fibril stabilities are correlated**. J. Mol. Biol. 2010, 401(3):503-17.

Krishnan R, Tsubery H, Proschitsky MY, Asp E, Lulu M, Gilead S, Gartner M, Waltho JP, Davis PJ, Hounslow AM, Kirschner DA, Inouye H, Myszka DG, Wright J, Solomon B, Fisher RA. **A bacteriophage capsid protein provides a general amyloid interaction motif (GAIM) that binds and remodels misfolded protein assemblies**. J Mol Biol 2014, 426(13): 2500-19.

Kumar S, Rajkumar SV, Kimlinger T, Greipp PR, Witzig TE. **CD45 expression by bone marrow plasma cells in multiple myeloma: clinical and biological correlations.** Leukemia. 2005, 19(8):1466-70.

Kurochkina N, Guha U. **SH3 domains: modules of protein-protein interactions**. Biophys Rev. 2013, 5(1):29-39.

Kumar S, Sharma AR, Sharma G, Chakraborty C, Kim J. **PLK-1: Angel or devil for cell cycle progression**. Biochim Biophys Acta. 2016, 1865(2):190-203.

Landau DA, Carter SL, Stojanov P, McKenna A, Stevenson K, Lawrence MS, Sougnez C, Stewart C, Sivachenko A, Wang L, Wan Y, Zhang W, Shukla SA, Vartanov A, Fernandes SM, Saksena G, Cibulskis K, Tesar B, Gabriel S, Hacohen N, Meyerson M, Lander ES, Neuberg D, Brown JR, Getz G, Wu CJ. **Evolution and impact of subclonal mutations in chronic lymphocytic leukemia**. Cell. 2013, 152(4):714-26.

Lee JW, Song J, Hwang MP, Lee KH. **Nanoscale bacteriophage biosensors beyond phage display.** Int J Nanomedicine 2013, 8:3917-25.

Lee SY, Jang C, Lee KA. **Polo-like kinases (plks), a key regulator of cell cycle and new potential target for cancer therapy**. Dev Reprod. 2014, 18(1):65-71.

Lee K, Yoon SS. **Pseudomonas aeruginosa Biofilm, a Programmed Bacterial Life for Fitness**. J Microbiol Biotechnol. 2017 ;27(6):1053-1064.

Lehmann A. **Ecallantide (DX-88), a plasma kallikrein inhibitor for the treatment of hereditary angioedema and the prevention of blood loss in on-pump cardiothoracic surgery.** Expert Opin Biol Ther 2008, 8(8):1187-99.

Lentini G, Franco D, Fazio E, De Plano LM, Trusso S, Carnazza S, Neri F, Guglielmino SPP, **Rapid detection of Pseudomonas aeruginosa by phage-capture system coupled with micro-Raman spectroscopy.** VIBSPE 2016, 86:1-7.

Lentini G, Fazio E, Calabrese F, De Plano LM, Puliafico M, Franco D, Nicolò MS, Carnazza S, Trusso S, Allegra A, Neri F, Musolino C, Guglielmino SPP. **Phage-AgNPs complex as SERS probe for U937 cell identification. Biosens Bioelectron. 2015,74:398-405.**

Leone P, Berardi S, Frassanito MA, Ria R, De Re V, Cicco S, Battaglia S, Ditonno P, Dammacco F, Vacca A, Racanelli V. **Dendritic cells accumulate in the bone marrow of myeloma patients where they protect tumor plasma cells from CD8+ T-cell killing.** Blood. 2015, 126(12):1443-51.

Le Ru E, Etchegoin P. **Principles of Surface Enhanced Raman Spectroscopy 1st Edition.** 2009 Elsevier, Amsterdam.

Le Ru EC, Meyer M, Etchegoin PG. **Surface Enhanced Raman Scattering Enhancement Factors: A Comprehensive Study**. J. Phys. Chem. C 2007, 111:13794–13803.

Liu JK, Lubelski D, Schonberg DL, Wu Q, Hale JS, Flavahan WA3, Mulkearns-Hubert EE, Man J, Hjelmeland AB, Yu J, Lathia JD, Rich JN. **Phage display discovery of novel molecular targets in glioblastoma-initiating cells.** Cell Death Differ 2014, 21(8):1325-39.

Lowman HB. **Bacteriophage display and discovery of peptide leads for drug development.** Annu Rev Biophys Biomol Struct 1997, 26:401-24.

Luzzago A, Felici F. Construction of disulfide-constrained random peptide libraries displayed on phage coat protein VIII. Methods Mol Biol. 1998, 87:155-64.

Lührs T, Ritter C, Adrian M, Riek-Loher D, Bohrmann B, Döbeli H, Schubert D, Riek R. **3D structure of Alzheimer's amyloid-beta(1-42) fibrils.** Proc Natl Acad Sci U S A. 2005, 102(48):17342-7.

Makowski L. **Phage display: structure, assembly and engineering of filamentous bacteriophage M13**.

Maftei M, Thurm F, Schnack C, Tumani H, Otto M, Elbert T, Kolassa I-T, Przybylski M, Manea M, von Arnim CAF. **Increased Levels of Antigen-Bound β-Amyloid Autoantibodies in Serum and Cerebrospinal Fluid of Alzheimer's Disease Patients.** PLoS One. 2013; 8(7): e68996.

Margulies M, Egholm M, Altman WE, Attiya S, Bader JS, Bemben LA, Berka J, Braverman MS, Chen YJ, Chen Z, Dewell SB, Du L, Fierro JM, Gomes XV, Godwin BC, He W, Helgesen S, Ho CH, Irzyk GP, Jando SC, Alenquer ML, Jarvie TP, Jirage KB, Kim JB, Knight JR, Lanza JR, Leamon JH, Lefkowitz SM, Lei M, Li J, Lohman KL, Lu H, Makhijani VB, McDade KE, McKenna MP, Myers EW, Nickerson E, Nobile JR, Plant R, Puc BP, Ronan MT, Roth GT, Sarkis GJ, Simons JF, Simpson JW, Srinivasan M, Tartaro KR, Tomasz A, Vogt KA, Volkmer GA, Wang SH, Wang Y, Weiner MP, Yu P, Begley RF, Rothberg JM. **Genome sequencing in microfabricated high-density picolitre reactors.** Nature. 2005, 437(7057):376-80.

Marino P, Norreel JC, Schachner M, Rougon G, Amoureux MC. **A polysialic acid mimetic peptide promotes functional recovery in a mouse model of spinal cord injury**. Exp Neurol. 2009, 219(1):163-74.

Marvin DA, Hale RD, Nave C, Helmer-Citterich M. **Molecular models and structural comparisons of native and mutant class I filamentous bacteriophages Ff (fd, f1, M13), If1 and IKe.** J Mol Biol. 1994, 235(1):260-86.

Matochko WL1, Cory Li S, Tang SK, Derda R. **Prospective identification of parasitic sequences in phage display screens.** Nucleic Acids Res 2014, 42(3):1784-98.

Mazzera L, Lombardi G, Abeltino M, Ricca M, Donofrio G, Giuliani N, Cantoni AM, Corradi A, Bonati A, Lunghi P. **Aurora and IKK kinases cooperatively interact to protect multiple myeloma cells from Apo2L/TRAIL**. Blood. 2013, 122(15):2641-53.

McLaurin J, Cecal R, Kierstead ME, Tian X, Phinney AL, Manea M, French JE, Lambermon MH, Darabie AA, Brown ME, Janus C, Chishti MA, Horne P, Westaway D, Fraser PE, Mount HT, Przybylski M, St George-Hyslop P. **Therapeutically effective antibodies against amyloid-beta**

peptide target amyloid-beta residues 4-10 and inhibit cytotoxicity and fibrillogenesis. Nat Med. 2002, 8(11):1263-9. Epub 2002 Oct 15.

Mediero A, Ramkhelawon B, Perez-Aso M, Moore KJ, Cronstein BN. **Netrin-1 is a critical autocrine/paracrine factor for osteoclast differentiation**. J Bone Miner Res. 2015, 30(5):837-54.

Messing J. **Phage M13 for the treatment of Alzheimer and Parkinson disease**. Gene, 2016, 583:85-9.

Mészáros B, Simon I, Dosztányi Z. **Prediction of protein binding regions in disordered proteins.** PLoS Comput Biol, 2009, 5(5): e1000376.

Mitchell AL, Attwood TK, Babbitt PC, Blum M, Bork P, Bridge A, Brown SD, Chang HY, El-Gebali S, Fraser MI, Gough J, Haft DR, Huang H, Letunic I, Lopez R, Luciani A, Madeira F, Marchler-Bauer A, Mi H, Natale DA, Necci M, Nuka G, Orengo C, Pandurangan AP, Paysan-Lafosse T, Pesseat S, Potter SC, Qureshi MA, Rawlings ND, Redaschi N, Richardson LJ, Rivoire C, Salazar GA, Sangrador-Vegas A, Sigrist CJA, Sillitoe I, Sutton GG, Thanki N, Thomas PD, Tosatto SCE, Yong SY, Finn RD. **InterPro in 2019: improving coverage, classification and access to protein sequence annotations.** Nucleic Acids Res. 2019, 47(D1): D351-D360.

Morag O, Sgourakis NG, Baker D, Goldbourt A. **The NMR-Rosetta capsid model of M13 bacteriophage reveals a quadrupled hydrophobic packing epitope.** Proc Natl Acad Sci U S A. 2015, 112(4):971-6.

Mruthinti S, Buccafusco JJ, Hill WD, Waller JL, Jackson TW, Zamrini EY, Schade RF. **Autoimmunity in Alzheimer's disease: increased levels of circulating IgGs binding Abeta and RAGE peptides**. Neurobiol Aging. 2004, 25(8):1023-32.

Münchberg U, Rösch P, Bauer M, Popp J. **Raman spectroscopic identification of single bacterial cells under antibiotic influence.** Anal Bioanal Chem. 2014, 406(13):3041-50.

Nagele EP, Han M, Acharya NK, DeMarshall C, Kosciuk MC, Nagele RG. **Natural IgG autoantibodies are abundant and ubiquitous in human sera, and their number is influenced by age, gender, and disease**. PLoS One. 2013, 8(4): e60726.

Nagoshi H, Taki T, Chinen Y, Tatekawa S, Tsukamoto T, Maegawa S, Yamamoto-Sugitani M, Tsutsumi Y, Kobayashi T, Matsumoto Y, Horiike S, Okuno Y, Fujiwara S, Hata H, Kuroda J, Taniwaki M. **Transcriptional dysregulation of the deleted in colorectal carcinoma gene in multiple myeloma and monoclonal gammopathy of undetermined significance.** Genes Chromosomes Cancer. 2015, 54(12):788-95.

Nandakumar R, Nandakumar MP, Marten MR, Ross JM. **Proteome analysis of membrane and cell wall associated proteins from Staphylococcus aureus.** J Proteome Res 2005, 4(2):250-7.

Nelson PT, Dickson DW, Trojanowski JQ, Jack CR, Boyle PA, Arfanakis K, Rademakers R, Alafuzoff I, Attems J8, Brayne C, Coyle-Gilchrist ITS, Fardo DW, Flanagan ME, Halliday G, Hunter S, Jicha GA1, Katsumata Y, Kawas CH, Keene CD, Kovacs GG, Kukull WA, Levey AI, Makkinejad N, Montine TJ, Murray ME, Nag S, Seeley WW, Sperling RA, White CL, Schneider JA. **Reply: LATE to the PART-y.** Brain. 2019, 142(9):e48.

Nemudraya AA, Richter VA, Kuligina EV. **Phage Peptide Libraries As a Source of Targeted Ligands**. Acta Naturae. 2016, 8(1):48-57.

Newton J, Deutscher SL. **Phage peptide display.** Handb Exp Pharmacol 2008, (185 Pt 2):145-63.

Neve RM, Chin K, Fridlyand J, Yeh J, Baehner FL, Fevr T, Clark L, Bayani N, Coppe JP, Tong F, Speed T, Spellman PT, DeVries S, Lapuk A, Wang NJ, Kuo WL, Stilwell JL, Pinkel D, Albertson DG, Waldman FM, McCormick F, Dickson RB, Johnson MD, Lippman M, Ethier S, Gazdar A, Gray JW. **A collection of breast cancer cell lines for the study of functionally distinct cancer subtypes.** Cancer Cell. 2006, 10(6):515-27.

Nixon AE, Sexton DJ, Ladner RC. **Drugs derived from phage display: from candidate identification to clinical practice.** MAbs 2014, 6(1):73-85.

Noren KA, Noren CJ. **Construction of high-complexity combinatorial phage display peptide libraries.** Methods 2001, 23(2):169-78.

Pande J, Szewczyk MM, Grover AK. **Phage display: concept, innovations, applications and future.** Biotechnol Adv. 2010, 28(6):849-58.

Paoli GC, Brewster JD. **A Listeria Monocytogenes-specific phage-displayed antibody fragment recognizes a cell surface protein whose expression is regulated by physiological conditions.** J RAP Meth Auto Microbiol 2007, 15: 77–91.

Papavoine CH, Christiaans BE, Folmer RH, Konings RN, Hilbers CW. **Solution structure of the M13 major coat protein in detergent micelles: a basis for a model of phage assembly involving specific residues**. J Mol Biol. 1998, 282(2):401-19.

Paschke M. **Phage display systems and their applications.** Appl Microbiol Biotechnol 2006, 70(1):2-11.

Pasqualini R, Ruoslahti E. **Organ targeting in vivo using phage display peptide libraries**. Nature 1996, 380(6572):364-6.

Petersen RC. **How early can we diagnose Alzheimer disease (and is it sufficient)? The 2017 Wartenberg lecture.** Neurology. 2018, 91(9):395-402.

Petrenko VA, Smith GP. **Phages from landscape libraries as substitute antibodies.** Protein Eng 2000, 13(8):589-92.

Petrenko VA, Vodyanoy VJ. **Phage display for detection of biological threat agents.** J Microbiol Methods 2003, 53(2):253-62.

Petrenko VA, Smith GP, Gong X and Quinn T. **A library of organic landscapes on filamentous phage**. Protein Eng 1996, 9:797-801.

Petrenko VA. **Autonomous self-navigating drug-delivery vehicles: from science fiction to reality.** Ther Deliv. 2017, 8(12):1063-1075.

Petrenko VA, Gillespie JW, Xu H, O'Dell T, De Plano LM. Combinatorial Avidity Selection of Mosaic **Landscape Phages Targeted at Breast Cancer Cells-An Alternative Mechanism of Directed Molecular Evolution**. Viruses. 2019, 11(9). pii: E785.

Polat G, Ugan RA, Cadirci E, Halici Z. **Sepsis and Septic Shock: Current Treatment Strategies and New Approaches**. Eurasian J Med. 2017, 49(1):53-58.

Qu BX, Gong Y, Moore C, Fu M, German DC, Chang LY, Rosenberg R, Diaz-Arrastia R. **Beta-amyloid auto-antibodies are reduced in Alzheimer's disease.** J Neuroimmunol. 2014,274(1-2):168-73.

Rao SV, Podagatlapalli GK, Hamad S. **Ultrafast laser ablation in liquids for nanomaterials and applications**. J Nanosci Nanotechnol. 2014, 14(2):1364-88.

Reddy MM, Wilson R, Wilson J, Connell S, Gocke A, Hynan L, German D, Kodadek T**. Identification of candidate IgG biomarkers for Alzheimer's disease via combinatorial library screening**. Cell. 2011, 144(1):132-42.

Rendtlew Danielsen JM, Knudsen LM, Dahl IM, Lodahl M, Rasmussen T. **Dysregulation of CD47 and the ligands thrombospondin 1 and 2 in multiple myeloma.** Br J Haematol. 2007, 138(6):756-60.

Riehemann K, Schneider SW, Luger TA, Godin B, Ferrari M, Fuchs H. **Nanomedicine--challenge and perspectives.** Angew. Chem. Int. Ed. 2009, 48: 872 – 97.

Richardson LJ, Rawlings ND, Salazar GA, Almeida A, Haft DR, Ducq G, Sutton GG, Finn RD. **Genome properties in 2019: a new companion database to InterPro for the inference of complete functional attributes.** Nucleic Acids Res. 2019, 47(D1):D564-D572.

Richter DC, Heininger A, Brenner T, Hochreiter M, Bernhard M, Briegel J, Dubler S, Grabein B, Hecker A, Kruger WA, Mayer K, Pletz MW, Storzinger D, Pinder N, Hoppe-Tichy T, Weiterer S, Zimmermann S, Brinkmann A, Weigand MA, Lichtenstern C. **Bacterial sepsis : Diagnostics and calculated antibiotic therapy.** Anaesthesist. 2019, 68(Suppl 1):40-62.

Roy P, Sarkar UA, Basak S. **The NF-κB Activating Pathways in Multiple Myeloma**. Biomedicines. 2018, 6(2). pii: E59.

Royston E, Lee SY, Culver JN, Harris MT. **Characterization of silica-coated tobacco mosaic virus.** J Colloid Interface Sci 2006, 298(2):706-12.

Ruoslahti E. **Drug targeting to specific vascular sites.** Drug Discov Today 2002, 7(22):1138-43.

Ruoslahti E. **Tumor penetrating peptides for improved drug delivery.** Adv Drug Deliv Rev 2017, 110-111:3-12.

Ruoslahti E. **RGD and other recognition sequences for integrins**. Annu Rev Cell Dev Biol 1996, 12:697-715.

Sabhnani L, Rao DN. **Identification of immunodominant epitope of F1 antigen of Yersinia pestis.** FEMS Immunol Med Microbiol. 2000, 27(2):155-62.

Saksela K, Permi P. **SH3 domain ligand binding: What's the consensus and where's the specificity?** FEBS Lett. 2012 Aug 14;586(17):2609-14.

Sato T, Kokabu S, Enoki Y, Hayashi N, Matsumoto M, Nakahira M, Sugasawa M, Yoda T. **Functional Roles of Netrin-1 in Osteoblast Differentiation**. In Vivo. 2017, 31(3):321-328.

Savitzky A, Golay MJE. **Smoothing and differentiation of data by simplified least squares procedures.** Anal. Chem. 1964, 36:1627–1639.

Schmid FX. **Biological Macromolecules: UV-visible Spectrophotometry** In R. Bridgewater (eds) ELS, American Cancer Society 2001, 1–4. Wiley, New Jersey.

Scibilia S, Lentini G, Fazio E, Franco D, Neri F, Mezzasalma AM, Guglielmino SPP. **Self-assembly of silver nanoparticles and bacteriophage**, Sens Biosens Res 2016 7 146–152.

Shetty G, Kendall C, Shepherd N, Stone N, Barr H. **Raman spectroscopy: elucidation of biochemical changes in carcinogenesis of oesophagus.** Br J Cancer 2006; 94(10):1460-4.

Shi J, Kantoff PW, Wooster R, Farokhzad OC. **Cancer nanomedicine: progress, challenges and opportunities.** Nat Rev Cancer 2017, 17(1):20-37.

Shrivastava A, Gupta VB. **Methods for the determination of limit of detection and limit of quantitation of the analytical method***s.* Chron. Young Sci. 2011, 2(1): 21–25.

Sidhu SS. **Phage display in pharmaceutical biotechnology**. Curr Opin Biotechnol 2000, 11(6):610-6.

Sidhu SS. **Engineering M13 for phage display**. Biomol Eng 2001, 18(2):57-63.

Sioud M. **Phage Display Libraries: From Binders to Targeted Drug Delivery and Human Therapeutics.** Mol Biotechnol 2019, 61(4):286-303.

Smith GP. **Filamentous fusion phage: novel expression vectors that display cloned antigens on the virion surface.** Science 1985, 228(4705):1315-7.

Smith GP, Petrenko VA. **Phage Display.** Chem Rev 1997, 97(2):391-410.

Smith GP. **The phage nanoparticle toolkit**. In Petrenko V and Smith GP (eds) Phage nanobiotechnology. Royal Society of Chemistry, London, 2011, 1–11.

Smith GP. **Surface presentation of protein epitopes using bacteriophage expression systems.** Curr Opin Biotechnol 1991, 2:668-673.

Smith GP and Scott JK. **Libraries of peptides and proteins displayed on filamentous phage**. Methods Enzymol 1993, 217:228-257.

Smith S, Giriat I, Schmitt A, de Lange T. **Tankyrase, a poly(ADP-ribose) polymerase at human telomeres.** Science 1998, 282(5393):1484-7.

Soendergaard M, Newton-Northup JR, Palmier MO, Deutscher SL. **Peptide Phage Display for Discovery of Novel Biomarkers for Imaging and Therapy of Cell Subpopulations in Ovarian Cancer.** J Mol Biomark Diagn 2011, S:2.

Soliakov A, Harris JR, Watkinson A, Lakey JH. **The structure of Yersinia pestis Caf1 polymer in free and adjuvant bound states.** Vaccine. 2010, 28(35):5746-54.

Stohl W. **Biologic differences between various inhibitors of the BLyS/BAFF pathway: should we expect differences between belimumab and other inhibitors in development?** Curr Rheumatol Rep 2012, 14(4):303-9.

Stolz LE, Horn PT. **Ecallantide: a plasma kallikrein inhibitor for the treatment of acute attacks of hereditary angioedema**. Drugs Today (Barc) 2010, 46(8):547-55.

Stone N, Kendall C, Smith J, Crow P, Barr H. **Raman spectroscopy for identification of epithelial cancers.** Faraday Discuss 2004, 126:141-57; discussion 169-83.

Stopar D, Spruijt RB, Wolfs CJ, Hemminga MA. **Structural characterization of bacteriophage M13 solubilization by amphiphiles.** Biochim Biophys Acta 2002, 1594(1):54-63.

Stopar D, Spruijt RB, Wolfs CJ, Hemminga MA. **Protein-lipid interactions of bacteriophage M13 major coat protein**. Biochim Biophys Acta 2003, 1611(1-2):5-15.

Strebhardt K, Ullrich A. **Paul Ehrlich's magic bullet concept: 100 years of progress**. Nat Rev Cancer. 2008, 8(6):473-80.

Szardenings M. **Phage display of random peptide libraries: Applications, limits, and potential**. J Recept Signal Transduct Res 2003 23:307-349.

Sutarlie L, Ow SY, Su X. **Nanomaterials-based biosensors for detection of microorganisms and microbial toxins**. Biotechnol J. 2017, 12(4).

Tatavarthy A, Cannons A. **Real-time PCR detection of Salmonella species using a novel target: the outer membrane porin F gene (ompF).** Lett Appl Microbiol. 2010, 50(6):645-52.

Teesalu T, Sugahara KN, Ruoslahti E. **Mapping of vascular ZIP codes by phage display**. Methods Enzymol 2012, 503:35-56.

Teyra J, Huang H, Jain S, Guan X, Dong A, Liu Y, Tempel W, Min J, Tong Y, Kim PM, Bader GD, Sidhu SS. **Comprehensive Analysis of the Human SH3 Domain Family Reveals a Wide Variety of Non-canonical Specificities.** Structure. 2017, 25(10):1598-1610.e3.

Thambisetty M, Lovestone S. **Blood-based biomarkers of Alzheimer's disease: challenging but feasible**. Biomark Med. 2010, 4(1):65-79.

Trøstrup H, Lerche CJ, Christophersen LJ, Thomsen K, Jensen PØ, Hougen HP, Høiby N, Moser C. **Chronic Pseudomonas aeruginosa biofilm infection impairs murine S100A8/A9 and neutrophil effector cytokines-implications for delayed wound closure?** Pathog Dis. 2017, 75(7).

Ulusoy Ghobadi TG, Ghobadi A, Okyay T, Topalli K, Okyay AK. **Controlling luminescent silicon nanoparticle emission produced by nanosecond pulsed laser ablation: role of interface defect states and crystallinity phase.** RSC Adv 2016, 6:112520-26.

Vigevani L, Valcárcel J. **Molecular biology. A splicing magic bullet. Science**. 2014, 345(6197):624-5.

Wachsmann-Hogiu S, Weeks T, Huser T. **Chemical analysis in vivo and in vitro by Raman spectroscopy: From single cells to humans**. Curr. Opin. Biotechnol. 2009, 20:63–73.

Walling MA, Novak JA, Shepard JR. **Quantum dots for live cell and in vivo imaging.** Int J Mol Sci. 2009, 10(2):441-91.

Wang AZ, Langer R, Farokhzad OC. **Nanoparticle delivery of cancer drugs.** Annu Rev Med. 2012, 63:185-98.

Wang H, Han M, Han Z. **Phage-displayed recombinant peptides for non-invasive imaging assessment of tumor responsiveness to ionizing radiation and tyrosine kinase inhibitors.** In: Nenoi M (eds) Current Topics in Ionizing Radiation Research 2012. INTECH Open Access Publisher, London.

Wang Y, Xu B, Hu WW, Chen LJ, Wu CP, Lu BF, Shen YP, Jiang JT. **High expression of CD11c indicates favorable prognosis in patients with gastric cancer**. World J Gastroenterol. 2015, 21(31):9403-12.

Webb B, Sali A. **Comparative Protein Structure Modeling Using MODELLER**. Curr Protoc Bioinformatics. 2016, 54:5.6.1-5.6.37.

Webster R. **Biology of the filamentous bacteriophage**. In Phage display of peptides and proteins: a laboratory manual. Academic Press, San Diego, 1996, 1-20.

Wu J, Li L. **Autoantibodies in Alzheimer's disease: potential biomarkers, pathogenic roles, and therapeutic implications**. J Biomed Res. 2016, 30(5):361-372.

Weksler ME, Relkin N, Turkenich R, LaRusse S, Zhou L, Szabo P. **Patients with Alzheimer disease have lower levels of serum anti-amyloid peptide antibodies than healthy elderly individuals**. Exp Gerontol. 2002, 37(7):943-8.

Yang W, Yoon A, Lee S, Kim S, Han J, Chung J**. Next-generation sequencing enables the discovery of more diverse positive clones from a phage-displayed antibody library**. Exp Mol Med. 2017, 49(3): e308.

Yip YL, Hawkins NJ, Smith G, Ward RL. **Biodistribution of filamentous phage-Fab in nude mice.** J Immunol Methods. 1999, 225(1-2):171-8.

Yoshiike Y, Minai R, Matsuo Y, Chen YR, Kimura T, Takashima A. **Amyloid oligomer conformation in a group of natively folded proteins.** PLoS One. 200, 3(9): e3235.

Zavialov AV, Berglund J, Pudney AF, Fooks LJ, Ibrahim TM, MacIntyre S, Knight SD. **Structure and biogenesis of the capsular F1 antigen from Yersinia pestis: preserved folding energy drives fiber formation.** Cell. 2003, 113(5):587-96.

Zavialov AV, Berglund J, Knight SD. **Overexpression, purification, crystallization and preliminary X-ray diffraction analysis of the F1 antigen Caf1M-Caf1 chaperone-subunit pre-assembly complex from Yersinia pestis**. Acta Crystallogr D Biol Crystallogr. 2003, 59(Pt 2):359-62.

Zavialov AV, Tischenko VM, Fooks LJ, Brandsdal BO, Aqvist J, Zav'yalov VP, Macintyre S, Knight SD. **Resolving the energy paradox of chaperone/usher-mediated fibre assembly**. Biochem J. 2005, 389(Pt 3):685-94.

Zhang ZM, Chen S, Liang YZ. **Baseline correction using adaptive iteratively reweighted penalized least squares.** Analyst. 2010, 135(5):1138-46.

Zimmermann K, Hagedorn H, Heuck CC, Hinrichsen M, Ludwig H. **The ionic properties of the filamentous bacteriophages Pf1 and fd.** J Biol Chem. 1986, 261(4):1653-5.

Zou M, Zhang L, Xie Y, Xu W. **NGR-based strategies for targeting delivery of chemotherapeutics to tumor vasculature.** Anticancer Agents Med Chem 2012, 12(3):239-46.